UNIVERSITY OF CALIFORNIA
SANTA CRUZ

# ANALYTICAL MODELING OF MEDIUM ACCESS CONTROL PROTOCOLS IN WIRELESS NETWORKS

A dissertation submitted in partial satisfaction of the
requirements for the degree of

DOCTOR OF PHILOSOPHY

in

COMPUTER ENGINEERING

by

**Marcelo Menezes de Carvalho**

March 2006

The Dissertation of Marcelo Menezes de Carvalho
is approved:

---

Professor J. J. Garcia-Luna-Aceves, Chair

---

Professor Katia Obraczka

---

Professor John Vesecky

---

Lisa C. Sloan
Vice Provost and Dean of Graduate Studies

# Report Documentation Page

*Form Approved*
*OMB No. 0704-0188*



| 1. REPORT DATE | 2. REPORT TYPE | 3. DATES COVERED |
|---|---|---|
| **MAR 2006** | | **00-03-2006 to 00-03-2006** |

| 4. TITLE AND SUBTITLE | 5a. CONTRACT NUMBER |
|---|---|
| **Analytical Modeling of Medium Access Control Protocols in Wireless Networks** | 5b. GRANT NUMBER |
| | 5c. PROGRAM ELEMENT NUMBER |
| 6. AUTHOR(S) | 5d. PROJECT NUMBER |
| | 5e. TASK NUMBER |
| | 5f. WORK UNIT NUMBER |
| 7. PERFORMING ORGANIZATION NAME(S) AND ADDRESS(ES) **University of California at Santa Cruz,Department of Computer Engineering,Santa Cruz,CA,95064** | 8. PERFORMING ORGANIZATION REPORT NUMBER |
| 9. SPONSORING/MONITORING AGENCY NAME(S) AND ADDRESS(ES) | 10. SPONSOR/MONITOR'S ACRONYM(S) |
| | 11. SPONSOR/MONITOR'S REPORT NUMBER(S) |

12. DISTRIBUTION/AVAILABILITY STATEMENT
**Approved for public release; distribution unlimited**

13. SUPPLEMENTARY NOTES
**The original document contains color images.**

14. ABSTRACT

15. SUBJECT TERMS

| 16. SECURITY CLASSIFICATION OF: | | | 17. LIMITATION OF ABSTRACT | 18. NUMBER OF PAGES | 19a. NAME OF RESPONSIBLE PERSON |
|---|---|---|---|---|---|
| a. REPORT | b. ABSTRACT | c. THIS PAGE | | | |
| **unclassified** | **unclassified** | **unclassified** | | **234** | |

# Contents

# List of Figures

# List of Tables

## Abstract

Analytical Modeling of Medium Access Control Protocols in Wireless Networks

by

Marcelo Menezes de Carvalho

A new modeling framework is introduced for the analytical study of medium access control (MAC) protocols operating in multihop wireless ad hoc networks, i.e., wireless networks characterized by the lack of any pre-existent infrastructure and where participating devices must cooperatively provide the basic functionalities that are common to any computer network. The proposed modeling framework focuses on the interactions between the physical (PHY) and MAC layers, and on the impact that each node has on the dynamics of every other node in the network. To account for the effects of both cross-layer interactions and the interference among all nodes, a novel linear model is introduced with which topology and PHY/MAC-layer aspects are naturally incorporated in what we define as interference matrices. A key feature of the model is that nodes can be modeled individually, i.e., it allows a per-node setup of many layer-specific parameters. Moreover, no spatial probability distribution or special arrangement of nodes is assumed; the model allows the computation of individual (per-node) performance metrics for any given network topology and radio channel model.

To show the applicability of our modeling framework, we model wireless ad hoc networks that operate according to the IEEE 802.11 standard. To accomplish this, we present a comprehensive analytical modeling of the IEEE 802.11 and the derivation of many perfor-

mance metrics of interest, such as delay, throughput, and energy consumption.

Following recent advances in communication technologies, we also investigate the use of multiple antenna elements in both ends of the wireless link to conduct the first analytical modeling of wireless ad hoc networks that considers the impact of realistic antenna-gain patterns on network performance. As such, our modeling approach allows the study of ad hoc networks in which nodes are equipped with directional antennas, i.e., systems of antennas that are able to transmit/receive energy over intended directions. This modeling capability stands out from all previous analytical models, which have only dealt with omnidirectional or over-simplified antenna gain patterns, and which have not addressed the specific mechanisms of the MAC protocols used (e.g., backoff mechanisms).

Lastly, we present the first analytical model for wireless ad hoc networks equipped with multiple-input multiple-output (MIMO) radios enabled with space-time coding (STC) that considers the impact of the underlying radio-based topology. In particular, we consider the space-time block coding (STBC) technique known as the "Alamouti scheme." We derive the effective signal-to-interference-plus-noise density ratio (SINR) of the Alamouti scheme under multiple access interference (MAI), and we propose the moment generating function (MGF) method to derive closed-form expressions for its symbol error probability under different modulation schemes and when fading paths are independent but not necessarily identically distributed. We apply the Alamouti scheme to IEEE 802.11 ad hoc networks with different antenna system configurations and compare their performance with respect to the basic single-input-single-output (SISO) system.

## Acknowledgements

First, and foremost, I would like to thank my advisor Prof. J. J. Garcia-Luna-Aceves for having accepted me as a Ph.D. student. Sometimes, the best support one can obtain in life is embodied in the simple act of trust and the gift of a second opportunity. For that, my deepest gratitude. I will always be indebted for all the support, guidance, encouragement, and understanding he has given me throughout these years. It was a real pleasure to work with someone so highly motivated, smart, enthusiastic, and passionate about his work. *Muito obrigado, JJ !*

I am very thankful to Prof. Katia Obraczka and Prof. John Vesecky for participating in my dissertation committee defense and for their invaluable suggestions, discussions, and wonderful feedback. Also, I would like to thank Prof. Patrick Mantey for serving in my qualifying exam committee, and for his insightful comments and suggestions in the early stages of my research. I also thank Prof. Hamid Sadjadpour for participating so actively in my dissertation defense with interesting comments and discussions.

I thank all the great colleagues I had the pleasure to meet at the Computer Communication Research Group (CCRG). In particular, I would like to thank Marco Spohn, Renato Moraes, Yu Wang, Hari Rangarajan, Ravindra Vaishampayan, Soumya Roy, Lori Flynn, Saravanan Balasubramaniyan, Ramesh Balakrishnan, Radhika Vullikanti, Long Yang, Mark Mosko, Brad Smith, Lichun Bao, Chane Fullmer, Ewerton Madruga, Zhenjiang Li, Wenyi, and Rolando Menchaca. Also, I would like to thank the members of the i-NRG Lab. In particular, Cíntia Margi, Kumar Viswanath, Ignacio Solis, and Venkatesh Rajendran.

To the great staff of SoE, I am very thankful to Carol Mullane and Jodi Rieger, who

have made my life so much easier at SoE with their prompt support, care, and great sense of humor. My thanks also go to the Computing Support, especially Haifang, Heidi Sitton and Lynne Sheehan. From the International Scholar and Student Services (ISSS), I thank Joni McFarlane for her prompt support and kind assistance in all matters related to being an international student at UCSC.

I would like to thank my wife Mylène Farias for her unconditional support throughout these years, especially during all the difficult times we went through while we had to live apart from each other in a foreign country for so long. In spite of all difficulties, I am extremely proud of all we have accomplished together in this long journey. For sure, this doctorate would have not been possible without her tremendous encouragement, love, patience, companionship, deep trust in me and, of course, the occasional swift kicks in the pants!

My deepest gratitude also go to my parents José Maria and Maria Neusa, who have always filled my life with generous love, unconditional support, and everything I needed to pursue my highest dreams. This doctorate is truly theirs! To my lovely sisters Eliane and Ana Maria, and my dear brother Evandro, my big thanks for all the support and encouragement they have always given to me. Also, I would like to thank my parents-in-law Afonso Gutemberg and Célia Farias for all their kind and generous support along these years.

Finally, I want to thank the financial support I have received from the Coordenação de Aperfeiçoamento de Pessoal de Nível Superior (CAPES/Brazil), the Baskin Chair of Computer Engineering at UCSC, the National Science Foundation under Grant CNS-0435522, the UCOP CLC under Grant SC-05-33, and the U.S. Army Research Office under grants No. W911NF-04-1-0224 and No. W911NF-05-1-0246.

*To my wife Mylène Farias*

*and my parents*

*José Maria and Maria Neusa.*

# Chapter 1

# Introduction

In the dawn of a new millennium, we have witnessed an explosive growth of information and communication technologies (ICTs) that have ignited profound changes in the way society will evolve in the years to come. The catalytic effect that ICTs have on the development of modern society is undeniable and, to attest to this fact, the importance of ICTs has been explicitly acknowledged in the elaboration of the *Millennium Development Goals* [128], which constitute the world's targets for reducing extreme poverty in its many dimensions in the near future. The eighth goal—developing a global partnership for development—proposes a means of achieving the other seven goals, which vary from eradication of extreme poverty and hunger to the achievement of universal primary education. Target 18 of Goal 8 calls upon the Declaration's adherents to: "*In cooperation with the private sector, make available the benefits of new technologies, especially information and communication technologies*." In other words, the *Millennium Development Goals* acknowledge ICTs as important tools to achieve its overall goals, and believe that ICTs can help alleviate poverty, improve the delivery of education

and health care, make governments more accessible and accountable to people, etc. Following the declaration of the Millennium Development Goals, the World Summit on the Information Society (WSIS) approved the Geneva Declaration of Principles [137], where it expresses its commitment to harness the potential of ICTs in the promotion of the Millennium Development Goals.

The importance attributed to ICTs in the development of society has certainly been fueled by the widespread growth of the *Internet* and *mobile wireless communications* in the past few decades. Today, the International Telecommunications Union (ITU) considers the level of access to these two technologies as one of the primary indicators of ICT availability in any country [66]. According to the ITU, almost every country in the world had a direct connection to the Internet by the turn of the new millennium and, in the end of 2001, over 90 per cent of the countries already had a mobile network, with almost 100 countries having more mobile than fixed telephone subscribers [65]. Although this represents an impressive achievement, access levels to ICTs vary among and within countries, creating the so-called "digital divide" between those with high and those with low access levels [66]. Today, the digital divide is the biggest challenge to be faced and, to reduce it, the ITU points to *mobile wireless communications* as the "missing link," reaffirming its belief on the potential of this technology by recognizing that "*Mobile has raised access to communications to new levels (...) Policy makers must look to mobile as a way of achieving social policy goals*" [65].

Ultimately, wireless communications can help not only to eliminate the digital divide, but also to realize the vision of *ubiquitous* and *pervasive computing* originally articulated by Mark Weiser [104, 134]. In his vision, Mark Weiser called for a new way of thinking

about computers in the world, one that takes into account the natural human environment and allows the computers themselves "to vanish into the background," in a way that computers become so seamlessly integrated in our lives that we cease to be aware of them. In fact, such "invisibility" is meant to happen not only in the metaphoric sense, with the development of user-friendly, task-oriented, intuitive computers, software and interfaces, but also in the strict sense, with the advent of small intelligent devices ubiquitously embedded in the physical world and globally connected through the Internet. To support this trend, a number of key technologies have emerged recently in the field of embedded systems. Most prominently, significant advances have been made in the fields of micro-electro-mechanical systems (MEMS) technology, nanotechnology, and sensor technology. In the future, embedded devices are expected to interact with each other to add intelligence to environments and create the so-called "smart spaces" [39]. Ultimately, the vision of ubiquitous and pervasive computing will lead to the ability of having seamless and transparent access to communications and computing services anytime, anywhere, on a global basis.

The inherent nature of ubiquitous and pervasive computing/communications demands an extremely flexible infrastructure to support a multitude of interconnections among highly heterogeneous devices. This demand for high flexibility makes wireless networks the easiest solution for the interconnection of ubiquitous devices [27]. Currently, however, most of the deployed wireless networks have a fixed infrastructure. By far, the most successful application of wireless networking has been the cellular telephone system, in which (mobile) telephone users communicate directly to a *fixed* and *central* base station that covers a certain geographic area and is responsible for most of the intelligence and control within the network.

Despite its advantages, the cellular concept (or infrastructure-based wireless networks, to be more general), has its drawbacks: it is of relatively low bandwidth, similar in many ways to wired dial-up access, and it generally takes time and potentially high cost to set up the necessary infrastructure [56]. Moreover, even if costs were reduced and efficiency improved, infrastructure-based networks may not always be possible, appropriate, or even desirable in many of the envisaged scenarios for ubiquitous and pervasive computing/communications.

To fulfill the vision of ubiquitous computing/communications, wireless networks need to evolve beyond the current infrastructure-type of networks. Fortunately, because of significant advances in hardware technology in the past decades—most notably in the areas of processing capability and storage capacity—it has now been possible to include more "intelligence" into smaller devices with significant reductions in power consumption. As a consequence, the deployment of wireless networks without any pre-existent infrastructure—the so-called *wireless ad hoc networks*—are now becoming possible.

In a wireless ad hoc network, all participating devices must cooperatively provide the "core" functionality that is usually "a given" in an infrastructure network, i.e., each "node" executes functions of routers, switches, clients, and servers. Given this characteristic, wireless ad hoc networks can be formed dynamically, "on the fly," by a group of nodes using the readily-available wireless channel, and without any centralized control or administration. Therefore, no pre-infrastructure is required to enable the exchange of information among users' devices. In case the devices are too distant apart that they cannot communicate directly to each other (due to signal power attenuation with distance and other phenomena typical of wireless channels), the packets can be forwarded via intermediate devices that relay the pack-

ets on a hop-by-hop basis. Depending on the application or the scenario, nodes in a wireless ad hoc network may be mobile and free to organize themselves arbitrarily. As a consequence, intermittent connectivity may happen and the network's topology may change rapidly and unpredictably. In those cases, routes to destination nodes may need to be computed dynamically and updated frequently. In addition, nodes may join or leave the network anytime, with their location and availability constrained by the characteristics of the surrounding wireless medium. Figure 1.1 shows an example of a wireless ad hoc network.

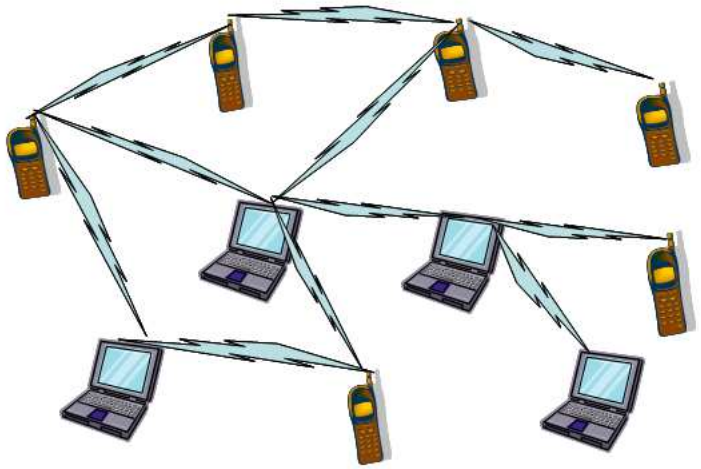

**Figure 1.1**: Example of a wireless ad hoc network.

The concept of wireless ad hoc networks is not new. Initial interest in this type of network emerged within the military arena with the Packet Radio Network (PRNet) project funded by the Defense Advanced Research Projects Agency (DARPA) in 1972, followed by the Survivable Radio Networks (SURAN) project in 1983, and DARPA's Global Mobile (GloMo) Information Systems program launched in 1994 [45]. In the commercial arena, however, the introduction of the Ethernet technology in the 1970's [82] for wired interconnection

of local area networks (LANs) kept the interest of companies away from wireless networking. Ethernet data rates were far higher than those provided by any radio-based technology at that time. Interest in the development of commercial products for wireless computer networks started to grow only in 1985, when the Federal Communications Commission (FCC) authorized the public use of the Industrial, Scientific, and Medical (ISM) frequency band for the development of wireless LAN products. The main advantage of the ISM band for the deployment of WLANs is the fact that no FCC license is required to operate in this band, as opposed to the frequency bands used in cellular telephone systems, whose license fees are extremely high. Unfortunately, the first wireless LAN products launched into the market had very poor performance [56]. Their poor performance, coupled with lack of standardization, security problems, and high prices (compared to wired Ethernet cards at that moment), resulted in weak sales. Thus, it was not until recently that commercial interest in radio technologies for wireless networking beyond cellular systems really took off. It all began in 1997, when the Institute of Electrical and Electronics Engineers (IEEE) released the first standard for WLANs, named IEEE 802.11, supporting data rates of up to 2 Mbps [64]. Later, in 1999, the IEEE task group 802.11b released an extension to support data rates of up to 11 Mbps. This extension, commonly referred to as Wireless Fidelity (Wi-Fi), became an instant success, igniting a true revolution in the segment of WLANs. Following this success, several IEEE 802.11 task groups (designated by the letters 'a', 'e', 'g', etc.) have been created to extend and improve the IEEE 802.11 standard in many aspects, which vary from the support to quality of service (QoS) features to higher data rates. Today, WLANs based on the IEEE 802.11 standard have become the preferred method of Internet access in many homes, offices, airports, libraries, and

many other environments because of their convenience and freedom from wires.

The importance and attractiveness of the IEEE 802.11 comes from its support for two operational modes: the *infrastructure* mode and the *ad hoc* mode. The infrastructure mode is similar to cellular infrastructure-based networks, where a node acts as the access point (AP) for other nodes to have access to the Internet. This is the most common operational mode used to build the so-called "Wi-Fi hotspots" for Internet access. Nevertheless, it is the ad hoc mode of operation that has caught the largest attention within the research community working in the field of wireless ad hoc networks. This is because the IEEE 802.11 standard is a platform that can be used to implement both single-hop and multi-hop ad hoc networks, and it gives specifications for two of the fundamental layers in the protocol stack of any wireless ad hoc network: the *physical* (PHY) layer and the *medium access control* (MAC) layer. Figure 1.2 shows the locations of the PHY and the MAC layers on the protocol stack defined by the International Standard Organization's Open System Interconnect (ISO/OSI) model.

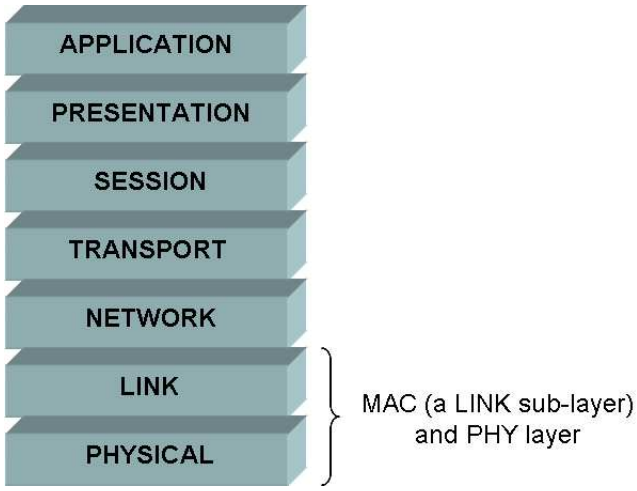


**Figure 1.2**: Location of the PHY and the MAC layers on the protocol stack defined by the ISO/OSI model. The MAC layer is considered as a sub-layer of the LINK layer.

The PHY layer defines the characteristics of, and methods of transmitting and receiving data through the medium that interconnects the nodes of the network. Therefore, it defines a number of parameters and procedures such as the bandwidth and channels to be used, signal modulation schemes, transmit power levels, and error correcting/detecting codes, to name a few. The PHY layer is also responsible for mapping the information bits received from the upper network layers into a framing format suitable for transmission over the physical medium and, correspondingly, for the de-mapping operation of the information received over the medium.

The medium access control (MAC) protocol, on the other hand, is a major component of many multiuser communication systems in which users transmit information over a *common, shared channel* (which is the case in wireless ad hoc networks). Thus, the main task of the MAC layer is to enable nodes in the network to determine their right to access the available channel(s), while attempting to enforce a fair and efficient usage of the channel(s). The establishment of such access rights is far more difficult in a wireless ad hoc network than in a wired long haul network or a wired local area network (LAN), because the radio channels of an ad hoc network are broadcast in nature, and radio connectivity is such that the topology of an ad hoc network is not as clearly defined as with point-to-point wired networks. Unlike wired channels that are fairly stationary and predictable, radio channels are extremely random, and connectivity between two nodes depends on many factors, such as the radio frequency in use, power of the transmitters, terrain, antenna type, transmitter/receiver distance, multipath fading, and the like. Furthermore, the quality of a radio link depends on the transmission activity of all other nodes in the entire system, whose aggregate signal powers can severely

degrade the signal-to-noise ratio (SNR) at a particular receiver and, consequently, compromise the successful reception of any on-going packet transmission. Last, but not least, thermal and other background noise sources can also contribute to the failure of a packet reception at a given receiver.

Consequently, the performance analysis of a MAC protocol in an ad hoc network must consider the interactions between the PHY and the MAC layers. In fact, a cross-layer perspective to both analysis and design of multiaccess communications has been brought to attention with recent advances in wireless communications. As pointed out by Gallager [49] and later by Ephremides and Hajeck [36], the fundamental challenge lies in the choice of a proper model that interfaces the physical layer with the upper network layers. Unfortunately, the bulk of the published work on ad hoc networks has focused on the modeling of medium access schemes where ideal channel conditions and unrealistic assumptions are made. Under the argument of separating the issues strictly related to the protocol operation from the issues intrinsically related to the physical layer, few studies have attempted to incorporate physical layer aspects *directly into the behavior of the protocol*, i.e., explicitly modeling the impact of the physical layer on the *dynamics* of the MAC protocol. Perhaps, more importantly, no attempt has ever been made to include not only the physical-layer aspects explicitly into the model, but also to include the interdependencies among nodes under a radio-based topology in a multihop ad hoc network. Although convenient for analytical modeling, it is *not* true that only the transmissions from "one hop" neighbors of a node can cause interference at the node.

Because of the limitations of existing analytical models for ad hoc networks, many researchers have opted to study the impact of physical layer on the dynamics of MAC proto-

cols via discrete-event simulations. However, even with such simulation packages as Qualnet [105], which are designed to scale with the number of nodes in the network, obtaining simulation results that are statistically meaningful (by using many seeds) requires hours of simulation time for scenarios corresponding to just a few minutes of simulated time in MANETs with hundreds of nodes with a given choice of physical-layer parameters. This is clearly not a promising approach for researchers to gain insight on the impact of multiple physical-layer parameters on the operation of MAC protocols.

In this dissertation, we introduce a new modeling framework for the analytical study of *any* MAC protocol operating in multihop ad hoc networks. The modeling framework we introduce focuses on the interactions between the PHY and MAC layers, and on the impact that each node has on the dynamics of every other node in the network. To account for the effects of both cross-layer interactions and the interference among all nodes, a novel linear model is introduced with which topology and PHY/MAC-layer aspects are naturally incorporated in what we define as *interference matrices*. A key feature of the model is that nodes can be modeled individually, i.e., it allows a per-node setup of many layer-specific parameters. Moreover, no spatial probability distribution or special arrangement of nodes is assumed; the model allows the computation of individual (per-node) performance metrics for any given network topology and radio channel model.

Because of the importance of the IEEE 802.11 standard in the development of current and future wireless ad hoc networks, we illustrate the applicability of our modeling framework through the analytical modeling of wireless ad hoc networks that operate according to the IEEE 802.11 standard. To accomplish this, we present a comprehensive analytical mod-

eling of the IEEE 802.11 distributed coordination function (DCF), which corresponds to the MAC specification for the ad hoc mode of operation. In this dissertation, we investigate the IEEE 802.11 DCF MAC in both single-hop and multihop scenarios, under ideal and realistic channel conditions. The study of single-hop scenarios is performed as an important "stepping stone" for the treatment of the more challenging scenarios oposed by multihop ad hoc networks. In contrast to traditional work in the literature, we use a bottom-up modeling approach to derive a number of performance metrics of interest for the IEEE 802.11 DCF MAC, which are based on its binary exponential backoff algorithm and the events underneath its operation.

Motivated by recent advances in communication technologies, we also investigate the use of multiple antenna elements in both ends of the wireless link and provide the first analytical modeling of wireless ad hoc networks that considers the impact of realistic antenna-gain patterns on network performance. As such, our modeling approach allows the study of ad hoc networks in which nodes are equipped with *directional antennas*, i.e., systems of antennas that are able to transmit/receive energy over intended directions, as opposed to omnidirectional antennas, which (ideally) radiate or absorb energy equally well along all directions. This modeling capability stands out from all previous analytical models, which have only dealt with omnidirectional or over-simplified antenna gain patterns, and which have not addressed the specific mechanisms of the medium access control (MAC) protocols used (e.g., the backoff mechanism). Using our new analytical modeling framework, which allows the study of different carrier-sensing mechanisms, we model the *directional virtual carrier sensing* (DVCS) protocol to validate our analytical model and show its applicability. Our numerical results show that our new analytical model predicts the results obtained by discrete-event simulation

very accurately, and does it with a processing time that is orders of magnitude faster than the time required by simulations. Furthermore, we show that the simplistic "pie slices" used in prior analytical models for antenna patterns over-estimate the throughput of the protocols dramatically compared to the results obtained using realistic antenna patterns.

Lastly, we present the first analytical model for wireless ad hoc networks in which nodes are equipped with multiple-input multiple-output (MIMO) radios and use space-time coding (STC). In particular, we consider the space-time block coding (STBC) technique known as the "Alamouti scheme." We derive the effective signal-to-interference-plus-noise density ratio (SINR) of the Alamouti scheme and closed-form expressions for its symbol error probability under different modulation schemes. The impact of the Alamouti scheme on IEEE 802.11 ad hoc networks is studied by using our new modeling framework and the new analytical model for the IEEE 802.11 DCF MAC. We apply the Alamouti scheme to different antenna system configurations and compare their performance with respect to the basic single-input-single-output (SISO) IEEE 802.11 DCF MAC.

## 1.1 Summary of Contributions

More specifically, the main contributions of this dissertation are as follows:

- The development of the first analytical model to compute the first two moments of the service time experienced by a packet when transmitted in a saturated IEEE 802.11 ad hoc network [16, 17];
- Modeling and performance evaluation of the impact of fading channels on single-hop

ad hoc networks operating according to the IEEE 802.11 DCF MAC [18];

- The first analytical model to predict energy consumption in saturated IEEE 802.11 single-hop ad hoc networks under ideal channel conditions [22];

- Development of a new modeling framework for the analytical study of MAC protocols operating in multihop ad hoc networks. The model focuses on the interactions between the PHY and the MAC layers, and on the impact that each node has on the dynamics of every other node in the network—all conveniently conveyed through the use of *interference matrices*. A key feature of the modeling framework is that nodes can be modeled *individually*, i.e., it allows the per-node setup of many layer-specific parameters. Moreover, no spatial probability distribution or special arrangement of nodes is assumed; the framework allows the computation of individual (per-node) performance metrics for any given network topology and radio channel model [19];

- A new analytical model for the binary exponential backoff algorithm of the IEEE 802.11 DCF MAC based on Markov processes. The new model is the first to include the impact of errors in both control and data frames, the carrier-sensing mechanism, and the finite-retry limits of the IEEE 802.11 DCF MAC [20, 21];

- The first analytical modeling of wireless ad hoc networks that considers the impact of realistic antenna-gain patterns on network performance. In particular, the modeling approach allows the study of wireless ad hoc networks in which nodes are equipped with *directional antennas*, i.e., antennas that are able to transmit/receive energy over intended directions [21];

- The first analytical model for wireless ad hoc networks in which nodes are equipped with multiple-input multiple-output (MIMO) radios and use space-time coding (STC), i.e., code design techniques that exploit both temporal and spatial dimensions inherent in the use of multiple spatially-distributed antennas per node [20];

## 1.2 Related Work

The bulk of the analytical modeling of wireless ad hoc networks has concentrated on the analysis of MAC protocols in fully-connected segments of networks (e.g., satellite networks, cellular networks, or single-hop wireless LANs (WLANs)), because they are simpler to analyze than multihop networks. The majority of this work has followed the formalism and assumptions introduced by Abramson [1, 2] for the analysis of the ALOHA protocol, and by Tobagi and Kleinrock [73, 124] for the analysis of the carrier sense multiple access (CSMA) protocol. The model typically adopted assumes that all nodes have infinite buffers and transmissions are scheduled according to *independent* Poisson point processes. This implies that packets which were either inhibited from being transmitted or were unsuccessfully transmitted are rescheduled after a "sufficiently long" randomized time out to preserve the Poisson property (i.e., no correlation between new packet arrivals and their rescheduling). Packet lengths are exponentially distributed and are independently generated at each transmission attempt (including retransmissions). In many cases, acknowledgments are assumed to happen instantaneously or, in cases where propagation delay is taken into account, acknowledgment traffic is simply ignored, and periods of collisions are restricted to the propagation time, after which all other nodes are able to perceive any activity in the channel (through the

single-hop and perfect-channel assumptions). Regarding the quality of the radio links, they are generally considered error free, and the event of unsuccessful transmission is restricted to packet collisions at the receiver. Examples where such assumptions have been made include [9, 31, 47, 48, 69, 72, 78, 101].

Other works consider physical-layer aspects more explicitly within the context of single-hop scenarios. Raychauduri [100] analyzed slotted ALOHA with code division; Gronemeyer and Davis [33] considered spread-spectrum slotted ALOHA with capture due to time of arrival. Musser and Daigle [84] derived the throughput of pure ALOHA with code division. Pursley [93] studied the throughput of frequency-hopped spread-spectrum communications for packet radio networks. In other cases, the error-free link assumption was relaxed and multipath fading channels where considered while preserving other original assumptions (e.g., Poisson scheduling). This is the case in the works by Arnbak and Blitterswijk, who studied the capacity of slotted ALOHA in Rayleigh-fading channels [5].

More recently, with the advent of the IEEE 802.11 standard for WLANs, a significant amount of work has been carried out to provide an analytical model for its operation. However, the vast majority of this effort has considered only single-hop networks under ideal channel conditions [12, 15, 17, 42, 70]. As far as imperfect channel conditions is concerned, Hadzi-Velkov and Spasenovski [60, 61] have investigated the impact of capture on the capacity of the IEEE 802.11 in both Rayleigh- and Rician-fading channels. However, no provision was made to consider a multihop ad hoc network and the interdependencies among the nodes.

Gitman [54] published what is arguably the first paper that actually dealt with a multihop system. Gitman considered a two-hop centralized network consisting of a large number

of terminals communicating with a single station via some repeaters located around the station. Subsequently, Tobagi [120, 121] considered the same topology to compute the network capacity and throughput-delay characteristics of both slotted ALOHA and CSMA. However, it was not until the work by Boorstyn et al. [13] that a methodology for the steady-state throughput analysis of a multihop packet radio network was introduced. Based on assumptions like independent Poisson scheduling at each node, exponentially-distributed packet lengths, zero propagation delay, and instantaneous acknowledgments, Boorstyn et al. were able to represent a CSMA multihop network as a continuous-time Markov chain, with the state at each time being the set of transmitting nodes. This analysis lead to a product-form solution and an iterative procedure was used to obtain the scheduling rates corresponding to given desired link traffic rates. The complexity of the algorithm by Boorstyn et al., although exponential in general, grows quadratically or cubically with the *number of links* for most networks on the order of 100 nodes. Tobagi and Brazio [123] considered the same model and observed that it is applicable to ALOHA and C-BTMA (a variant of BTMA). They also observed that not all schemes could be modeled by simply tracking the set of transmitting nodes. Shepard [107] considered fundamental physical-layer aspects in the modeling of large, dense packet-radio networks. Although Shepard's model considered aspects closer to the underlying physics of radio communications, it did not target the modeling of the interaction among the nodes and their interdependencies.

Chhaya and Gupta provided one of the first analytical models of the IEEE 802.11 DCF that considered a multihop scenario and where both capture and hidden terminals were taken into account [26]. Like prior work, however, all nodes were assumed to transmit inde-

pendently according to some Poisson point process. Moreover, in their numerical results, they considered that *all* individual scheduling processes offered the *same load*, regardless of network topology, therefore ignoring the many interdependencies among nodes and their impact on individual scheduling rates. Subsequently, Wang and Garcia-Luna-Aceves [130] provided a model for the saturation throughput of collision avoidance protocols that included the IEEE 802.11 DCF. Their modeling approach is based on the work by Wu and Varshney [139], in which nodes are spatially distributed according to a two-dimensional Poisson distribution, and two Markov models are used to represent the channel around a node and its activity. To obtain the Markov models, the channel is modeled as a circular region in which nodes within the region can communicate with each other, while weak interactions are assumed with nodes outside this region.

Another important venue of research emerged in the last few years that focuses on the problem of *network capacity*. The main objective of this line of work consists of finding fundamental limits on achievable communication rates in wireless networks. In such a problem formulation, a set of rates between source-destination pairs is called achievable if there exists a network control policy that guarantee those rates. The closure of the set of achievable rates is the capacity region of the network. In their seminal work, Gupta and Kumar [59] considered a joint optimization of transmission powers and schedules, showing that the maximum per-node throughput scales proportionally to $1/\sqrt{n}$, where $n$ is the number of nodes. Subsequent works have studied network capacity from various viewpoints (e.g., [52, 58, 83, 92, 126, 143]) while others considered the joint optimization of resource allocation and scheduling [46, 50], or the optimal cross-layer design of PHY and MAC layers [79, 125].

Despite the undeniable importance of such studies, a gap still remains on the modeling of wireless ad hoc networks under *specific* (optimally designed or not) MAC and PHY layers, in a way that the impact of their interactions and the interdependence among the nodes in a multihop environment are all taken into account in the performance evaluation of each node.

## 1.3 Organization of the Dissertation

Chapter 2 introduces the analytical model to compute the average service time and jitter experienced by a packet when transmitted in a saturated IEEE 802.11 ad hoc network. The model we introduce is general enough to be applied to any IEEE 802.11 wireless ad hoc network where the channel state probabilities driving a node's backoff operation are known. In particular, we apply the model to saturated single-hop ad hoc networks under ideal channel conditions.

In Chapter 3 we introduce aspects of the physical layer directly into the dynamics of the events underneath the operation of the IEEE 802.11 DCF MAC binary exponential backoff algorithm. To show its application, we study the impact of frequency-selective, slowly time-variant Rician fading channels on the performance of saturated IEEE 802.11 single-hop ad hoc networks.

Chapter 4 presents the first analytical model to predict energy consumption in saturated IEEE 802.11 single-hop ad hoc networks under ideal channel conditions. In contrast to previous work that attempted to characterize the energy consumption of IEEE 802.11 cards in isolated, contention-free channels (i.e., single sender/receiver pair), we investigate the extreme opposite case, i.e., when nodes need to contend for channel access under saturation

conditions.

Chapter 5 contains the main contribution of this dissertation, which is the development of a new modeling framework for the analytical study of any medium access control protocol operating in multihop ad hoc networks. The modeling framework focuses on the interactions between the PHH and MAC layers, and on the impact that each node has on the dynamics of every other node in the network—all conveniently conveyed through the use of *interference matrices*.

Chapter 6 shows the application of the general modeling framework developed in Chapter 5 to the modeling of wireless ad hoc networks that operate according to the IEEE 802.11 DCF. In particular, we introduce a new analytical model for the operation of the IEEE 802.11 DCF MAC based on Markov chains. Due to the new Markov model, we extend the performance metrics relative to the IEEE 802.11 and validate our analytical model against numerical results driven from discrete-event simulations.

Chapter 7 contains the analytical modeling of wireless ad hoc networks that considers the impact of realistic antenna-gain patterns on network performance. In particular, we apply the model to the study of ad hoc networks in which nodes are equipped with directional antennas.

In Chapter 8, we present the analytical modeling of wireless ad hoc networks in which nodes are equipped with multiple-input multiple-output (MIMO) radios and use space-time coding (STC) as the signaling technique of choice.

Finally, in Chapter 9, we present the conclusions of this dissertation, and we provide directions for future work.

# Chapter 2

# Delay Analysis of IEEE 802.11 in Single-Hop Ad Hoc Networks

In this chapter, we present an analytical model to compute the average service time and jitter experienced by a packet when transmitted in a saturated IEEE 802.11 ad hoc network. In contrast to traditional work in the literature, in which a distribution is usually fitted or assumed, we use a bottom-up approach and build the first two moments of the service time based on the IEEE 802.11 binary exponential backoff algorithm and the events underneath its operation. Our model is general enough to be applied to any type of IEEE 802.11 wireless ad hoc network where the channel state probabilities driving a node's backoff operation are known. We apply our model to saturated single-hop ad hoc networks under ideal channel conditions. We validate our model through extensive simulations and conduct a performance evaluation of a node's average service time and jitter for both direct sequence and frequency-hopping spread spectrum physical layers.

## 2.1 Introduction

During the past few years we have witnessed an ever-growing interest in wireless technologies and their application to portable devices. As the number of users of such technologies has increased, the demand for real-time traffic and delay-sensitive applications has become more critical. Along the efforts to satisfy such needs, standards for wireless local area networks (WLANs) have been proposed, and the IEEE 802.11 medium access control (MAC) protocol [64] is the *de facto* standard and the most widely used protocol nowadays. In the IEEE 802.11, the main mechanism to access the medium is the distributed coordination function (DCF), which is a random access scheme based on the carrier sense multiple access with collision avoidance (CSMA/CA). The DCF provides two access schemes: the default, called *basic access mechanism*, and an optional, four-way handshake scheme. The standard also defines the optional point coordination function (PCF), which is a centralized MAC protocol that uses a point coordinator to determine which node has the right to transmit. The PCF suppports collision free and time bounded services. However, because the PCF cannot be used in multihop or single-hop ad hoc networks, the DCF is the access network widely assumed, which implies varying delays for all traffic. Curiously, the majority of the work on analyzing the performance of IEEE 802.11 DCF has concentrated on its throughput [12, 15, 26, 130] and not much attention has been given to analyzing its delay.

In this chapter, we provide an analytical model to compute the *average service time* and *jitter* experienced by a packet when transmitted in a saturated IEEE 802.11 ad hoc network. By "service time" we refer to the total time interval between the transmissions of two consecutive data packets from a node's ouput queue (note that we are dealing with saturated

networks). Accordingly, by "jitter" we refer to the variation of the service time with respect to its average value. More specifically, we refer to the square root of the mean squared difference between the service time and its average value, i.e, the *standard deviation*.

In contrast to traditional work in the literature, in which a distribution is usually fitted or assumed [15, 42, 48, 73], we use a bottom-up approach and build the first two moments of a node's service time based on the IEEE 802.11 binary exponential backoff algorithm and the events underneath its operation. The strength of our model relies on the fact that it can be applied to many network scenarios. The key to its successful application is the knowledge of the channel state probabilities driving a node's backoff operation. Here, we apply our model to saturated, single-hop ad hoc networks with ideal channel conditions, operating under the four-way handshake mechanism of the DCF. For this case, the channel state probabilities we obtain are based on the work by Bianchi [12], which provides a set of nonlinear equations that relates a packet's collision probability with its transmission probability (in steady-state). We linearize Bianchi's model and find simple equations to these quantities. The reason for our approximation is twofold: ease of computation and the need to better understand the impact of system parameters on channel and system probabilities (something that is not so clear under a nonlinear system of equations). We validate both our model and the linearized system through extensive simulations and conduct a performance evaluation of a node's average service time and jitter for the direct sequence spread spectrum (DSSS) and frequency-hopping spread spectrum (FHSS) physical layers under the same scenario. We investigate their performance as we vary such parameters as initial contention window size, slot time size, packet size, and maximum backoff stage.

The remainder of the chapter is organized as follows. Section 2.2 briefly reviews the DCF mechanism. Section 2.3 presents our analytical model. Following that, in Section 2.4, we validate our model through simulations. Section 2.5 presents a performance evaluation of both DSSS and FHSS physical layers. In Section 2.6 we present our conclusions.

## 2.2 The IEEE 802.11 Distributed Coordination Function (DCF)

The DCF describes two techniques for packet transmission: the default, a two-way handshake scheme called basic access mechanism, and an optional four-way handshake mechanism. In the basic access mechanism, a node monitors the channel to determine if another node is transmitting before initiating the transmission of a new packet. If the channel is idle for an interval of time that exceeds the *distributed interframe space* (DIFS), the packet is transmitted. Otherwise, the node monitors the channel until it is sensed idle for a DIFS interval, when it then generates a random backoff interval for an additional deferral time before transmitting. This collision avoidance feature of the protocol intends to minimize collisions during contention among multiple nodes. In addition, to avoid channel capture, a node must wait a random backoff time between two consecutive new packet transmissions, even if the medium is sensed idle in the DIFS time.

DCF has a discrete-time backoff timer. The backoff timer is decremented only when the medium is idle and it is frozen when the medium is sensed busy. After a busy period, the decrementing of the backoff timer resumes only after the medium has been free longer than a DIFS period. A transmission takes place when the timer zeros out. The slot size of the backoff timer is denoted by $\sigma$, and equals the time needed by any node to detect the transmission of a

packet by any other node. It is, therefore, dependent on the physical layer and accounts for the propagation delay, the transmit-to-receive turn-around time, and the time to signal the state of the channel to the MAC layer. At each packet transmission, the backoff time is uniformly chosen in the range $(0, W-1)$. The value $W$ is called the *contention window* and depends on the number of failed transmissions for a packet, i.e., for each packet queued for transmission, the contention window $W$ takes an initial value $W_{\min}$ that doubles after each unsuccessful packet transmission, up to a maximum of $W_{\max}$ (the values of $W_{\min}$ and $W_{\max}$ are physical-layer specific). The contention window remains at $W_{\max}$ for the remaining attempts. This is the so-called exponential backoff scheme. In the sequel, each attempt to transmit a packet during the exponential backoff will be referred to as a *backoff stage*. An ACK is transmitted by the destination node to signal the successful packet reception. The ACK is immediately transmitted at the end of the packet, after a period of time called *short interframe space* (SIFS). If the transmitting node does not receive the ACK within a specified timeout, or if it detects the transmission of a different packet on the channel, it reschedules the packet transmission according to the given backoff rules. Figure 2.1(a) illustrates the basic access mechanism.

The four-way handshake mechanism involves the transmission of the *request-to-send* (RTS) and *clear-to-send* (CTS) control frames prior to the transmission of the actual data frame. A successful exchange of RTS and CTS frames attempts to reserve the channel for the time duration needed to transfer the data frame under consideration. The rules for the transmission of an RTS frame are the same as those for a data frame under the basic access scheme. After receiving an RTS frame, the receiver responds with a CTS frame after a SIFS. After the successful exchange of RTS and CTS frames, the data frame can be sent

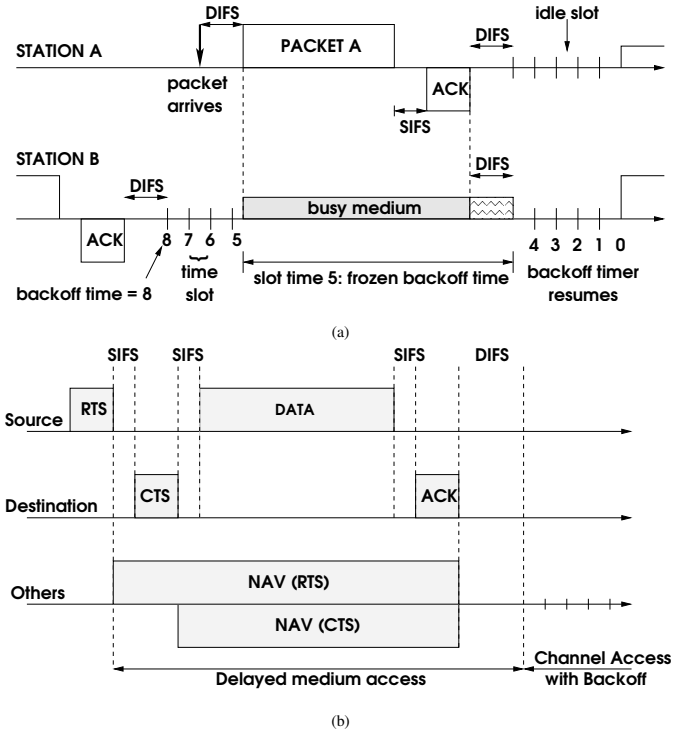


**Figure 2.1**: IEEE 802.11 access methods: (a) Basic Access. (b) RTS/CTS.

by the transmitter after waiting for a SIFS interval. In case a CTS frame is not received within a predetermined time interval, the RTS is retransmitted following the backoff rules as specified in the basic access procedures described above. The frames RTS and CTS carry the information of the length of the packet to be transmitted. This information can be read by any listening node, which is then able to update a network allocation vector (NAV) containing the information of the period of time in which the channel will remain busy. Therefore, when a node is hidden from either the transmitting or the receiving node, by detecting just one frame among the RTS and CTS frames, it can suitably delay further transmissions to try to avoid collisions. Figure 2.1(b) illustrates the four-way handshake mechanism, which we simply call the RTS/CTS mechanism.

## 2.3 Analytical Model

In this Section, we present the analytical model for the average service time and jitter experienced by a packet in a saturated IEEE 802.11 ad hoc network. For this purpose, we first derive the average service time and jitter as functions of the channel state probabilities. Following that, we present the computation of the channel state probabilities for the case of a single-hop ad hoc network under ideal channel conditions.

### 2.3.1 Service Time Characterization

As mentioned in Section 2.2, once a node goes to backoff, its backoff time counter decrements according to the perceived state of the channel. If the channel is sensed idle, the backoff time counter is decremented. Otherwise, it is frozen, staying in this state until the channel is sensed idle again for a time interval that lasts more than a DIFS interval, at which time the decrementing operation is resumed. While the backoff timer is frozen, only two mutually exclusive events can happen in the channel: either a successful transmission takes place or a packet collision occurs. Therefore, if we denote the three possible events a node can sense during its backoff by $E_s = \{\text{successful transmission}\}$, $E_i = \{\text{idle channel}\}$, and $E_c = \{\text{collision}\}$, each of the time intervals between two consecutive backoff counter decrements, which we call "backoff steps", will contain one of these three mutually exclusive events. In other words, during a node's backoff, the $j$-th "backoff step" will result in either a collision, a transmission, or the channel being sensed idle. We assume that events in successive backoff steps are independent, which is a reasonable assumption if the WLAN is relatively large and if the time a node spends on collision resolution is about the same as the time the

channel is sensed bus due to collisions by noncolliding nodes. In the DCF, a node finds out that a collision has taken place if it does not receive the acknowledgment to its transmission after a certain timeout (the ACK_Timeout in the basic access mechanism and the CTS_Timeout in the RTS/CTS mechanism). In other words, if a collision happens in a backoff step, the colliding nodes are assumed to go through the collision resolution process in this *same* backoff step and, therefore, can be ready for transmission in the following backoff step. This way, we avoid dependencies on the number of colliding nodes at previous backoff steps.

Given the above considerations, let $k$ denote the backoff stage at which a specific node is at a certain instant of time, and let $n_k$ be the number of backoff time slots randomly chosen at the $k$-th stage. Assuming that the events $E_i$, $E_s$, and $E_c$ have probabilities $p_s = P\{E_s\}$, $p_i = P\{E_i\}$, and $p_c = P\{E_c\}$, respectively, and given that these events are independent and mutually exclusive at each backoff step, then the probability that in $n_k$ slots we have $r_i$ "idle slots", $r_c$ "collision slots", and $r_c$ "successful slots" is given by the multinomial probability distribution

$$P\{\mathbf{r} \,|\, n_k, \mathbf{p}\} = \frac{n_k}{r_i!\, r_c!\, r_s!}\, p_i^{r_i} p_c^{r_c} p_s^{r_s}, \tag{2.1}$$

where $\mathbf{r} = [r_i \; r_c \; r_s]^T$, $\mathbf{p} = [p_i \; p_c \; p_s]^T$, $p_i + p_c + p_s = 1$, and $r_i + r_c + r_s = n_k$. Let $\mathbf{t} = [\sigma \; t_c \; t_s]^T$, where $\sigma$ is the time used when the channel is sensed idle (i.e., one backoff slot), $t_s$ is the average time the channel is sensed busy due to a successful transmission, and $t_c$ is the average time the channel is sensed busy due to a collision in the channel. If we denote by $T_B^k(\mathbf{r}; n_k)$ the total backoff time spent at the $k\text{-th}$ backoff stage when $r_i$ slots are idle, $r_c$ slots have collisions, and $r_s$ slots have successful transmissions within the randomly chosen

$n_k$ slots, then

$$T_B^k(\mathbf{r}; n_k) = \mathbf{r}^T \mathbf{t} = \sigma r_i + t_c r_c + t_s r_s. \tag{2.2}$$

Note that the event $E = \{\, r_i$ idle slots, $r_c$ collision slots, $r_s$ successful slots $\mid n_k\}$ is the same as the event $E' = \{$backoff timer zeros out after $r_i\sigma + r_c t_c + r_s t_s$ time slots $\mid n_k\}$. Therefore,

$$P\left\{\mathbf{r}^T \mathbf{t} \,|\, n_k, \mathbf{p}\right\} = P\{\mathbf{r} \,|\, n_k, \mathbf{p}\}. \tag{2.3}$$

From the above results, the average time a node spends at the $k$-th backoff stage when $n_k$ backoff steps are chosen is simply

$$\begin{aligned}\overline{T}_B^k(n_k) &= E\left\{T_B^k(\mathbf{r}; n_k) \,|\, n_k\right\} = E\left\{\mathbf{r}^T \mathbf{t} \,|\, n_k\right\} = E\left\{\mathbf{r}^T \,|\, n_k\right\} \mathbf{t} = [n_k p_i \; n_k p_c \; n_k p_s]^T \mathbf{t} \\ &= n_k(\sigma p_i + t_c p_c + t_s p_s),\end{aligned} \tag{2.4}$$

where $\overline{T}_B^k(n_k)$ indicates that $E\{T_B^k(\mathbf{r}; n_k) \,|\, n_k\}$ is a function of the randomly chosen value $n_k$ at the $k$-th backoff stage. We can finally compute the average backoff time $\overline{T}_B^k$ at the $k$-th stage by averaging over $n_k$ as follows:

$$\overline{T}_B^k = \sum_{n_k=0}^{W_k-1} \overline{T}_B^k(n_k) P\{n_k\} = \sum_{n_k=0}^{W_k-1} \frac{n_k(\sigma p_i + t_c p_c + t_s p_s)}{W_k} = \frac{\alpha(W_k - 1)}{2}, \tag{2.5}$$

where $\alpha = \sigma p_i + t_c p_c + t_s p_s$. This last result is quite intuitive: it simply states that the average time a node spends at the $k$-th backoff stage is nothing but the product of the average number of backoff steps, $(W_k - 1)/2$, times the average backoff step size $\alpha$.

We are now able to consider the more general case of the binary exponential backoff algorithm. Let $\mathbf{R}_k$ be a $3 \times k$ matrix whose columns are the $k$ "counting events" $\mathbf{r}_i$, $i = 1, 2, \ldots, k$ of each backoff stage up to the $k$-th stage, i.e, $\mathbf{R}_k = [\mathbf{r}_1 \; \mathbf{r}_2 \ldots \mathbf{r}_k]$. We are

interested in computing $P\{\mathbf{R}_k \,|\, \mathbf{n}_k\}$, where $\mathbf{n}_k = [n_1\ n_2\ \ldots\ n_k]^T$ is a column vector of the number of time slots chosen in each of the $k$ stages. By our independence assumption, the events that happen while a node is in its $(k-1)$-th backoff stage are independent of the events that happen while the node is in the $k$-th stage. Therefore,

$$\begin{aligned} P\{\mathbf{R}_k \,|\, \mathbf{n}_k\} &= P\{\mathbf{r}_1 \,|\, \mathbf{n}_k\} \cdot P\{\mathbf{r}_2 \,|\, \mathbf{n}_k\} \cdot \ldots \cdot P\{\mathbf{r}_k \,|\, \mathbf{n}_k\} \\ &= P\{\mathbf{r}_1 \,|\, n_1\} \cdot P\{\mathbf{r}_2 \,|\, n_2\} \cdot \ldots \cdot P\{\mathbf{r}_k \,|\, n_k\}, \end{aligned} \tag{2.6}$$

where the last equality expresses the independence, among stages, on the randomly-chosen number of backoff steps. Given $\mathbf{R}_k$ and $\mathbf{n}_k$, the total backoff time can be computed as follows:

$$T_B(\mathbf{R}_k; \mathbf{n}_k) = \sum_{i=1}^{k-1} \left(\mathbf{r}_i^T \mathbf{t} + t_c\right) + \mathbf{r}_k^T \mathbf{t} = \sum_{i=1}^{k} \mathbf{r}_i^T \mathbf{t} + (k-1)t_c, \tag{2.7}$$

where $t_c$ accounts for the time a node spends on collision resolution (according to our previous remark). We can now compute the average time it takes to successfully transmit a packet after $k$ backoff stages:

$$\begin{aligned} \overline{T}_B(\mathbf{n}_k) = E\{T_B(\mathbf{R}_k; \mathbf{n}_k) \,|\, \mathbf{n}_k\} &= \sum_{\mathbf{R}_k} \left[\sum_{i=1}^{k} \mathbf{r}_i^T \mathbf{t} + (k-1)t_c\right] P\{\mathbf{R}_k \,|\, \mathbf{n}_k\} \\ &= \sum_{i=1}^{k} \overline{T}_B(n_i) + (k-1)t_c. \end{aligned} \tag{2.8}$$

By averaging over $\mathbf{n}_k$, and observing that the selected number of backoff steps at a specific backoff stage is independent of the selected number of backoff steps at previous stages, we have that

$$\begin{aligned} \overline{T}_B(k) = E\{\overline{T}_B(\mathbf{n}_k)\} = \sum_{\mathbf{n}_k} \overline{T}_B(\mathbf{n}_k) P\{\mathbf{n}_k\} &= \sum_{\mathbf{n}_k} \overline{T}_B(\mathbf{n}_k) \prod_{i=1}^{k} P\{n_i\} \\ = \sum_{\mathbf{n}_k} \left[\sum_{i=1}^{k} \overline{T}_B(n_i) + (k-1)t_c\right] \prod_{i=1}^{k} P\{n_i\} &= \sum_{i=1}^{k} \overline{T}_B^i + (k-1)t_c, \end{aligned} \tag{2.9}$$

where $\overline{T}_B^i$ is given by Eq.(2.5). This last result simply tells us that the backoff time is a non-linear function of the discrete random variable $K$ of the number of backoff stages a node has to go through before transmitting a packet successfully. Consequently, the backoff time probability distribution is the same as the probability distribution of the number of backoff stages $K$[1], which in turn is directly related to the probability that a packet is succesfully transmitted at the end of the $k\text{-th}$ stage. Therefore, if we let $q_k$ be the probability of success that a packet experiences when it is transmitted at the end of the $k$-th backoff stage, and if we make the reasonable assumption that $P\{$packet collides at the $k\text{-th}$ stage $|$ packet collided at the 1st, 2nd, $\ldots$, $(k-1)\text{-th}$ stages$\}$ = $P\{$packet collides at the $k\text{-th}$ stage$\}$ then,

$$P\{K=k\} = \left[\prod_{i=1}^{k-1}(1-q_i)\right] q_k. \tag{2.10}$$

Note that if the probabilities $q_i$ are independent of the backoff stage and constant, i.e., $q_i = q,\ \forall\, i \in \mathbb{N}$, then we simply have the geometric distribution

$$P\{K=k\} = (1-q)^{k-1}q. \tag{2.11}$$

For simplicity, let us assume from now on that $q_i = q,\ \forall\, i \in \mathbb{N}$. In fact, very accurate throughput results were obtained by Bianchi [12] by assuming a constant and independent collision probability. Given that, we can now compute the first two moments of the backoff time $T_B(k)$. Let us start with the average backoff time $\overline{T}_B$. From Eq. (2.9), we have

$$\begin{aligned}\overline{T}_B = E\{\overline{T}_B(k)\} &= \sum_{k=1}^{\infty}\overline{T}_B(k)P\{K=k\} = \sum_{k=1}^{\infty}\left[\left(\sum_{i=1}^{k}\overline{T}_B^i\right) + (k-1)t_c\right](1-q)^{k-1}q \\ &= \sum_{k=1}^{\infty}\left(\sum_{i=1}^{k}\frac{\alpha}{2}W_i\right)(1-q)^{k-1}q - \frac{\alpha}{2q} + \frac{(1-q)}{q}t_c. \end{aligned}\tag{2.12}$$

[1]In one-to-one mappings of discrete random variables, if $\mathbf{y} = g(\mathbf{x})$ then $P\{\mathbf{y}=y\} = P\{\mathbf{x}=x\}$ [89].

To compute the first term of Eq. (2.12), we first observe that

$$W_i = \begin{cases} 2^{i-1}W_{\min} & \text{if } 1 \le i \le m \\ \\ 2^m W_{\min} & \text{if } m < i \end{cases} \tag{2.13}$$

where $m$ is the "maximum backoff stage", i.e., the value such that $W_{\max} = 2^m W_{\min}$. We can now compute the remaining summation in Eq. (2.12) by splitting it into two terms as follows:

$$\sum_{k=1}^{\infty}\left(\sum_{i=1}^{k}\frac{\alpha}{2}W_i\right)(1-q)^{k-1}q = \sum_{k=1}^{m}\left(\sum_{i=1}^{k}\frac{\alpha}{2}W_i\right)(1-q)^{k-1}q + \\ + \sum_{k=m+1}^{\infty}\left(\sum_{i=1}^{k}\frac{\alpha}{2}W_i\right)(1-q)^{k-1}q = S_1 + S_2. \tag{2.14}$$

For $S_1$ we have:

$$S_1 = \sum_{k=1}^{m}\left(\sum_{i=1}^{k}\frac{\alpha}{2}W_i\right)(1-q)^{k-1}q = \frac{\alpha W_{\min}}{2}\left\{2q\left[\frac{1-[2(1-q)]^m}{1-2(1-q)}\right] + (1-q)^m - 1\right\}. \tag{2.15}$$

To find $S_2$, we notice first that, for $k = m+1$,

$$\sum_{i=1}^{k}\frac{\alpha W_i}{2} = \frac{\alpha W_{\min}}{2}\sum_{i=1}^{m+1}2^{i-1} = \frac{\alpha W_{\min}}{2}\left(2^{m+1}-1\right). \tag{2.16}$$

Hence, for $k = m+2$,

$$\sum_{i=1}^{k}\frac{\alpha W_i}{2} = \frac{\alpha W_{\min}}{2}\left[\sum_{i=1}^{m+1}2^{i-1} + \sum_{i=m+2}^{m+2}2^m\right] = \frac{\alpha W_{\min}}{2}\left[\left(2^{m+1}-1\right) + 2^m\right]. \tag{2.17}$$

In general, for $k = m+\gamma$,

$$\sum_{i=1}^{k}\frac{\alpha W_i}{2} = \frac{\alpha W_{\min}}{2}\left[\sum_{i=1}^{m+1}2^{i-1} + \sum_{i=m+2}^{m+\gamma}2^m\right] = \frac{\alpha W_{\min}}{2}\left[\left(2^{m+1}-1\right) + (\gamma-1)\cdot 2^m\right]. \tag{2.18}$$

Making the change of variable $j = k - (m+1)$ in $S_2$, we have:

$$\begin{aligned} S_2 &= \frac{\alpha W_{\min}}{2} \sum_{j=0}^{\infty} \left[ \left(2^{m+1} - 1\right) + j \cdot 2^m \right] (1-q)^{j+m} q \\ &= \frac{\alpha W_{\min}}{2} \left[ \left(2^{m+1} - 1\right) (1-q)^m + \frac{2^m (1-q)^{m+1}}{q} \right]. \end{aligned} \tag{2.19}$$

By adding $S_1$ to $S_2$ we obtain that the average backoff time equals

$$\overline{T}_B = \frac{\alpha(W_{\min}\beta - 1)}{2q} + \frac{(1-q)}{q}\, t_c, \tag{2.20}$$

where

$$\beta = \frac{q - 2^m (1-q)^{m+1}}{1 - 2(1-q)}. \tag{2.21}$$

Therefore, the average time a packet spends in backoff is simply the average number of backoff stages it goes through $(1/q)$ times the average time it spends in each backoff stage, added to the respective average time spent on collision resolution. Note here that the term $W_{\min}\beta$ works as an "effective window size", scaling the initial contention window size according to the maximum backoff stage $m$ and the success probability $q$. In the specific case in which the contention window is constant at every backoff stage, i.e., $\overline{T}_B^i = T^* = \alpha(W^* - 1)/2$, $\forall k \in \mathbb{N}$, $\overline{T}_B(k)$ is simply $\overline{T}_B(k) = kT^* + (k-1)t_c$. In this case, the average backoff time reduces to

$$\overline{T}_B = \frac{\alpha(W^* - 1)}{2q} + \frac{(1-q)}{q}\, t_c \tag{2.22}$$

If we make $m = 0$ in Eq. (2.21), i.e., if we fix the contention window size to the initial contention window size, we have

$$\overline{T}_B = \frac{\alpha(W_{\min} - 1)}{2q} + \frac{(1-q)}{q}\, t_c. \tag{2.23}$$

In the same way, if the contention window size is constant at every stage $k$, the variance of the total backoff time is given by

$$\text{Var}\left\{\overline{T}_B(k)\right\} = \text{Var}\left\{\sum_{i=1}^{k} \overline{T}_B^i + (k-1)t_c\right\} = \text{Var}\left\{kT^* + (k-1)t_c\right\} = (T^* + t_c)^2 \frac{(1-q)}{q^2}$$
$$= \left[\frac{\alpha(W^* - 1)}{2} + t_c\right]^2 \frac{(1-q)}{q^2}. \tag{2.24}$$

In the case of the binary exponential backoff algorithm, we need to apply the same techniques we applied before to squared and cross-product terms. For conciseness, we omit here the intermediate steps and give the final expression obtained after some algebra:

$$\text{Var}\left\{\overline{T}_B(k)\right\} = \left[\frac{\alpha(W_{\min}\gamma - 1)}{2} + t_c\right]^2 \frac{(1-q)}{q^2}, \tag{2.25}$$

where

$$\gamma = \frac{\left\{[2q^2 - 4q + 1 - m(-1+2q)q][2(1-q)]^m + 2q^2\right\}}{(-1+2q)^2},$$

and, if we make $m = 0$ we obtain Eq. (2.24). Given the backoff time characterization, the *average service time* $\overline{T}$ equals

$$\overline{T} = \overline{T}_B + T_s, \tag{2.26}$$

where $T_s$ is the time to successfully transmit a packet at the end of the backoff operation. Because $T_s$ is a constant,

$$\text{Var}\{\overline{T}(k)\} = \text{Var}\{\overline{T}_B(k)\}. \tag{2.27}$$

Note that the service time distribution is the same as that of the backoff time, which, in this case, is a non-linear function of a geometric random variable with parameter $q$.

### 2.3.2 Channel Probabilities

The model we have just presented is applicable whenever the channel state probabilities $\mathbf{p} = [p_i\ p_c\ p_s]^T$ driving a node's backoff operation are known. In this Section, we compute the values of $\mathbf{p}$ for a saturated, single-hop ad hoc network under ideal channel conditions. For this purpose, we rely on the work by Bianchi [12], which provides a model to evaluate the saturation throughput of the IEEE 802.11 MAC protocol under the hypothesis of ideal channel conditions (i.e., no hidden terminals and capture). Following Bianchi's analysis, we also assume a fixed number of nodes, with each node always having a packet available for transmission, i.e., the transmission queue of each node is assumed to be always nonempty. The key approximation of his model, which we adopt here too, is that each packet, at each transmission attempt, collides with constant and independent probability $p = 1 - q$ regardless of the number of retransmissions suffered[2]. This probability is called the *conditional collision probability*, meaning that this is the probability of a collision experienced by a packet being transmitted on the channel. Bianchi modeled the stochastic process representing the backoff time counter for a given node as a bidimensional discrete-time Markov process. According to his development, the probability $\tau$ that a node transmits in a randomly chosen slot time is [12]

$$\tau = \frac{2(1-2p)}{(1-2p)(W_{\min}+1) + pW_{\min}(1-(2p)^m)}, \tag{2.28}$$

which is a function of the conditional collision probability $p$, still unknown. To find the value of $p$, it is sufficient to note that the probability $p$ that a transmitted packet faces a collision in the channel is the probability that at least one of the $n-1$ remaining nodes transmit in a given time slot. By the independence assumption given above, each transmission experiences the

[2]Note that the probability $q$ is the same as the one we used in Section 2.3.1.

system in the same state, i.e., in steady state. Each remaining node transmits a packet with probability $\tau$ in steady state. Therefore,

$$p = 1 - (1 - \tau)^{n-1}. \tag{2.29}$$

Equations (2.28) and (2.29) form a nonlinear system in the two unknowns $\tau$ and $p$ that can be solved using numerical techniques. In fact, Bianchi showed [12] that this system has a unique solution. To make things simpler, and to better understand the effect of different parameters on these two probabilities, we will find an approximate solution to this nonlinear system by linearizing both equations. For this purpose, let $\gamma = 1 - \tau$ be the probability that a node *does not* transmit in a randomly chosen slot time, i.e.,

$$\gamma = \frac{(1-2p)(W_{\min}-1) + pW_{\min}(1-(2p)^m)}{(1-2p)(W_{\min}+1) + pW_{\min}(1-(2p)^m)}. \tag{2.30}$$

Given the continuity of both $\gamma(p)$ and its derivatives[3] in the interval $p \in (0,1)$, the Taylor series expansion of $\gamma(p)$ at $p = 0$ is given by

$$\gamma(p) = \frac{W_{\min}-1}{W_{\min}+1} + \frac{2W_{\min}}{(W_{\min}+1)^2}p + O(p^2), \tag{2.31}$$

where $O(p^2)$ accounts for the second and high order terms in the Taylor series expansion. Hence, a first order approximation of $\gamma(p)$ is simply

$$\gamma(p) = \frac{W_{\min}-1}{W_{\min}+1} + \frac{2W_{\min}}{(W_{\min}+1)^2}p, \tag{2.32}$$

which, in terms of $q = 1 - p$ becomes

$$\begin{aligned} \gamma(q) &= \frac{-2W_{\min}}{(W_{\min}+1)^2}\, q + \frac{W_{\min}^2 + 2W_{\min} - 1}{(W_{\min}+1)^2} \\ &\approx \frac{-2W_{\min}}{(W_{\min}+1)^2}\, q + 1. \end{aligned} \tag{2.33}$$

[3]Continuity with respect to the critical value $p = 1/2$ can be shown by simply rewriting $\gamma(p)$ in the same way as it was done for $\tau(p)$ in [12].

Given that $\tau = 1 - \gamma$, we have

$$\tau(q) = \frac{2W_{\min}}{(W_{\min}+1)^2}\, q = \frac{2W_{\min}}{(W_{\min}+1)^2}\,(1-p). \tag{2.34}$$

Figure 2.2 shows the comparison between the nonlinear relationship of Eq. (2.28) with the linear approximation of Eq. (2.34) for DSSS parameters ($W_{\min} = 32$ and $m = 5$). The error in the approximation becomes more significant as the collision probability grows. However, given the range at which $\tau$ is varying, the error tends to be very small. In Section 2.5 we evaluate the performance of our approximation.

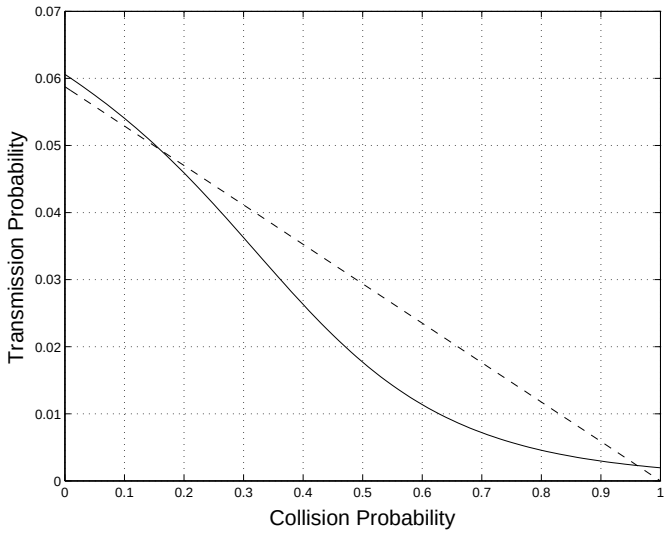


**Figure 2.2**: Transmission probability $\tau$: comparison of nonlinear relationship versus linear approximation.

We can now substitute our approximation of $\tau(q)$ in the equation that relates the probability that *no* node is transmitting at any randomly chosen slot time, i.e., $q = (1-\tau)^{n-1}$. Because $W_{\min}$ can assume values such as 16 or 32 (depending on the physical layer of choice, according to the IEEE 802.11 specifications), we have that $2W_{\min}/(W_{\min}+1)^2 << 1$. Also,

since $0 \leq q \leq 1$, a first-order approximation of $q = (1-\tau)^{n-1}$ is simply given by

$$q = \left[1 - \frac{2W_{\min}}{(W_{\min}+1)^2} q\right]^{n-1} \approx 1 - \frac{2(n-1)W_{\min}}{(W_{\min}+1)^2}\, q$$
$$\approx \frac{(W_{\min}+1)^2}{(W_{\min}+1)^2 + 2(n-1)W_{\min}}, \tag{2.35}$$

which leads to the following approximation for the collision probability $p$ :

$$p = \frac{2W_{\min}(n-1)}{(W_{\min}+1)^2 + 2W_{\min}(n-1)}. \tag{2.36}$$

Equations (2.34) and (2.36) clearly show the decoupling we have achieved by linearizing the original system of equations. Figure 2.3 shows the conditional collision probability $p$ as a function of the number of nodes $n$ and the minimum contention window $W_{\min}$. As we can see, for the current parameters of the IEEE 802.11 protocol, i.e., $W_{\min} = 16$ (FSSS) and $W_{\min} = 32$ (DSSS), the collision probability is higher than 0.5 if the number of nodes in the wireless LAN exceeds 20 nodes.

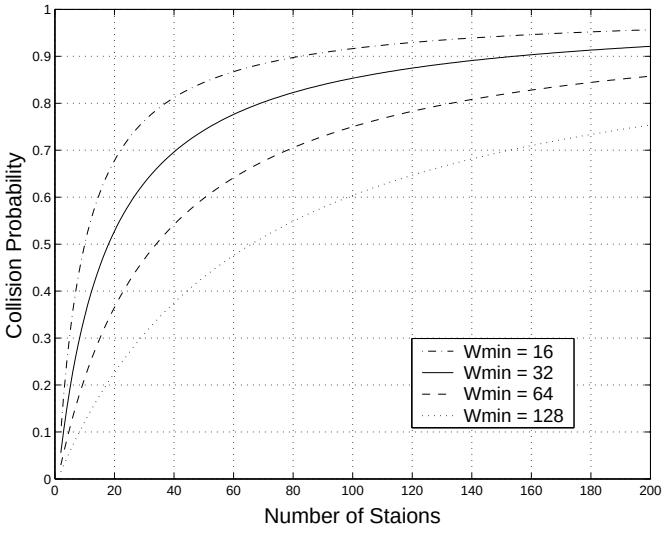


**Figure 2.3**: Collision probability as a function of number of nodes in the network.

We can now turn to the problem of finding the conditional channel probabilities,

represented here by the vector $\mathbf{p}$. For this purpose, let $P_{tr}$ be the probability that there is at least one transmission in the considered time slot. Because we are considering the events experienced by a node during its backoff period, only the remaining $n-1$ nodes can be contending for channel access. Therefore, because each of the remaining $n-1$ nodes transmits a packet with probability $\tau$ at steady state, we have

$$P_{tr} = 1 - (1-\tau)^{n-1}. \tag{2.37}$$

The probability $P_{suc}$ that a transmission occurring on the channel is successful is given by the probability that exactly one node transmits on the channel, conditioned on the fact that at least one node transmits, i.e.,

$$P_{suc} = \frac{\binom{n-1}{1}\tau(1-\tau)^{n-2}}{P_{tr}} = \frac{(n-1)\tau(1-\tau)^{n-2}}{1-(1-\tau)^{n-1}}. \tag{2.38}$$

Therefore, the probability that a successful transmission occurs in a given time slot is $p_s = P\{E_s\} = P_{tr}P_{suc}$. Accordingly, $p_i = P\{E_i\} = 1 - P_{tr}$ and $p_c = P\{E_c\} = P_{tr}(1 - P_{suc})$. Figure 2.4 shows these three probabilities as a function of $n$, the number of nodes. Finally, for the time intervals $t_s$ and $t_c$, we follow the definitions given by Bianchi [12], where[4]

$$t_s = \text{RTS} + \text{SIFS} + \tau + \text{CTS} + \text{SIFS} + \tau + \text{H} + E\{P\} + \text{SIFS} + \tau + \text{ACK} + \\ + \text{DIFS} + \tau, \tag{2.39}$$

$$t_c = \text{RTS} + \text{DIFS} + \tau, \tag{2.40}$$

where $E\{P\} = P$ for fixed packet sizes.

[4]It is shown in [48] that, for correct floor acquisition to occur, CTS packets have to be at least the same size as RTS packets plus the turnaround time plus twice the propagation delay, which does not happen in the IEEE 802.11 protocol. We will ignore this and consider that collisions involve RTS packets only.

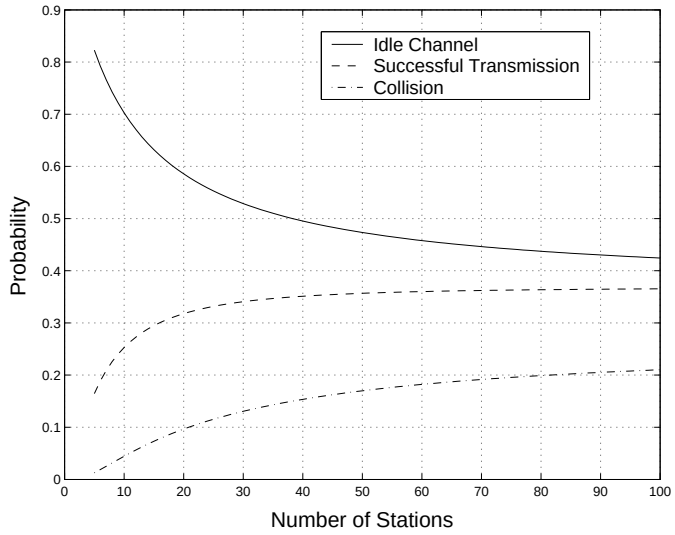


**Figure 2.4**: Conditional channel probabilities.

## 2.4 Model Validation

In this section we evaluate the accuracy of our model in predicting the first two moments of a node's service time in a single-hop IEEE 802.11 WLAN. For this purpose, we use the simulator Ns-2 [87] to run simulations on network sizes varying from 8 to 56 nodes (in steps of 8). All nodes transmit to some other node in the network according to the same CBR source rate with fixed packet sizes of 1500 bytes (IP packet). We pick a source rate high enough to saturate the nodes for each network size. Nodes are randomly placed in an area of $20 \times 20$ meters and have no mobility. Each run corresponds to 6 minutes of data traffic. We trace each node in the network and compute both the mean and variance of its service time. We repeat the experiment for 20 different seeds. We do that not just for statistical reasons, but also because of the *fairness problem* inherent in the IEEE 802.11 DCF. As already reported in the literature [10, 130], the available bandwidth is not equally shared among competing nodes under the IEEE 802.11 protocol. We noticed the same behavior during our simulations in some

**Table 2.1**: IEEE 802.11 Physical Layer Parameters Used in Simulations.

| | DSSS | FHSS |
|---|---|---|
| $W_{\min}$ | 32 | 16 |
| $W_{\max}$ | 1024 | 1024 |
| MAC Header | 34 bytes | 34 bytes |
| ACK | 38 bytes | 30 bytes |
| CTS | 38 bytes | 30 bytes |
| RTS | 44 bytes | 36 bytes |
| Slot Time | 20 $\mu$sec | 50 $\mu$sec |
| SIFS | 10 $\mu$sec | 28 $\mu$sec |
| DIFS | 50 $\mu$sec | 128 $\mu$sec |
| ACK_Timeout | 212 $\mu$sec | — |
| CTS_Timeout | 348 $\mu$sec | — |

of the randomly-chosen topologies, where some nodes were more successful in acquiring the channel than others. Regarding the physical layer, we use Direct-Sequence Spread Spectrum (DSSS) with a raw bit rate of 2Mbps. Table 2.1 summarizes the parameters used for our simulations. FHSS standard-specific paramaters are listed for completeness (ACK_Timeout and CTS_Timeout are not specified in the standard). We compute the average service time and jitter of each node in each run, and take the average over all nodes in the network. We repeat this computation for all 20 seeds and report the results averaged over the 20 seeds. Figure 2.5 shows the numerical results for the average service time for both simulations and analytical models (linear and nonlinear). As we can see, our analytical model performs quite well, especially in small to medium-size networks, providing us with an upper bound on the average service time. Regarding the increasing discrepancy observed as the number of nodes grows, we note two main reasons. First, in our analytical model, a packet can backoff infinitely in time, whereas in simulations (as in the standard) retry counters help the MAC determine when it is no longer worth it to continue attempting to transmit a packet. Therefore, only packets

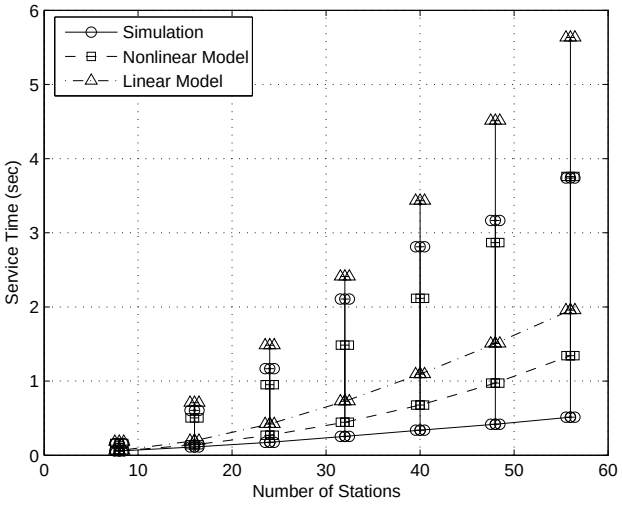


**Figure 2.5**: Average service time as the number of nodes increases. Error bars show the standard deviation (jitter) in both simulations and analytical models.

that were not discarded had their service time considered in the statistics. The second reason stems from our assumption that periods of collision experienced by colliding nodes have the same duration as the periods in which the channel is sensed busy by noncolliding nodes. As mentioned before, this is not necessarily true, because the CTS timeout is usually longer than the assumed $t_c$, which lasts RTS + DIFS + $\tau$ $\mu$sec for noncolliding nodes. Fortunately, this discrepancy is practically irrelevant if we note the high variance (jitter) of the service time as the number of nodes grows, and the fact that the average service time predicted by both linear and nonlinear models are within standard deviation of simulation results, as shown in Figure 2.5. Another important result is shown in Figure 2.6, where we can see how accurate our analytical model is in predicting the magnitude of the jitter experienced by each node in the network. The similarity is quite striking, with the jitter predicted by the nonlinear model slightly less than that in simulations. From Figures 2.5, and 2.6, we see that the linear model

is a more conservative model, providing higher values for both delay and jitter. This is due to the fact that, for the same values of $n$ and $W_{\min}$, the probability of having transmissions and collisions in the channel during a node's backoff time is usually higher for the linear model than for the nonlinear model. Consequently, the delay and jitter are also higher.

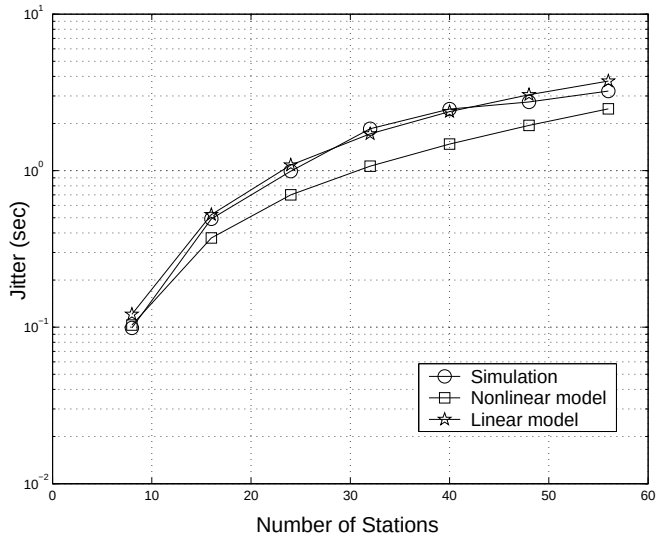


**Figure 2.6**: Jitter magnitude as the number of nodes in the network increases.

## 2.5 Performance Evaluation

This section addresses the impact of some of the IEEE 802.11 parameters on the average service time and jitter for both DSSS and FHSS physical layers, based on the model we developed in Section 2.3 for saturated networks. Unless stated otherwise, the parameters used are the ones in Table 2.1. First, we consider the impact of the initial contention window size on the average service time and jitter. Figures 2.7(a) and 2.7(c) show the results for the DSSS physical layer and Figures 2.7(b) and 2.7(d) show the results for the FHSS physical layer. From the results, we see that, overall, DSSS performs better than FHSS in both average

service time and jitter. This can certainly be explained by the significant sizes of the SIFS and DIFS time intervals specified for the FHSS, as shown in Table 2.1. The length of the DIFS and SIFS time intervals affect the average time a node stays in backoff, leading to significant higher average service time and jitter. In particular, if we look at the performance for their real parameters ($W_{\min} = 32$ for DSSS and $W_{\min} = 16$ for FHSS), we see that FHSS average service time is, roughly speaking, twice the values of the DSSS physical layer, specially for large networks. DSSS and FHSS exhibit the same behavior in terms of jitter. An important observation to be made here is that, as far as delay and jitter in saturated networks is concerned, increasing the initial contention window size improves the performance of the system in both physical layers. Figures 2.7(e), 2.7(f), 2.7(g), and 2.7(d) show very clearly the impact of the initial contention window size on service time and jitter. The results refer to window sizes of 8, 16, 32, 64, 128, 512, and 1024. Both metrics drop dramatically as we increase the initial contention window size to values such as 512 or 1024. For small to medium-size networks (around 20 nodes) the jitter is very small and the average service time is practically constant for window sizes higher than 128. For small values of window sizes, DSSS still performs better than FHSS. Their performance becomes similar when window sizes are bigger than 128. Such results can be easily explained by observing Figure 2.3, which clearly shows that, as the minimum contention window size increases, the collision probability decreases. Consequently, transmitted packets are more likely to be successful.

Figures 2.8(a), 2.8(b), 2.8(c), and 2.8(d) show the performance of DSSS and FHSS physical layers for packet sizes of 32, 64, 128, 512, and 1024 bytes (IP packets). We see again that DSSS outperforms FHSS in both average service time and jitter. From the graphs, we

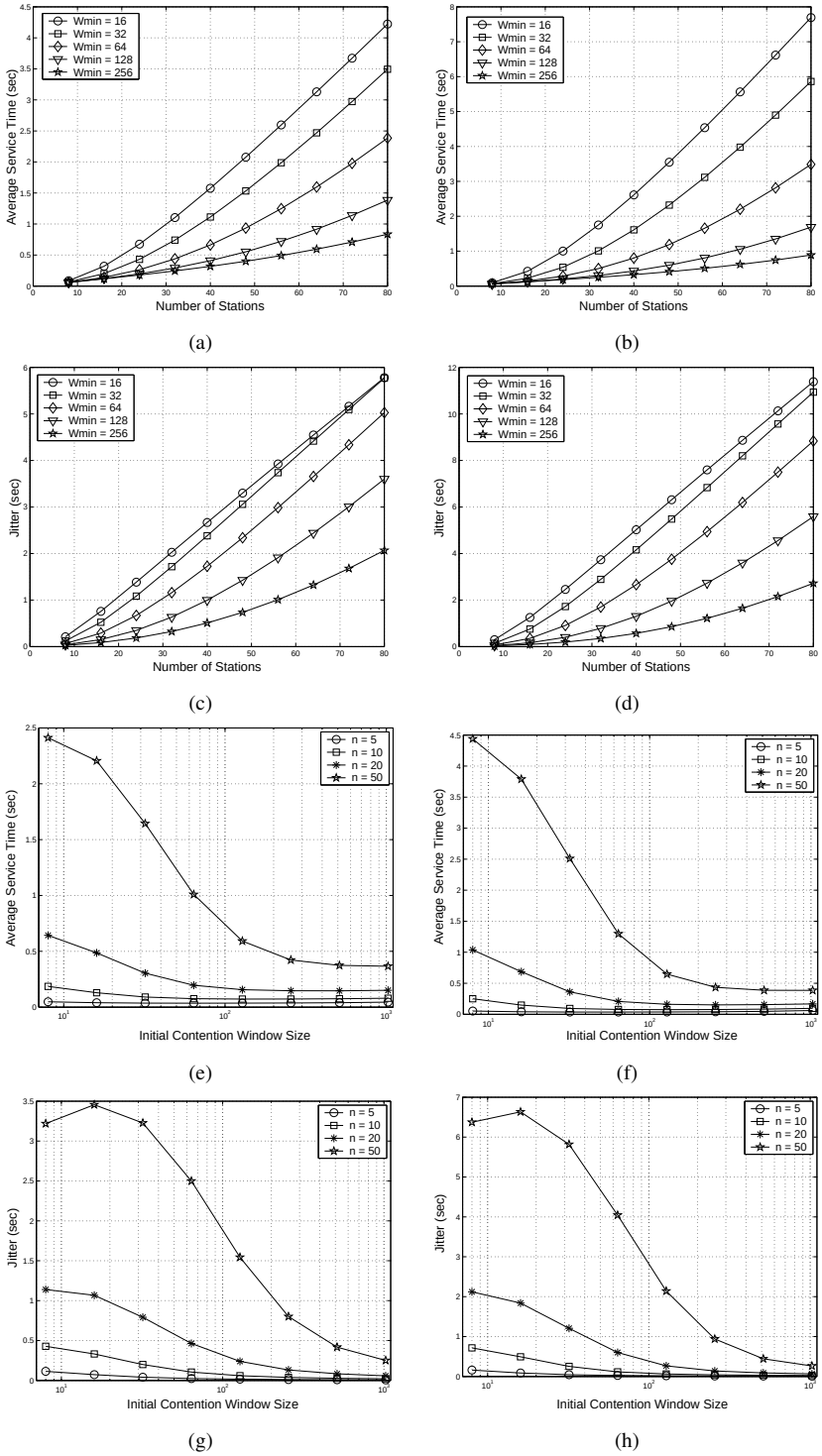


**Figure 2.7**: Average service time versus number of nodes for different initial contention window sizes: (a) DSSS (b) FHSS. Jitter versus number of nodes for different initial contention window sizes: (c) DSSS (d) FHSS. Average service time versus initial contention window size for different network sizes: (e) DSSS (f) FHSS. Jitter versus initial contention window size for different network sizes: (g) DSSS (h) FHSS.

see that performance is not very affected for medium-sized networks. However, the impact on system performance is more critical for large networks, where a considerable increase in mean service time and jitter is noticeable as packet size increases. This result can be explained if we refer to Figure 2.4. In this figure, it is shown that, as the number of nodes increases, the probability of having an idle channel decreases significantly, whereas the probabilites of collision and successful transmission increase (with the successful transmission probability still greater than the collision probability). Therefore, the time $t_s$ the channel is perceived busy due to successful transmissions becomes more relevant in large networks. From Eq. (2.39), the time $t_s$ depends on the average packet size. Consequently, the average packet size will have a higher impact on the average service time and jitter in large networks. From these results, it is interesting to note that, even though it is commonly stated that the RTS/CTS mechanism is throughput-effective when the packet size increases [12], we are facing here a clear trade-off on delay/throughput performance as the number of nodes increases.

Figures 2.8(e) and 2.8(g) show the average service time and jitter as we vary the slot time size for the case of the DSSS physical layer. Figures 2.8(f) and 2.8(h) show the results for the FHSS physical layer. Data packet size is fixed to 1024 bytes. From the graphs, we see that, even though we have a big packet size, the slot time size has neglible impact on system performance for both DSSS and FHSS physical layers. This result parallels the one reported by Bianchi [12], where throughput does not change much as we vary the slot time size. The fact is that, the amount of idle channel time still remains marginal with respect to the time spent in transmissions and collisions regardless of how much we increase the slot size.

Figures 2.9(a), 2.9(b), 2.9(c), and 2.9(d) show the results quantifying the impact of

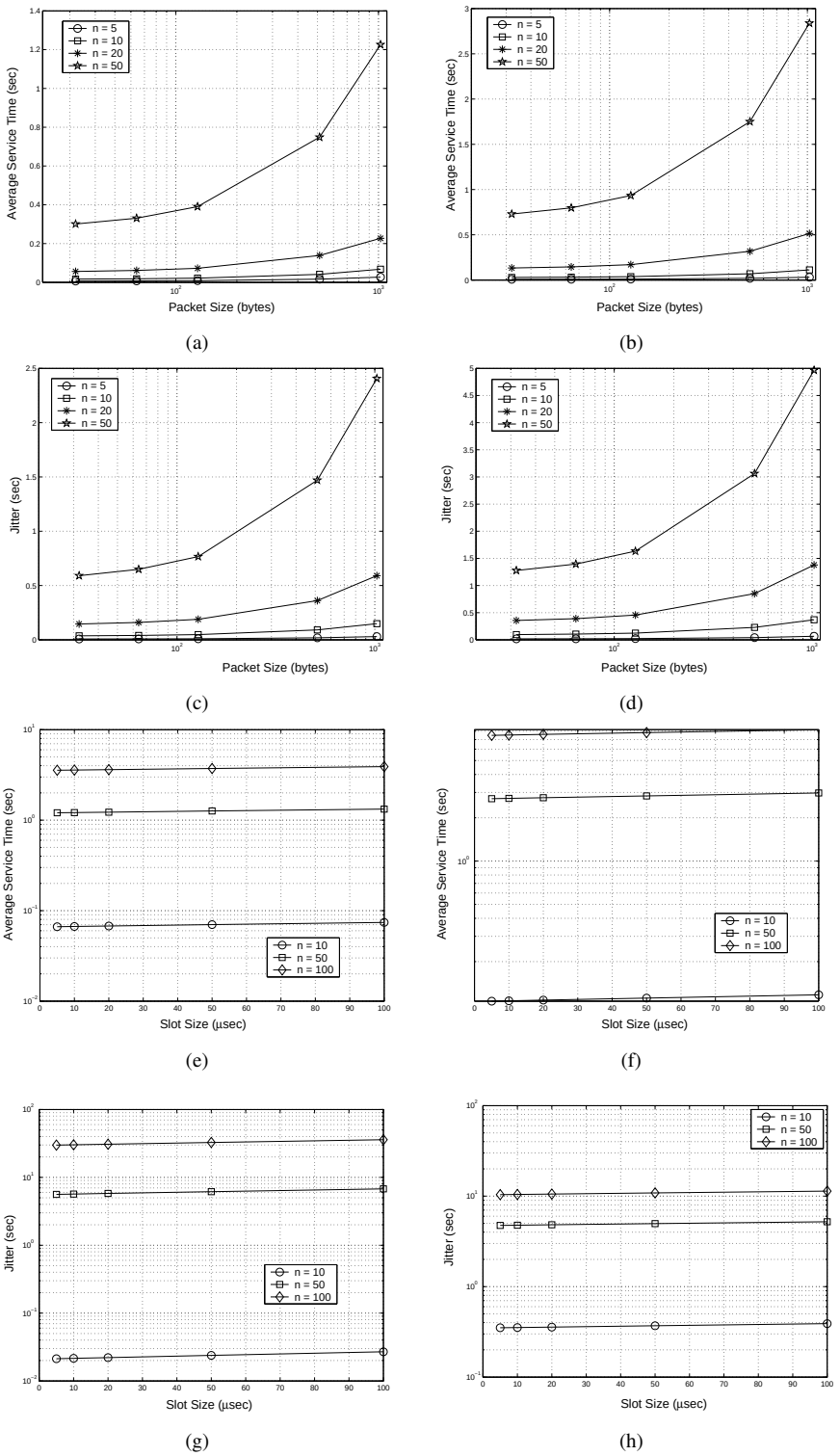


**Figure 2.8**: Average service time versus packet size for different network sizes: (a) DSSS (b) FHSS. Jitter versus packet size for different network sizes: (c) DSSS (d) FHSS. Average service time versus slot size for different network sizes: (e) DSSS (f) FHSS. Jitter versus slot size for different network sizes: (g) DSSS (h) FHSS.

the maximum backoff stage (parameter $m$) on the service time for DSSS and FHSS physical layers. The results show that, as far as service time and jitter are concerned, the binary exponential backoff algorithm can be very harmful in large, saturated networks if the maximum backoff stage is high. In both DSSS and FHSS we see that the fewer backoff stages, the better is the performance, specially for large networks. This fact suggests that, in saturated networks where nodes always have a packet ready to be sent in the head of their queues, the binary exponential backoff algorithm seems to be inappropriate. In fact, nodes will constantly have to backoff. However, according to our results, it is more effective to keep a constant, large contention window size than to increase the size of the contention window exponentially. This way, nodes will be more aggressive in acquiring the floor, providing lower delays.

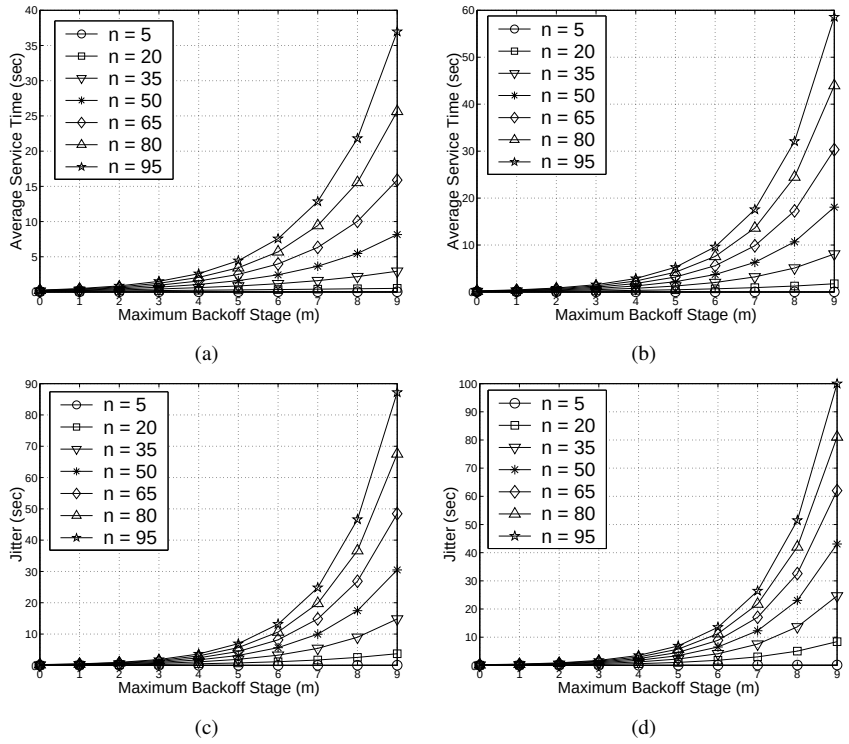


**Figure 2.9**: Average service time versus maximum backoff stage: (a) DSSS (b) FHSS. Jitter versus maximum backoff stage: (c) DSSS (d) FHSS.

## 2.6 Conclusions

In this chapter, we presented an analytical model for computation of the average service time and jitter experienced by a packet when transmitted in a saturated ad hoc network in which the IEEE 802.11 DCF is used. Using a bottom-up approach, we built the first two moments of the service time based on the IEEE 802.11 binary exponential backoff algorithm and the events underneath its operation. We provided a general model that can be applied to many scenarios where the channel state probabilities that drive a node's backoff operation are known. Here, we applied our model to saturated single-hop networks with ideal channel conditions and we carried out a performance evaluation of a node's average service time and jitter for the DSSS and FHSS physical layers. According to our results, as far as delay and jitter are concerned, DSSS performs better than FHSS. In addition to this, we found that, in contrast to previous studies on throughput in which the RTS/CTS mechanism was found to be practically independent of the initial contention window size and network size, these parameters have a major impact on system performance if delay is the metric in which we are interested. In this case, the higher the initial contention window size, the smaller the average service time and jitter are, especially for large networks. On the other hand, if we consider packet size, the opposite applies: the smaller the packet, the smaller the average service time and jitter are. Regarding the slot time size, we found that it has neglible impact on delay performance for both DSSS and FHSS. Finally, for the maximum backoff stage, the binary exponential backoff algorithm was found to be harmful if both the maximum backoff stage and the number of nodes in the network are large. As far as delay in saturated IEEE 802.11 networks is concerned, the binary exponential backoff algorithm seems to be inapropriate,

and a large and constant contention window size was showed to be more efficient, with packet sizes being selected according to the network size.

# Chapter 3

# Modeling IEEE 802.11 Single-Hop Networks under Fading Channels

In this chapter, we introduce a simple, yet effective, analytical model that incorporates the impact of the physical layer on the operation of the IEEE 802.11 DCF in saturated single-hop ad hoc networks. To show an application of the analytical model, we study the impact of frequency-nonselective slowly time-variant Rician fading channels on the performance of saturated IEEE 802.11 single-hop ad hoc networks.

## 3.1 Introduction

In the previous chapter, we introduced an analytical model to characterize the service time of a node in saturated IEEE 802.11 ad hoc networks. The advantage of our model is the fact that it takes a bottom-up approach and builds the first two moments of the ser-

vice time based on the events underlying the operation of the IEEE 802.11 binary exponential backoff algorithm (rather than assuming or fitting a probability distribution to a node's service time). A key characteristic of the model is the fact that it is general enough to be applied to any kind of IEEE 802.11 ad hoc network where the channel state probabilities governing the binary exponential backoff algorithm are known. Previously, we applied our results to single-hop networks under ideal channel conditions. In this chapter, we find the channel state probabilities when the physical layer is explicitly taken into account and Rician fading channel is considered. We validate our model through simulations and study the throughput performance of the standard-defined four-way handshake mechanism under direct sequence spread spectrum (DSSS) physical layer with differential binary phase shift keying (DBPSK) modulation.

The rest of the chapter is organized as follows. In Section 3.2 we present our analytical model. Section 3.3 contains our model validation and performance evaluation, and in Section 3.4 we present our conclusions.

## 3.2 Analytical Model

The model we presented in the previous chapter is applicable whenever the channel state probabilities $\mathbf{p} = [p_i \ p_c \ p_s]^T$ driving a node's backoff operation are known. We now compute the values of $\mathbf{p}$ for a saturated, single-hop ad hoc network when aspects of the physical layer are taken into consideration. For this purpose, we extend the work by Bianchi [12], who provided a model to evaluate the saturation throughput of the IEEE 802.11 MAC protocol under the hypothesis of ideal channel conditions. Following Bianchi's analysis, we also

assume a fixed number $n$ of nodes, with each node always having a packet available for transmission, i.e., the transmission queue of each node is assumed to be always nonempty. The key approximation of his model, which we adopt here too, is that each packet collides with constant and independent probability $p = 1 - q$ at each transmission attempt regardless of the number of retransmissions experienced. This probability is called the *conditional collision probability*, meaning that this is the probability of a collision experienced by a packet being transmitted on the channel. As mentioned in the previous chapter, Bianchi modeled the stochastic process representing the backoff time counter for a given node as a bidimensional discrete-time Markov process. According to his development, the probability $\tau$ that a node transmits in a randomly chosen slot time is given by Eq. (2.28), which is a function of the conditional collision probability $p$.

In a real situation, one might expect that each node $i$ would transmit a packet with an *individual* transmission probability $\tau_i$ dependent on the individual conditional collision probability $p_i$ (characterized by physical layer constraints such as path-loss propagation to receiver, fading, interference, etc). But, because our focus is on single-hop networks, and we want to consider the general scenario where nodes move constantly and randomly around an area (and, therefore, their distances to the intended receivers are changing constantly), by the independence assumption given above, we will assume that each transmission experiences the system in the *same state*. Therefore, at steady state, all nodes transmit a packet with the same probability $\tau$, and packets will collide with the same probability $p$. In effect, we are assuming that, on the average, all nodes experience the same channel conditions (e.g., fading, path-loss

propagation, and interference)[1].

Now, we can compute the conditional collision probability $p$ by first considering the probability $q$ that the packet does not collide. Notice that, in the basic access scheme, this packet refers to a *data packet*, whereas in the four-way handshake mechanism this is an *RTS*. By the previous considerations, the average power of the packets at any receiver is about the same. Therefore, we assume that, if two or more packets are transmitted at about the same time they will collide in any given receiver in the single-hop network. This means that we are not considering the capture phenomenon. Given that, the probability $q$ that a transmitted packet does not collide is given by

$$q = P\{\text{packet does not collide}\} = P\{\text{no neighbor transmits} \cap \text{packet correctly received}\}$$
$$= P\{\text{packet correctly received} \mid \text{no neighbor transmits}\}P\{\text{no neighbor transmits}\}. \quad (3.1)$$

The first probability is related to the successful reception of a packet by a given receiver. Therefore, it is a function of physical layer aspects such as the modulation/demodulation scheme used, forward error control coding (FEC), receiver structure, thermal and background noise, etc. In Section 3.2.1, we compute this probability according to specific physical layer and channel conditions. For the moment, let us simply assume that

$$\phi = P\{\text{packet correctly received} \mid \text{no neighbor transmits}\}. \quad (3.2)$$

From the independence assumptions, the second probability in Eq. (3.1) will be given by

$$P\{\text{no neighbor transmits}\} = (1-\tau)^{n-1}. \quad (3.3)$$

[1]Chapters 5 and 6 consider the general case, where nodes are treated individually.

Therefore,

$$q = \phi(1-\tau)^{n-1}, \tag{3.4}$$

or, in terms of the conditional collision probability $p$,

$$p = 1 - \phi(1-\tau)^{n-1}. \tag{3.5}$$

Eqs. (2.28) and (3.5) form a nonlinear system in the unknowns $\tau$ and $p$ that can be solved using numerical techniques. By using similar arguments as in [12], we can show that this system has a unique solution (see details in Appendix 3.5).

For simplicity, and to better understand the effects of different parameters on the probabilities $\tau$ and $p$, we find an approximate solution to the previous nonlinear system by linearizing Eqs. (2.28) and (3.5). We have shown in the previous chapter that a first-order approximation to Eq. (2.28) is given by

$$\tau = \frac{2W_{\min}}{(W_{\min}+1)^2}\,(1-p) = \frac{2W_{\min}}{(W_{\min}+1)^2}\,q. \tag{3.6}$$

We can now substitute the above approximation for $\tau(q)$ in Eq. (3.4), which defines the probability of a successful RTS reception. Because $2W_{\min}/(W_{\min}+1)^2 << 1$ (in 802.11, $W_{\min} >> 1$) and $0 < q < 1$, we have that

$$\begin{aligned} q &= \phi\left[1 - \frac{2W_{\min}}{(W_{\min}+1)^2}q\right]^{n-1} \approx \phi - \frac{2\phi W_{\min}(n-1)}{(W_{\min}+1)^2}q \\ &\approx \frac{\phi(W_{\min}+1)^2}{(W_{\min}+1)^2 + 2\phi(n-1)W_{\min}}, \end{aligned} \tag{3.7}$$

or, in terms of $p$,

$$p = \frac{(1-\phi)(W_{\min}+1)^2 + 2\phi(n-1)W_{\min}}{(W_{\min}+1)^2 + 2\phi W_{\min}(n-1)}, \tag{3.8}$$

which leads to the results presented in Chapter 2 by making $\phi = 1$. Eqs. (3.6) and (3.8) clearly show the decoupling we have achieved by linearizing the original system of nonlinear Eqs. (2.28) and (3.5).

We can now turn to the problem of finding the conditional channel state probabilities in $\mathbf{p}$ by following similar procedures as in Chapter 2. For this purpose, let $P_{tr}$ be the probability that there is at least one transmission in the considered time slot. Because we are considering the events experienced by a node during its backoff period, only the remaining $n-1$ nodes can be contending for channel access. Therefore, because each of the remaining $n-1$ nodes transmits a packet with probability $\tau$ at steady state, we have

$$P_{tr} = 1 - (1-\tau)^{n-1}. \tag{3.9}$$

The probability $P_{suc}$ that a transmission occurring on the channel is successful is given by the probability that exactly one node transmits on the channel and its handshake is successful, conditioned on the fact that at least one node transmits, i.e.,

$$P_{suc} = \frac{\binom{n-1}{1}\phi\tau(1-\tau)^{n-2}}{P_{tr}} = \frac{(n-1)\phi\tau(1-\tau)^{n-2}}{1-(1-\tau)^{n-1}}. \tag{3.10}$$

Therefore, the probability that a successful transmission occurs in a given time slot is $p_s = P\{E_s\} = P_{tr}P_{suc}$. Accordingly, $p_i = P\{E_i\} = 1 - P_{tr}$ and $p_c = P\{E_c\} = P_{tr}(1 - P_{suc})$.

### 3.2.1 Probability of Successful Packet Reception

Now let us consider the computation of the probability $\phi$ that a packet is correctly received. For this purpose, we need to characterize the radio channel under consideration.

We assume that all nodes are in line-of-sight (LOS) of each other, at an indoor environment such as a conference room. As far as the large-scale path loss is concerned, we adopt the simple model in which the path loss is a function of the transmitter/receiver distance $d$, with a path loss exponent $\eta$. Such models have been used extensively in the literature and are given by [99]

$$P_r = P_t \kappa \left( \frac{d_0}{d} \right)^{\eta}, \tag{3.11}$$

where $\kappa$ is a unitless constant which depends on factors such as antenna characteristics, and $d_0$ is the close-in reference distance. According to recent indoor measurements for the LOS path loss in the 2.4 GHz ISM band (the one in which the IEEE 802.11 operates), the exponent $\eta$ was found to be 1.91 [25]. Accordingly, for simplicity, we use the well-know *free-space* propagation model, in which $\eta = 2$ and $\kappa = (G_T G_R \lambda^2)/(4\pi d_0)^2 L$, where $G_T$ and $G_R$ are the transmitter and receiver antenna gains, $\lambda$ is the carrier wavelength in meters, and $L$ is the system loss factor not related to propagation ($L \geq 1$). Let us denote

$$G_{\text{loss}}(d) = \kappa \left( \frac{d_0}{d} \right)^2 \tag{3.12}$$

the *attenuation factor* of the free space model.

As far as multipath fading is concerned, we adopt the Rician fading model because of the LOS nature of the channel [99]. Wysocki and Zepernick [141] carried out indoor measurements in the 2.4 GHz band and reported mean excess delays $T_m$ in the range of 43.40 ns up to 57.04 ns. If we approximate the coherence bandwidth[2] $(\Delta f)_c$ by $(\Delta f)_c \approx 1/T_m$ [56], and take a mean delay spread of about 45.0 ns, then $(\Delta f)_c \approx 22.22$ MHz. According to the IEEE

[2]There is no exact definition for the coherence bandwidth [99]. Other definitions consider the coherence bandwidth as the bandwidth over which the frequency correlation function is above 0.9 or 0.5.

802.11 standard, the assigned channel bandwidth is about 22 MHz (after spreading), which means that, under such conditions, the channel can be considered a *frequency non-selective* channel (i.e., signal bandwidth $<$ coherence bandwidth). It is important to mention that the spread spectrum operation specified in the 802.11 helps to reduce intersymbol interference (ISI), which is the main effect of a *frequency-selective* channel. Moreover, real implementations of matched-filter demodulators [67] generally correlate the *whole* PN sequence with the incoming signal, i.e., the sampling time is equal to the original symbol duration, bringing the samples from the chip rate back to the original data rate (instead of performing per-chip demodulation). This way, possible effects of some frequency-selective fading on each transmitted *chip* are, in effect, averaged over the symbol period and rejected during the de-spread operation.

Now, if we consider a low mobility scenario (maximum velocity of 5 m/s), the maximum doppler frequency is $f_D = v_{\max}/\lambda = v \cdot f_c/c = (5 \times 2.4 \times 10^9)/(3 \times 10^8) = 40$ Hz. In other words, the *coherence time* $T_C \approx 1/f_D = 0.025$ s. Therefore, because the symbol duration is much smaller than the coherence time, the channel can be considered as a *slowly time-variant* fading channel. Finally, when data are transmitted over a *frequency-nonselective slowly time-variant* Rician fading channel, the average bit-error probability for conventional (two-symbol observation) differentially coherent detection of DBPSK is given by [108]

$$P_b = \frac{1}{2}\left(\frac{1+K}{1+K+\overline{\gamma}}\right)\exp\left(-\frac{K\overline{\gamma}}{1+K+\overline{\gamma}}\right), \tag{3.13}$$

where $K$ is given by

$$K = \frac{\text{Power of the line-of-sight component}}{\text{Total power of all other scattered components}} = \frac{a_0^2}{2\sigma_z^2},$$

and $\overline{\gamma}$ is the average signal-to-noise ratio, defined by

$$\overline{\gamma} = \frac{E_b}{N_0} E\{\psi^2\}, \tag{3.14}$$

with $E_b$ denoting the energy per bit, $N_0$ the power spectrum density of the additive thermal and background noise (assumed white Gaussian), $E\{\psi^2\}$ the mean squared value of $\psi$ (the Rician-distributed envelope of the multiplicative fading).

In Qualnet [105] (the simulator we use), it is assumed that $E\{\psi^2\} = G_{\text{loss}}(d)$. At any time, the distance between any transmitter/receiver pair is largely dependent on the mobility pattern of the nodes. In simulations, we use the *Random Waypoint* mobility model. From the findings by Royer et al. [102], we can postulate that a reasonable candidate for the pdf of the transmitter/receiver distance is a Maxwell distribution, i.e.,

$$f_X(x) = \sqrt{\frac{2}{\pi}}\, a^{3/2} x^2 \exp\left(\frac{-ax^2}{2}\right), \quad x \geq 0, \tag{3.15}$$

where $a$ is a constant and $E\{X\} = \sqrt{8/\pi a}$. Rigorously speaking, we should average $P_b$ over the transmitter/receiver distance $d$. Instead, to make things simpler, we average the path-loss attenuation factor $G_{\text{loss}}(d)$ over the distance $d$, and substitute the result back in Eq. (3.13). By doing this, we are basically computing $P_b$ for an average attenuation factor $\overline{G_{\text{loss}}}$, given by

$$\overline{G_{\text{loss}}} = \int_{d_0}^{d_{\max}} G_{\text{loss}}(x) f_X(x) dx = a\kappa d_0^2 \,\text{erf}\left(\sqrt{\frac{a}{2}}\, d_{\max}\right). \tag{3.16}$$

Considering a square area of side $l$, and the fact under the random waypoint mobility model nodes are likely to concentrate near the center of the area [11], we will assume that $d_{\max} \approx l/2$. If we assume that $E\{X\} \approx d_{\max}/\,2$, we have $a = 128/\pi l^2$ and

$$\overline{G_{\text{loss}}} = \frac{128\kappa d_0^2}{\pi l^2} \,\text{erf}\left(\frac{4}{\sqrt{\pi}}\right). \tag{3.17}$$

Finally, for the additive noise at the receiver front end, we have $N_0/2 = \xi k_B T_0$ W/Hz, where $k_B$ is the Boltzmann's constant ($1.38 \times 10^{-23}\, W\, s/K$), $T_0$ is the noise temperature in Kelvin, and $\xi$ is a constant, the noise factor, used to calculate the thermal noise level of the physical model [105].

Once $P_b$ has been found, we can compute the probability that a packet is correctly received in Eq. (3.1). In a slow fading channel, errors are likely to be correlated, occurring in bursts. In Qualnet, though, it is assumed that errors are independent from bit to bit (memoryless channel). We will follow their assumption for purposes of performance evaluation. Notice that, in the IEEE 802.11, the scrambling/descrambling operation works as an *interleaver*, helping the bit errors to appear as random when contiguous bits are descrambled. As a final remark, it has been shown that the undetected error probability for the 16-bit CCITT code (the one used in the preambles of the 802.11) is very small [6]. For this reason, we assume that all single and burst errors are correctly detected at the receiver. Given these considerations, if the transmitted packet is $x$ bits long, the probability $\phi$ that a packet is correctly received is simply

$$\phi = (1 - P_b)^x. \tag{3.18}$$

## 3.3 Numerical Results

We use Qualnet v.3.5 [105] to run simulations on network sizes ranging from 10 to 60 nodes (in steps of 10). Nodes are randomly placed in an area of $50 \times 50$ m and move around the terrain with velocities in the range $[0, 5]$ m/s according to the random waypoint algorithm. Each node transmits to one and only one receiver during the entire length of the

simulation with the same CBR source rate. We pick source rates high enough to saturate all nodes in the network. Packet sizes are fixed to 1500 bytes (IP packet) and each simulation run corresponds to 5 minutes of data traffic. Regarding the physical layer, we use direct sequence spread spectrum (DSSS) with a raw bit rate of 1Mbps with DBPSK modulation. Table 3.1 summarizes the rest of the parameters used in the simulations.

Figure 3.1(a) depicts simulation results for throughput versus the number of nodes for different values of the Rice parameter $K$. As we can see, throughput varies according to the number of nodes and the parameter $K$. As the number of nodes increases, throughput obviously decays as a result of higher contention within the network. Regarding the parameter $K$, as it increases, throughput increases as well. This is due to the fact that we have Rayleigh fading when $K = -\infty$ dB, which corresponds to the worst case scenario, where there is no line-of-sight component. As $K$ increases, fading goes away, and the channel gets closer to an AWGN channel. From the results, we notice that smaller networks are more sensitive to changes in $K$ than larger networks. As the number of nodes increases (and, consequently, contention) packet collisions dominate the packet reception rate, and fading becomes less of an issue. It is interesting to note that both behaviors (i.e., throughput versus $K$ and number of nodes) are captured by the analytical models, as shown in Figure 3.1(b). However, the analytical models provide a more conservative picture when compared to simulations, especially the linear model, given that it is already an approximation to the nonlinear model. As the number of nodes increases, the average throughput is smaller than in simulations, and sensitivity to $K$ is more prominent for smaller numbers of nodes, while it is practically irrelevant for bigger network sizes. There are three main reasons for the behavior just observed in the analytical

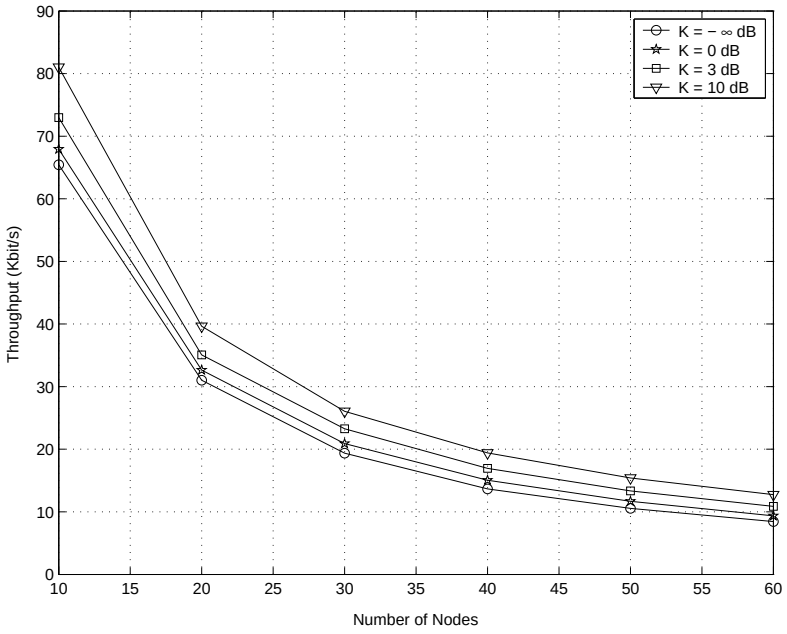


(a)

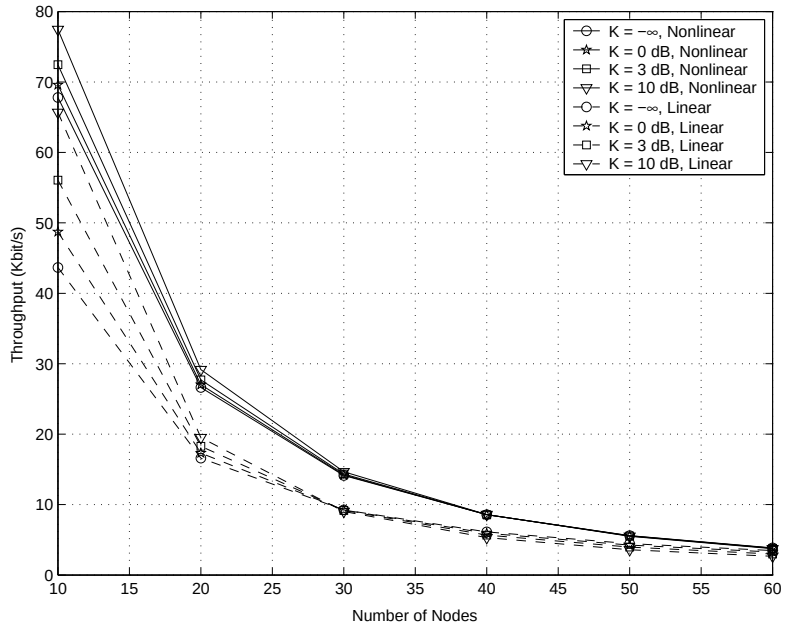


(b)

**Figure 3.1**: (a) Simulation results. (b) Analytical models.

**Table 3.1**: Simulation Parameters for both PHY and MAC Layers.

| | | | |
|---|---|---|---|
| $W_{\min}$ | 32 | Temperature (Kelvin) | 290 |
| $W_{\max}$ | 1024 | Noise Factor | 700 |
| MAC Header (bytes) | 34 | Transmission Power (dBm) | 1 |
| ACK (bytes) | 38 | Sensitiviy of PHY (dBm) | -79.0 |
| CTS (bytes) | 38 | Minimum Power for received packet (dBm) | -77.0 |
| RTS (bytes) | 44 | $G_T$ | 1 |
| Slot Time ($\mu$sec) | 20 | $G_R$ | 1 |
| SIFS ($\mu$sec) | 10 | $L$ | 1 |
| DIFS ($\mu$sec) | 50 | $d_0$ (meters) | 1 |
| ACK_Timeout ($\mu$sec) | 212 | $v_{\max}$ (m/s) | 5 |
| CTS_Timeout ($\mu$sec) | 348 | | |

models. First, in the model developed in Chapter 2, packets are allowed to backoff infinitely, as opposed to simulations, which follow the IEEE standard and have retransmission counters to limit the number of times a frame is retransmitted. In our simulations, a fraction of the packets is actually dropped because of this reason, especially in large network scenarios. Secondly, our model assumes that periods of collisions experienced by colliding nodes have the same duration as periods in which the channel is sensed busy by non-colliding nodes. This assumption has a direct impact on the number of nodes contending for the channel at any given time. When two or more nodes transmit at about the same time, if their packets collide, they will wait CTS_timeout seconds until they figure out that a collision has occurred. On the other hand, nodes that did not transmit at that particular time will sense a "clear channel" much earlier before colliding nodes do and, therefore, are more likely to be ready to transmit before the colliding nodes. For this reason, our model implies a more "aggressive" network, where the probability of having a node transmitting at any given time is higher than in real scenarios. Last, but not least, we have the impact of the capture phenomenon. As mentioned in Section 3.2, our model does not take into account the capture effects, which are present

in Qualnet simulations and are known to affect throughput considerably. Regardless of these limitations, both linear and non-linear models perform close to simulation results. It is important to point out here that, in simulations, nodes are constantly moving in different patterns with transmitter/receiver distances varying according to some unknown probability distribution. Despite this fact, our model is able to capture the general behavior by simply computing the average attenuation factor, as given by Eq. (3.17). In simulations, signal-to-noise ratios can vary by more than 33 dB at distinct receivers due to path-loss propagation effects. Considering such a dynamic range, the results provided by the analytical models have a striking correlation with simulation results. It is actually the computation of a good "representative" of the average signal-to-noise ratio the key to diminish the differences between simulations and analytical models with respect to variations in $K$, which certainly depends on how accurate is our estimation of the probability distribution of the transmitter-receiver distance.

In order to better show this problem, Figure 3.2 shows the theoretical throughput as a function of the average signal-to-noise ratio $\overline{\gamma}$ as predicted by the analytical models. In this figure, we show analytical results for network sizes of 10 and 50 nodes, as well as the case when the channel has no fading (AWGN channel, DBPSK modulation). For these cases, fading becomes relevant when the average signal-to-noise ratio is around 20 dB or less. Also, as we can see, there is a difference in signal-to-noise ratio of about 2 dB with respect to the point where fading kicks off in both network sizes. For a fixed SNR, throughput variation is more dramatic in small network sizes, as mentioned before. As the SNR decreases, fading becomes also relevant in bigger network sizes. Although not shown in the graphs, the performance for AWGN channels also decreases for smaller SNR values.

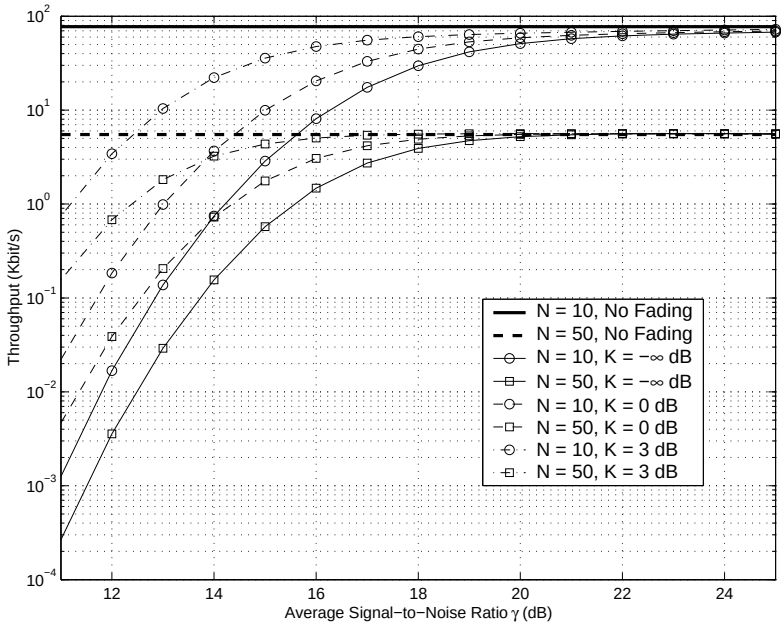


**Figure 3.2**: Throughput versus signal-to-noise ratio: performance comparison for channels with and without Rician fading.

## 3.4 Conclusions

In this Chapter, we introduced a simple, yet effective, analytical model for saturated IEEE 802.11 single-hop ad hoc networks that considers the impact of the physical layer on protocol operation and network performance. Using a bottom-up approach, aspects of the physical layer were explicitly incorporated in the dynamics of the events governing the operation of the IEEE 802.11 binary exponential backoff algorithm, leading to a more realistic computation of a node's average service time and throughput. We studied the impact of frequency-nonselective slowly time-variant Rician fading channels on the performance of saturated IEEE 802.11 single-hop ad hoc networks. We validate our model through simulations and studied the throughput performance of the four-way handshake mechanism under direct sequence spread spectrum (DSSS) with differential binary phase shift keying (DBPSK)

modulation. According to our results, smaller networks are more sensitive to fading variations than larger networks. As the number of nodes increases, packet collisions dominate the packet reception rate, and fading becomes less of an issue.

## 3.5 Appendix

If we invert Eq. (3.5), we obtain $\tau^*(p) = 1 - [(1-p)/\phi]^{1/(n-1)}$. If $\phi \neq 0$, this is a continuous and monotone increasing function in the range $p \in (0,1)$, which starts at $\tau^*(0) = 1 - \phi^{-1/(n-1)}$ (it can be negative) and grows up to $\tau^*(1) = 1$ . On the other hand, Eq. (2.28) is also continuous in the range $p \in (0,1)$ and is a monotone decreasing function that starts at $\tau(0) = 2/(W_{\min}+1)$ and reduces to $\tau(1) = 2/(1+2^m W_{\min})$. Uniqueness of the solution can be proven if we can show that $\tau(0) > \tau^*(0)$ and $\tau(1) < \tau^*(1)$, i.e., the two curves intercept at some point $p \in (0,1)$. From the above, we clearly have that $\tau(1) < \tau^*(1)$. Now, observe that $\tau^*(0) > \tau(0)$ if and only if $1 - (1/\phi)^{1/(n-1)} > 2/(W_{\min}+1)$, i.e., $\phi > [(W_{\min}+1)/(W_{\min}-1)]^{n-1}$. Because the initial contention window size $W_{\min} > 1$ (802.11 standard), the right-hand side is always greater than 1, which implies that we need to have $\phi > 1$ in order for $\tau^*(0) > \tau(0)$. However, because $\phi$ is a probability, i.e., $0 \leq \phi \leq 1$, there exists no value of $\phi$ such that $\tau^*(0) > \tau(0)$. On the other hand, $\tau(0) > \tau^*(0)$ if and only if $2/(W_{\min}+1) > 1 - (1/\phi)^{1/(n-1)}$, i.e., $\phi < [(W_{\min}+1)/(W_{\min}-1)]^{n-1}$, which is certainly true; therefore, $\tau(0) > \tau^*(0)$.

# Chapter 4

# Modeling Energy Consumption in Single-Hop IEEE 802.11 Networks

This Chapter presents an analytical model to predict energy consumption in saturated IEEE 802.11 single-hop ad hoc networks under ideal channel conditions. The model we introduce takes into account the different operational modes of the IEEE 802.11 DCF MAC, and is validated against packet-level simulations. In contrast to previous works that attempted to characterize the energy consumption of IEEE 802.11 cards in isolated, contention-free channels (i.e., single sender/receiver pair), we investigate the extreme opposite case, i.e., when nodes need to contend for channel access under saturation conditions. In such scenarios, our main findings include: (1) contrary to what most previous results indicate, the radio's *transmit* mode has marginal impact on overall energy consumption, while other modes (*receive, idle, etc.*) are responsible for most of the energy consumed; (2) the energy cost to transmit useful data increases almost linearly with the network size; and (3) transmitting large payloads is

more energy efficient under saturation conditions; and (4) data transmissions at higher rates have marginal impact on overall energy consumption in saturated networks under ideal channel conditions.

## 4.1 Introduction

Since most ad hoc networks include nodes that are connected to limited power sources (e.g., batteries), energy is a precious resourse. As a result, in the past few years, the design of "energy-efficient" or "energy-aware" protocols for ad hoc networks has become an area of intense research. Understanding the energy consumption at all network layers—as well as the energy consumed due to inter-layer interactions—is a fundamental step in the design of power-efficient protocols for wireless ad hoc networks.

As it has already been reported in the literature [110], [41], energy consumption of a wireless network interface card (NIC) can be significant, especially when small, power-anemic devices are considered. Typically, NICs implement two layers of the protocol stack, namely the medium access control (MAC) and the physical (PHY) layers. Nowadays, most commercial wireless NICs are based on the IEEE 802.11 standard [64]. The IEEE 802.11 MAC (its distributed coordination function (DCF), in particular) is also widely available in many discrete-event network simulators, and is the MAC of choice in the evaluation of many higher-layer protocols for ad hoc networks. In addition, the IEEE 802.11 DCF contains various mechanisms and features upon which many of the recently-proposed MAC protocols rely, such as carrier sensing, collision avoidance, exponential backoff, and others. For these reasons, the study of energy consumption in the IEEE 802.11 DCF represents an important step

towards the design of future energy-efficient protocols.

This chapter presents advances in two fundamental aspects of energy-aware protocols: it introduces an analytical model to predict energy consumption in single-hop IEEE 802.11 ad hoc networks (under ideal channel conditions), and it validates this model with discrete-event simulations using Qualnet v3.6 [105], for which an extended and improved energy consumption accounting was implemented [80]. In particular, we are interested in addressing the following questions: (1) How accurate is the analytical model compared to discrete-event simulations? (2) What is the relative energy consumption among the MAC operational modes (e.g., transmit, receive, and idle) when nodes are actively contending for channel access (under saturation)? (3) What is the efficiency (Joule/Bit) incurred at each node for a specific network size? (4) How does efficiency changes as the network size increases? (5) What is the impact of payload size on energy consumption as the number of nodes increases? (6) What are the energy savings if we transmit data at higher rates under saturation and ideal channel conditions?

Section 4.2 presents a brief overview of relevant work in energy consumption in the recent past. Section 4.3 presents the analytical model based on service-time characterization. Following that, Section 4.4 validates the model by comparing its results against data obtained using packet-level simulations. Finally, Section 4.5 presents our conclusions.

## 4.2 Related Work

A number of papers have characterized energy consumption in the IEEE 802.11 DCF. Stemm and Katz [110] have measured the power consumption of some NICs when used

by different end-user devices. They also report on transport- and application-level strategies to reduce the burden of energy consumption at NICs. Feeney and Nilsson [41] have reported detailed energy consumption measurements of some commercially-available IEEE 802.11 NICs operating in ad hoc mode. Along the same lines, Ebert et. al. [34], [35] have measured the impact of transmission rate, transmit power, and packet size on energy consumption in a typical wireless network interface. In all previous works, however, the focus was on characterizing energy consumption during the many modes of operation of a NIC, under extremely simple scenarios: only two nodes operating in ad hoc mode, with one node acting as the sender and the other as the receiver. None of the efforts investigated the energy consumption that is drained from the MAC operation itself, i.e., *when nodes need to contend for channel access*. Such studies, as pointed out by Feeney [41], are difficult to reproduce experimentally, and discrete-event simulations or probabilistic analysis are more appropriate.

The modeling of energy consumption at the MAC layer has already been treated previously in the context of cellular networks. Chockalingam and Zorzi [29] have developed an analytical framework to study the energy efficiency of MAC schemes whose operations can be described by finite state-space Markov chains. In particular, they have compared different versions of a hybrid protocol using slotted ALOHA and reservation concepts, and evaluated their performance with respect to the fading characteristics of the wireless channel. Within the same context, Chen et. al. [24] have conducted an energy consumption analysis of some MAC protocols, including the IEEE 802.11 itself. They showed that MAC protocols that aim to reduce the number of contentions perform better from an energy consumption perspective. As far as the modeling of the IEEE 802.11 is concerned, however, their approach falls short in

providing an accurate description of 802.11 DCF's behavior, because it ignores the binary exponential backoff operation, which is at the heart of the protocol. Instead, retransmissions and newly-generated packets are treated collectively as a single Poisson process. Moreover, because the analysis targets the infrastructure (WLAN) mode, the energy that is consumed when nodes act as *receivers* is not taken into account and, therefore, the model is not appropriate for an analysis of energy consumption in ad hoc networks, even fully-connected ones.

Qiao et. al. [94] have explored power-conserving strategies for IEEE 802.11a/h systems that adaptively select appropriate power-rate settings for each data transmission attempt. Their approach is based on an off-line computation of a lookup table that contains power-rate combinations indexed by the data transmission status (frame retry counts, payload, etc.). To compute the lookup table, an energy consumption analysis of the MAC operation was developed, and a recursive calculation of the average total energy consumption was provided. However, because the goal of their analysis was the generation of the lookup table—not the analysis of the IEEE 802.11 itself—the account of energy consumption was built from the standpoint of a *sending* node and, again, the model is not suitable for the analysis of an ad hoc network as a whole, where nodes can play both the *sender* and *receiver* roles. Additionally, a more careful analysis of the events that happen during the times the backoff counter is frozen is lacking, and an upper bound was obtained instead for the energy spent during those periods.

Recently, Gobriel et al. [55] have investigated the effect of transmission power control on overall throughput and energy savings in power-aware ad hoc networks. The drawback of their analysis, which targeted the IEEE 802.11 DCF, is the fact that the binary exponential backoff algorithm is ignored and a *constant* contention window size is assumed instead. For

this reason, as far as energy consumption is concerned, this model is not a good candidate to accurately reflect the energy consumption in IEEE 802.11 ad hoc networks. In addition, because the model was not validated/compared with discrete-event simulations, the accuracy of the model itself demands more study.

Concurrently with our previous work [22], Zanella and Pellegrini [147] have provided an analytical model for the energy consumption of single-hop IEEE 802.11 networks under ideal channel conditions. In their work, they assume that packets can be retransmitted indefinetly. Their work focuses on the analytical computation of a node's lifetime. As in the work by Gobriel et al. [55], no validation of the analytical model is carried out (e.g., against packet-level simulations).

## 4.3 Energy-Aware Model

Typically, the various tasks performed by a MAC protocol correspond to different radio modes, which exhibit different power requirements. In the particular case of the IEEE 802.11 DCF, two power management mechanisms are supported: *active* and *power-saving* (PS) [64]. In this paper, we only consider the *active* mechanism, in which a node may be in one of three different radio modes, namely, *transmit, receive*, and *idle* modes. In an ad hoc network under saturation conditions, each node actively contends for channel access while at the same time is a potential receiver of some other node's transmission. Therefore, while attempting to transmit its *own* data frame, each node needs to respond to transmission requests from other nodes. Consequently, understanding the service time in a network under saturation conditions is fundamental, because nodes have to constantly switch to different power modes

according to the perceived state of the channel and their own operation.

In Chapter 2, we introduced an analytical model to characterize the first two moments of the service time of a node in a saturated IEEE 802.11 ad hoc network. One of the drawbacks of the model is the fact that frames are allowed to backoff *infinitely* in time. This is not consistent with what is defined in the standard, where retransmission counters limit the number of attempts to transmit a particular data frame, after which the frame is dropped. The infinite backoff abstraction makes the model much more tractable, but makes it too conservative, predicting higher service times (and consequently, lower throughputs) than what actually happens in the IEEE 802.11 DCF. In this Chapter, we extend the model to include a more realistic approach regarding the IEEE 802.11 binary exponential backoff algorithm by developing the average service time for the case of a *finite* backoff operation. For this purpose, we keep our previous assumption that the conditional probability of a successful handshake per transmission attempt, $q$, is constant. In other words, at the end of a backoff stage, the probability of a successful handshake is constant, regardless of the number of previous attempts.

Now, let $M$ be the maximum number of times a frame can be retransmitted, i.e., the maximum number of backoff stages a frame can undergo (defined in the standard). In this case, we have a *truncated geometric distribution*, given by

$$P\{B = k\} = \frac{(1-q)^{k-1}q}{1-(1-q)^M}, \;\; k = 1, 2, \ldots, M. \tag{4.1}$$

Hence, following the same developments adopted in Chapter 2, the average service time is now given by (omitting intermediate steps, which are straigthforward but tedious):

$$\overline{T}_B = \frac{\alpha W_{\min}}{2}\beta_1 - \frac{\alpha}{2}\beta_2 + \beta_3\, t_c, \tag{4.2}$$

where

$$\beta_1 = \frac{A_1 + A_2 + A_3}{1-(1-q)^M}, \tag{4.3}$$

$$A_1 = \frac{2q\{1-[2(1-q)]^m\}}{2q-1} - 1 + (1-q)^m, \tag{4.4}$$

$$A_2 = \left(2^{m+1}-1\right)(1-q)^m\left[1-(1-q)^{M-m}\right], \tag{4.5}$$

$$A_3 = \frac{2^m\left\{(1-q)^{m+1} - (1-q)^M[1+q(M-m-1)]\right\}}{q}, \tag{4.6}$$

$$\beta_2 = \frac{1-(1-q)^M(1+qM)}{q[1-(1-q)^M]}, \tag{4.7}$$

$$\beta_3 = \frac{(1-q)-(1-q)^M[1+q(M-1)]}{q[1-(1-q)^M]}, \tag{4.8}$$

where the parameters $\alpha$, $m$, $W_{\min}$, and $t_c$ are defined as before. Because we are dealing with a saturated network under ideal channel conditions, the computation of the channel state probabilities $p_i, p_s$, and $p_c$ follow the derivations in Section 2.3.2.

### 4.3.1 Energy Consumption Model

To account for the energy consumption under saturation conditions, we need to consider the many events that take place while a node is trying to transmit its own data frame. For this purpose, let us first look at Eq. (4.2), which describes the average time a node spends in backoff. As described in Section 2.3.1, decrementing a node's backoff time counter depends on the node's perception of the *channel state*. As we have pointed out, there are three main channel states (or "events" during backoff): *successful transmission*, *collision*, and *idle channel* states. Notice that, these "states" do not correspond to the "modes of operation" of a network interface.

In the *successful transmission channel state*, the node in backoff experiences a suc-

cessful transmission happening over the channel. This transmission, however, can either refer to a successful transmission between any two nodes in the network, or to a successful transmission having the node itself as the target receiver. In the former case, the node in backoff overhears an RTS and updates its network allocation vector (NAV) accordingly [64], freezing its backoff time counter for the duration of someone's else four-way handshake (or two-way handshake if the basic access mode is used). Notice that, in this case, the node in backoff first *overhears* the RTS and then stays *idle* for the duration of the advertised transfer, as recorded in the NAV. In the latter case, i.e., when the node itself is the recipient of the transfer, it has to *receive* the RTS and DATA frames from the sender, and *transmit* the corresponding CTS and ACK frames back to the sender. Meanwhile, power is also consumed during the time intervals corresponding to SIFS's, DIFS's, and propagation delays $\delta$, during which the node stays *idle* or *senses* the channel[1].

In the *collision channel state*, similar events can take place from the standpoint of the node in backoff, i.e., the node is either overhearing or being the target of a transmission. Here, however, the node in backoff is overhearing an unsuccessful transmission or is being the target of a failed handshake. As before, energy is consumed while in overhearing and receiving modes, respectively. Nodes also consume power during the DIFS interval as the node waits before resuming its own backoff operation, after overhearing/receiving a failed handshake. Finally, during the *idle channel state*, the node in backoff basically *senses* the channel and decrements its backoff time counter each time no activity is detected for the duration of a time slot [64], [17].

[1]In reality, some power is also consumed when the network interface switches from one mode to another as, for instance, from the *receive* mode to the *transmit* mode (or *idle* mode). In this paper, we disregard the power costs of switching from one mode to another.

All these three states correspond to times when the node is in backoff, perceiving the channel activity, and before attempting its own handshake, i.e., during the course of a backoff stage, as mentioned in Section 2.3.1. The node attempts to establish a handshake with its intended receiver only at the end of a backoff stage. Each time the handshake fails, the node backs off again and repeats the process, until it finally succeeds in establishing the handshake and before it reaches the maximum number of allowed retransmissions, in which case, it drops its current data frame. In each of its handshake attempts, the node waits for a `cts _timeout` period before deciding that its RTS was not successful. In our analytical model (Eq. (4.2)), this collision resolution period is indicated by $t_c$, which, as described in Eq. (2.40), includes the time to *transmit* the RTS frame. Therefore, from Eq. (2.40), DIFS $+ \delta$ seconds are spent in *sensing* the channel, waiting for the CTS frame that is never received.

During a successful four-way handshake with the node's intended receiver, the NIC switches through a number of modes of operation. During the four-way handshake time interval $\overline{T}_s$ (i.e., $t_s -$ DIFS), the node *transmits* an RTS and a DATA frame (expressed in Eq. (2.39) by the header $H$ and payload $P$), *receives* the CTS and ACK back from the receiver, and *stays idle* during the time intervals corresponding to SIFSs and propagation delays $\delta$. According to experimental results reported by Feeney et. al. [41], the costs of *overhearing* a frame, staying *idle*, or *sensing* the channel are only marginally different from the cost of actually *receiving* a frame (in the IEEE 802.11 network interfaces evaluated). Note that these costs are not provided by manufacturers in data sheets. They were all measured in experiments. For this reason, many network simulators assume (implicitly or explicitly) the same power level for the *idle, overhear, sense*, and *receive* modes [105]. Consequently, because we want

to compare our analytical model with simulation results, we follow this same assumption and consider two power levels only: *passive*, or $P_{pas}$, for the cases when the NIC is in any of the four aforementioned modes, and *active*, or $P_{act}$, for the mode in which the NIC is actually transmitting something. Given these considerations, all we need to do is to account for the time intervals in which the network interface stays either in the "passive" or "active" modes.

From our previous remarks, a node will be in "passive" mode during backoff except for the case when it is the target receiver of a handshake request, in which case it has to transmit CTS and ACK frames back to the sender. If we denote by $T_{pas}^{back}$ the time a node is in *passive* mode during its backoff, we have, from Eq. (4.2),

$$T_{pas}^{back} = \frac{\alpha(W_{\min}\beta_1 - \beta_2)}{2}. \tag{4.9}$$

At the end of a backoff stage, the node attempts to perform a handshake with its intended receiver. Before succeeding in doing that, however, the node will spend $\beta_3 t_c$ seconds, on average, in collision resolutions due to unsuccessful attempts (as shown in Eq. (4.2)). In each collision resolution time interval $t_c$, the node spends DIFS$+\delta$ seconds in "passive" mode. Hence, if $T_{pas}^{col\_res}$ denotes the average time spent in passive mode during collision resolutions and, likewise, $T_{act}^{col\_res}$ the average time spent on "active" mode during collision resolution, we have that

$$T_{pas}^{col\_res} = \beta_3(\text{DIFS} + \delta) \quad \text{and} \quad T_{act}^{col\_res} = \beta_3 \text{RTS}. \tag{4.10}$$

When the node succeeds in performing a handshake, it will spend $T_{pas}^{4\_way}$ seconds in passive mode during the four-way handshake. From Eq. (2.39), this time interval corresponds to

$$T_{pas}^{4\_way} = \text{CTS} + \text{ACK} + 3 \times \text{SIFS} + 4\delta, \tag{4.11}$$

whereas in transmission the node will spend

$$T_{act}^{4\_way} = \text{RTS} + \text{H} + E\{P\}. \tag{4.12}$$

Finally, we need to take into account the case when the node is the target receiver of a handshake request during its backoff, in which case it needs to transmit CTS and ACK frames back to the sender. In a single-hop ad hoc network under ideal channel conditions, no capture or hidden terminal problems happen. Therefore, it is always assumed that all frame collisions are due to RTS collisions *at the intended receiver*. This means that, under such assumptions, *no CTS or ACK frame is ever transmitted unsuccessfully*. Therefore, the recipient of a handshake request only transmits a single CTS and a single ACK frame for each data transmission request, i.e., only those frames corresponding to the completion of a successful handshake. Furthermore, assuming a balanced and fair distribution of load in the network [2], if $T_{total}$ denotes the total observation time, then, on average, $T_{total}/\overline{T}$ data frames will be received by any node during the time interval $T_{total}$. From the remarks, for each data frame transmitted successfully, there is one and only one CTS and ACK frame sent by the intended receiver. Therefore, the average time $T_{act}^{back}$ a node spends transmitting CTS and ACK frames back to other nodes (while the node itself is in backoff) is given by

$$T_{act}^{back} = \overline{N}(\text{CTS} + \text{ACK}), \tag{4.13}$$

where $\overline{N} = T_{total}/\overline{T}$ is the average number of data frames transmitted over the interval $T_{total}$. Hence, if $\mathcal{E}_{passive}$ and $\mathcal{E}_{active}$ denote the energy consumptions in the *passive* and *active* modes,

[2] This assumption is realistic in ad hoc network scenarios such as n-way conferencing, and sensor network monitoring. Motivated by applications that may produce non-uniform traffic distributions, one of our directions of future work is to extend our model accordingly.

respectively, during the observation time $T_{total}$, then, from above,

$$\mathcal{E}_{passive} = \overline{N} P_{pas} \left( T_{pas}^{back} + T_{pas}^{col\_res} + T_{pas}^{4\_way} \right) \tag{4.14}$$

and

$$\mathcal{E}_{active} = \overline{N} P_{act} \left( T_{act}^{back} \overline{N}^{-1} + T_{act}^{col\_res} + T_{act}^{4\_way} \right), \tag{4.15}$$

where the $\overline{N}^{-1}$ term accounts for the $\overline{N}$ already included in the computation of $T_{act}^{back}$. Finally, the total energy consumption $\mathcal{E}_{total}$ is simply

$$\mathcal{E}_{total} = \mathcal{E}_{passive} + \mathcal{E}_{active}. \tag{4.16}$$

## 4.4 Model Validation and Performance Analysis

We validate our energy-aware model through packet-level simulations using the Qualnet v3.6 simulator [105] with improved energy consumption instrumentation [80]. We then use the model to account for energy consumption of saturated IEEE 802.11 single-hop ad hoc networks in a variety of ad hoc scenarios with different network- and payload sizes. Results correspond to the average of 10 runs with different seeds and different transmission start times (necessary to reduce IEEE802.11 unfairness). Table 4.1 summarizes the simulation parameters used. It is important to note that simulation parameters were chosen in order to provide a simulation environment as close as possible to the assumptions made in our model.

Figures 4.1 and 4.2 show the average energy consumption per node (in Joules) for the *active* and *passive* modes, as well as their sum (i.e., the total energy consumption) for different network sizes. Figure 4.1 plots results for the 1472-byte payload, whereas Figure 4.2 shows the results for a payload of 20-bytes. As we can observe, the analytical model predicts

**Table 4.1**: Simulation parameters used for validation of the IEEE 802.11 energy consumption model.

| Parameter | Value | Parameter | Value |
|---|---|---|---|
| Area | 50 × 50 m | Phy model | phy-IEEE802.11 |
| Number of nodes | 10, 20, 30, 40, 50 | RX model | SNR-based |
| Node placement | random | RX-SNR-THRESHOLD | 10.0 |
| Node mobility | none | Routing protocol | static |
| Simulation time | 300 sec | Traffic | CBR |
| Bandwidth | 1 Mbps | Payload size | 20 and 1472 bytes |
| TX-POWER | 10 dBm | Packet interval | 0.024 sec |
| RX-POWER | -82.045 dBm | Power consumption in TX | 1650 mW |
| Path loss model | free-space | Power consumption in RX | 1400 mW |
| Fading model | none | | |

quite well the simulation results. Because the analytical model is more conservative in terms of throughput [17], it leads to slightly smaller energy consumption values for the *active* mode and, consequently, slightly bigger values for the *passive* mode, compared to simulations. It is worth mentioning that, when compared to the model, Qualnet simulations use more "realistic" PHY-layer parameters, as shown in Table 4.1. Despite this fact, the analytical model proved to be a good abstraction of the simulated scenarios, supporting our earlier assumptions of restricting collisions to RTS frames only (for fully-connected networks).

Regarding individual contributions of the operational modes to overall energy consumption, the *passive* mode is responsible for the largest fraction of the total energy consumed. For the network sizes investigated, the *passive* mode consumes more than 88% of the total energy drained (for the chosen parameters). This result is a direct consequence of the fact that, under saturation and high contention, nodes spend most of their time backing off and listening to the channel, instead of actually transmitting data. For all network sizes investigated, the average total energy consumption is about 420 J, leading to an average power consumption of

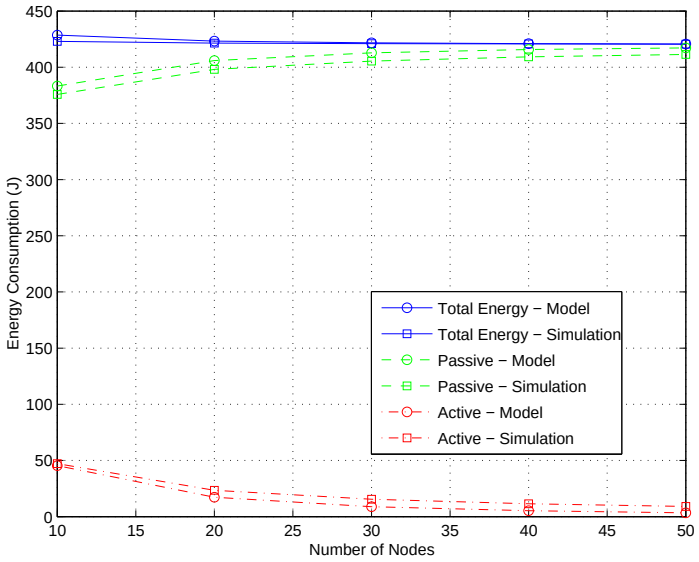


**Figure 4.1**: Per-node average energy consumption versus network size for a 1472-byte payload.

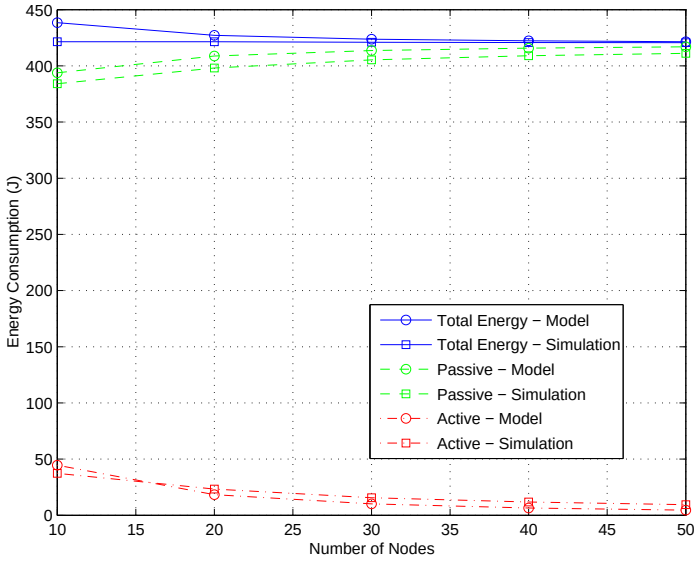


**Figure 4.2**: Per-node average energy consumption versus network size for a 20-byte payload.

1.4 W for the 300 s period, i.e., equivalent to the nominal power setting for the passive modes (energy consumption in RX) as shown in Table 4.1. This is consistent with the observation that passive modes are responsible for most of the energy dissipated. As the number of nodes increases, the power consumption in *passive* mode increases from 1.25 W up to 1.37 W. In other words, although the nominal value for the *transmit* (active) mode is 250 mW higher than the value for the *receive* (passive) mode, its impact is practically insignificant as far as the MAC operation in saturation conditions is concerned. This result opposes the findings in [41] and [34] which, under the perspective of a two-node scenario (sender/receiver) without contention, transmit mode is the largest overall energy consumer.

In cases where power-saving methods cannot be employed for some reason (like the IEEE 802.11 power saving (PS) mode [64], not available at some NICs), this result suggests that one can design energy-efficient WLAN devices by focusing on the optimization of circuits that are mainly active during *passive* modes of operation (see [94] for a simplified block diagram of a WLAN device). In fact, in typical WLAN devices, the RF power amplifier is a key component that, alone, demands most of the nominal power consumption, and it is used only in the transmit mode [34], [94]. According to our results, this is exactly the component that will *affect performance the least*, as far as energy consumption under channel contention is concerned.

Another interesting observation from Figures 4.1 and 4.2 is that the energy spent on both 20- and 1472-byte transfers are equivalent in all modes of operation. In other words, from the standpoint of energy-efficiency, it is better to transmit bigger payloads than smaller payloads, because the net energy consumption is the same. This last result can be better

illustrated by the *energy efficiency to transmit useful data*, $E_{\text{eff}}$ given by

$$E_{\text{eff}} = \frac{\text{Total Power Consumption}}{\text{Goodput}} \frac{\text{J}/s}{\text{Bit}/s}. \tag{4.17}$$

Figure 4.3 shows the behavior of $E_{\text{eff}}$ for the cases of 20- and 1472-byte data payloads as the number of nodes increases. Surprisingly, the energy cost appears to have an *almost linear* increase with network size. Moreover, the energy cost to transmit a 20-byte data payload grows at a rate that is about one order of magnitude higher than the cost to transmit a 1472-byte payload. For the 1472-byte scenario, the energy cost grows at a rate of approximately 0.002 mJ/Bit, whereas in the 20-byte scenario, the energy cost grows at 0.02 mJ/Bit.

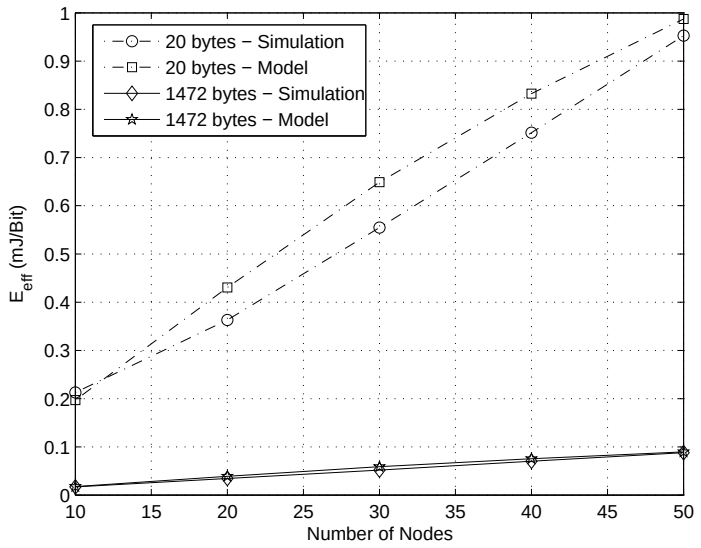


**Figure 4.3**: Energy efficiency (millijoules per bit) versus network size for 20-byte and 1472-byte payloads.

The usefulness of an analytical model such as the one we provide here is the ability to provide quick answers without resorting to simulations. As an example, we use it to analyze

the energy consumption of commercially-available NICs, namely the Lucent WaveLan card transmitting at both 1 Mbps (TX = 1650 mW and RX = 1400 mW) and 11 Mbps (TX = 1400 mW and RX = 900 mW), and the Cisco Aironet PC4800 at 1 Mbps (TX = 2200 mW and RX = 1350 mW) [34]. Figure 4.4 shows that, as expected, the power setting that provides the smallest energy consumption is exactly the one with the smallest power level in *passive* mode, i.e, the 11-Mbps WaveLan. Another interesting result is the little impact that transmit power has on overall results. All three settings showed similar performance in active mode, despite their relative nominal power differences.

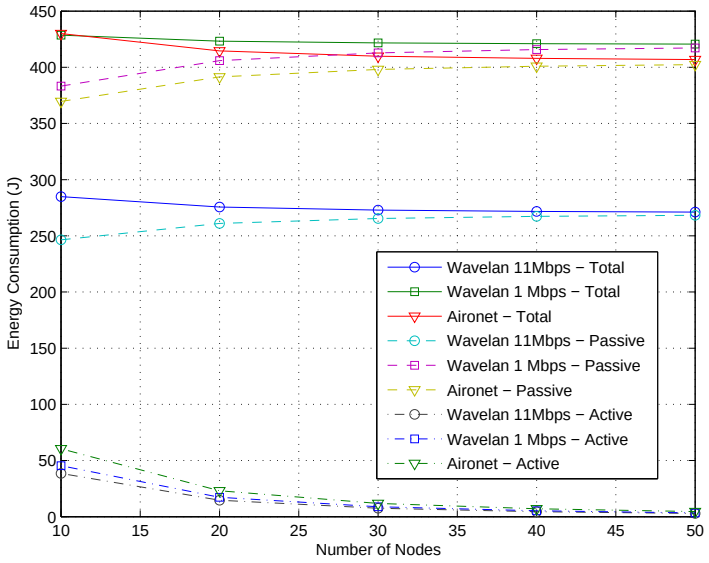


**Figure 4.4**: Energy consumption from the analytical model for different power settings.

This last set of results prompts the following question: what is the actual impact of the data rate on energy efficiency if power levels are kept constant (in reality, power levels change for different modulation schemes)? To answer this question, we investigate what is the energy consumption for the four data rates supported by the IEEE 802.11 b, namely: 1

Mbps (BPSK), 2 Mbps (QPSK), 5.5 Mbps (CCK), and 11 Mbps (CCK). Figure 4.5 shows the energy consumption results when TX = 1400 mW, RX = 900 mW, and the payload size is 1472 bytes. We choose this payload size to emphasize the impact of the data rate, since the headers are always transmitted at 1 Mbps using DBPSK. As we can see, the higher the data rate is, the higher the energy savings become. Unfortunately, such energy savings are not very significant, implying that, as far as single-hop saturated networks under ideal channel conditions are concerned, different data rates have little impact on overall energy consumption. Notice that, our focus here is on how much energy can be saved by simply transmitting data at higher speeds. Obviously, when channel impairments are considered, it is extremely important to select an appropriate power-rate setting that can overcome significant channel losses, as pointed out by Qiao et al. [94], for example.

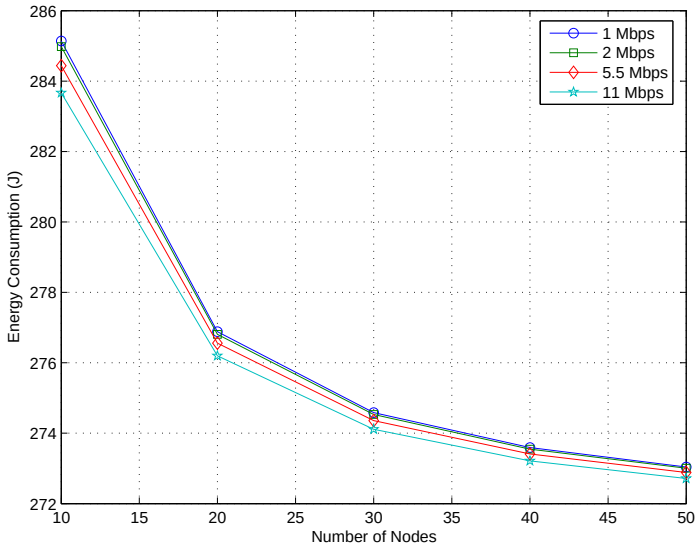


**Figure 4.5**: Overall energy consumption for different transmit data rates and fixed power levels (TX = 1400 mW and RX = 900 mW).

## 4.5 Conclusions

In this Chapter, we have introduced a simple analytical model to predict energy consumption in saturated IEEE 802.11 single-hop ad hoc networks under ideal channel conditions. In contrast to previous work that has focused on power consumption of IEEE 802.11 NICs without any channel contention, the opposite case was investigated here, with nodes actively contending for channel access under saturation conditions. In that case, the *passive* modes of the MAC operation dominate the energy consumption, whereas the *active* mode has just marginal impact (even when different power settings were used). In addition, we have found that the energy cost to transmit useful data grows almost linearly with the network size, and that the transmission of large data payloads is more advantageous from the standpoint of energy consumption under saturation conditions. Finally, we have also observed that transmitting at higher data rates does not translate into significant energy savings in saturated single-hop networks under ideal channel conditions.

# Chapter 5

# A Modeling Framework for MAC Protocols in Ad Hoc Networks

In this chapter, we introduce a new modeling framework for the analytical study of medium access control (MAC) protocols operating in multihop ad hoc networks. The model focuses on the interactions between the PHY and the MAC layers, and on the impact that each node has on the dynamics of every other node in the network—all conveniently conveyed through the use of *interference matrices*. A key feature of the model is that nodes can be modeled individually, i.e., it allows a per-node setup of many layer-specific parameters. Moreover, no spatial probability distribution or special arrangement of nodes is assumed; the model allows the computation of individual (per-node) performance metrics for any given network topology and radio channel model.

## 5.1 Introduction

As mentioned in Chapter 1, the main task of the medium access control (MAC) protocol of a computer network is to enable nodes to determine their right to access the available channel(s) while attempting to enforce a fair and efficient usage of the channel(s). To accomplish this task, the MAC protocol makes use of *input* and/or *feedback information* that other layers of the protocol stack may convey to it directly or indirectly. Typically, however, the MAC layer is mostly interested in the information it receives from the underlying physical (PHY) layer regarding the state(s) of the channel(s) and/or the occurrence of any events that are key to its operation (e.g., the successful transmission of a frame over the channel). Based on the input/feedback information, the MAC protocol dynamically adjusts its behavior in order to better allocate the channel(s) among competing nodes within the network.

The PHY layer, on the other hand, has the main job of receiving the bits of information from the MAC layer and, at the MAC's discretion, transmit the bits across the underlying communication channel(s) as fast and reliable as possible, according to appropriate (de)coding and (de)modulation schemes. The likelihood with which a transmission is successful will depend on how well the signaling used defends against channel impairments and interference from any source.

In wireless ad hoc networks, in particular, the signal transmissions from any node can potentially interfere with signal receptions at *any other node in the network* due to the broadcast nature of the radio channels. Hence, the quality of a radio link depends on the transmission activity of *every node* in the entire system, whose aggregate signal powers can severely degrade the signal-to-noise ratio (SNR) at a particular receiver and, consequently,

compromise the successful reception of any on-going packet transmission. As a result, each node's transmission activity can affect the PHY-layer performance at every node in the network, which, in turn, can affect back their MAC dynamics. Clearly, *the dynamics of the MAC layer is tightly connected to the dynamics of the PHY layer*, and the cross-layer interactions at each node will depend, fundamentally, on the activity of every node in the network.

In addition, because of radio wave propagation effects and multiaccess activity, connectivity among nodes is not a deterministic "boolean function" and, therefore, the underlying network *topology* is not as clearly defined as in wired networks, which makes interdependencies among nodes a complex matter. For this reason, the performance experienced by each node is a complex function of the signals used at the PHY layer, the scheduling established at the MAC layer, and the radio topology of the network.

Unfortunately, the bulk of the published work on ad hoc networks has focused on the modeling of medium access control schemes where ideal channel conditions and unrealistic assumptions are made. Under the argument of separating the issues strictly related to the MAC operation from the issues intrinsically related to the physical layer, few studies have attempted to incorporate physical layer aspects *directly into the behavior of the MAC protocol*, i.e., explicitly modeling the impact of the physical layer on the *dynamics* of the MAC protocol. Perhaps, more importantly, no attempt has ever been made to include not only the physical-layer aspects explicitly into the model, but also to include the interdependencies among nodes under a radio-based topology in a multihop ad hoc network. Although convenient for analytical modeling, it is *not* true that only the "one hop" neighbors of a node can cause interference at a node.

In this chapter, we introduce a new modeling framework for the analytical study of *any* MAC protocol operating in multihop ad hoc networks. The model focuses on the interactions between the PHY and the MAC layers, and on the impact that each node has on the dynamics of every other node in the network. To account for the effects of both cross-layer interactions and the interference among all nodes, a novel linear model is introduced with which topology and PHY/MAC-layer aspects are naturally incorporated in what we define as *interference matrices*. A key feature of the model is that nodes can be modeled individually, i.e., it allows a per-node setup of many layer-specific parameters. Moreover, no spatial probability distribution or special arrangement of nodes is assumed; the model allows the computation of individual (per-node) performance metrics for any given network topology and radio channel model.

In the sequel, we build our modeling framework in probabilistic terms, i.e., we express the input and/or feedback information conveyed to the MAC layer in terms of probabilities, as well as the output of the MAC layer, i.e., the scheduling rates (transmission probabilities).

## 5.2 Modeling the Medium Access Control (MAC) Layer

Let $\boldsymbol{\varphi}_i(t)$ denote a *vector* whose entries are the input and feedback information used by a particular MAC protocol at each node $i \in V$ at time $t$, where $V$ is a set of $|V| = n$ nodes in the network. Because we are proposing a probabilistic model, we assume that the entries of the vector $\boldsymbol{\varphi}_i(t)$ are, in fact, *probabilities*, i.e., they represent probabilities of events whose outcomes are important input and/or feedback information to the operation of the MAC proto-

col in place. In this sense, a MAC protocol can be seen as a *stochastic dynamic system* whose input and feedback information are contained in the vector of probabilities $\boldsymbol{\varphi}_i(t)$, and the corresponding output is the scheduling rate $\tau_i(t)$. Therefore, in principle, the MAC operation can be represented by some function that maps $\boldsymbol{\varphi}_i(t)$ into the desired output $\tau_i(t)$.

Strictly speaking, the MAC operation should be seen as a time-variant system, where probabilities should also be time-variant (a stochastic process). However, we will assume that in the long-run (or in steady-state), the operation of the MAC protocol can be represented by a time-invariant (linear or non-linear) function $h_i(\cdot)$ relating the steady-state probability vector $\boldsymbol{\varphi}_i$ to the steady-state scheduling rate $\tau_i$, i.e., if we let $\tau_i = \lim_{t\to\infty} \tau_i(t)$ and $\boldsymbol{\varphi}_i = \lim_{t\to\infty} \boldsymbol{\varphi}_i(t)$, we assume that there exists a function $h_i(\cdot)$ such that

$$\tau_i = h_i(\boldsymbol{\varphi}_i), \quad i \in V, \tag{5.1}$$

where the subscript $i$ in the mapping function $h_i(\cdot)$ denotes a node-specific instantiation of the MAC protocol in use.

The number and nature of input/feedback entries in the vector $\boldsymbol{\varphi}_i(t)$ will depend on the MAC protocol in place and the scenarios investigated. For instance, one should expect $\tau_i$ to be a function of the steady-state probability that a packet is available at a node's input queue, i.e., that the queue is not empty. Consequently, $\tau_i$ should also be a function of the input data traffic distribution at node $i \in V$. Many times, however, the throughput of an ad hoc network is studied by assuming saturation at all nodes, i.e., all buffers are considered to be full [122]. In this case, one is normally concerned with the maximum throughput attainable by the network when all nodes are actively seeking access to the channel.

In the case of carrier sense-based MAC protocols, an example of relevant feedback

information from the PHY layer is the probability that the *channel is sensed idle* by a node that wants to transmit a frame over the channel. In such protocols, a node only attempts to transmit a frame if the channel is sensed idle, i.e., if the signal power captured by the node's antenna(s) is below some signal power threshold, meaning that no on-going transmission over the channel is happening within the node's immediate neighborhood. Otherwise, the node refrains from transmitting the frame.

As far as a *reliable delivery service* at a given MAC protocol is concerned (contention or schedule-based MAC), the single most important feedback information is the *probability that a frame transmission is successful*. This is, in fact, the main information on which the MAC protocol basis its behavior in order to schedule retransmissions and transmissions of new frames. This information is the key link between the PHY and MAC layers. Depending on how well the signaling used defends against channel impairments determines the evolution of the MAC protocol itself. Moreover, due to the inherent broadcast nature of wireless networks, this feedback probability depends on the activity of *every other node in the network*, which, in turn, depends on how well the PHY layer guarantees the minimum interference among simultaneous transmissions and how well the MAC protocol avoids the concurrent scheduling of potential interfering transmissions over the channel.

In the next section, we model the impact of the PHY layer with respect to some of the aforementioned feedback probabilities.

## 5.3 Impact of the Physical (PHY) Layer

In this section, we present the modeling of the impact of the PHY layer by introducing the computation of some feedback probabilities. First, we present the computation of the *successful frame reception probability,* which reflects a node's capability to successfully receive a frame transmitted to it. Once this probability is known, we can compute the *probability of a successful handshake*, which represents the most important feedback information for a reliable delivery service at the MAC layer. Lastly, we show how to compute the *probability that the channel is busy*, a key information that is needed within the class of carrier sense-based MAC protocols.

### 5.3.1 The Successful Frame Reception Probability

The quality of the radio link between any two nodes in an ad hoc network may vary considerably over time, even in the case when the two nodes are within range of each other. The time-variant nature of a radio link is due to physical layer aspects, as well as the transmission activity of all other nodes in the network, which is controlled by the MAC scheme. Individually, a node's transmission may not interfere with some packet reception at a distant node. However, collectively, the aggregate interference from many simultaneous transmissions might do.

With few exceptions (e.g., [71, 151]), most prior models of MAC protocols assume that all packets received at the same time at a given receiver "collide" and, therefore, are destroyed. This assumption is reasonable if the powers of the received signals are nearly the same. In most situations, however, the powers of the received signals are subject to large-

scale path loss propagation, shadowing, and small-scale multipath fading [111]. Even when packets from different nodes overlap in time, it may still be possible to successfully decode the packet with the strongest received signal strength—the so-called capture phenomenon [77]. Moreover, a number of choices in system design at the PHY layer have a direct impact on the successful reception of a packet at a given receiver.

For all the above considerations, a link in a wireless ad hoc network may generally be seen as an *asymmetric* channel, and the conditions for a packet to be successfully received at one end of the link may be significantly different at the other end. Therefore, we need to consider network topology in a broader sense, in which asymmetries, unpredictability, and physical-layer aspects are explicitly incorporated into the model.

For the purposes of this work, we classify the channel signaling methods into two types [122]: *narrowband* and *spread-spectrum* systems. In narrowband signaling, data bits are modulated directly onto the carrier. On spread-spectrum systems, some form of coding is used to get a much wider bandwidth than narrowband schemes do for the same data rate. In many cases, spread-spectrum signaling is the signaling method of choice because of its anti-jamming capabilities, robustness to multi-path effects, lower power spectrum density, and potential for multiuser access through CDMA techniques, i.e., the use of orthogonal codes that can overlap in time with little or no effect on each other. As an example, the IEEE 802.11 standard supports both direct sequence spread spectrum (DSSS) and frequency-hopped spread spectrum (FHSS) systems [64].

In this work, we assume a direct sequence spread spectrum ad hoc network. In such networks, *multiple access interference* (MAI) plays a major role on network capacity [59],

[88]: in the demodulation of each signal, signals from other nodes transmitting simultaneously over the channel appear as interference. The level of such interference varies according to the number of active nodes at any time (dictated by the underlying medium access control scheme). For this reason, not only capacity, but many quality of service (QoS) measures in wireless ad hoc networks are intrinsically dependent on the received *signal-to-interference-plus-noise density ratio* (SINR). More specifically, let $P_k^r$ denote the received signal power at node $r$ for a signal transmitted by node $k \in V$. Then, the signal-to-interference-plus-noise density ratio $\text{SINR}_i^r$ for a signal transmitted by node $i$ and received at node $r$, is given by (using a conventional matched filter receiver) [127]:

$$\text{SINR}_i^r = \frac{P_i^r L_i}{\sum_{\substack{j \in V \\ j \neq i}} \chi_j P_j^r + \sigma_r^2}, \tag{5.2}$$

where $L_i$ is the spreading gain (or bandwidth expansion factor) of the spread-spectrum system, $\sigma_r^2$ is the background or thermal noise power at the front end of the receiver $r$, and $\chi_j$ is an on/off indicator, i.e.,

$$\chi_j = \begin{cases} 1, & \text{if } j \text{ transmits at the same time,} \\ 0, & \text{otherwise.} \end{cases} \tag{5.3}$$

In Eq. (5.2), it is assumed that nodes use long, orthogonal pseudo-random sequences [127], and that the thermal and background noise is modeled as a white Gaussian noise process. The same assumptions are used in such simulators as Glomosim, Ns-2, and Qualnet [105].

Each time node $i$ transmits a frame to node $r$, the (instantaneous) multiple access interference (MAI) level at node $r$ depends on which nodes in $V$ transmit concurrently with

node $i$, as indicated by the variable $\chi_j$, a Bernoulli-distributed random variable with probability $\tau_j$, the probability that node $j$ transmits a frame at any time, according to the MAC protocol in place. Because $|V| = n$, there are exactly $2^{n-2}$ combinations of potential active nodes (interferers) transmitting concurrently with $i$ (excluding both transmitter $i$ and receiver $r$). Let $\{c_{ik}^r\}_{k=1,\ldots,2^{n-2}}$ denote the set of such combinations, and $\mathcal{C}_i^r$ be a random variable that indicates the occurrence of a specific combination $c_{ik}^r$ of interferers. We also assume, for simplicity, that when node $i$ transmits a frame to node $r$, the set of interferers remains the same throughout the entire transmission of the frame. In reality, of course, some nodes may become active or inactive during the course of a frame transmission. However, this assumption is reasonable if frames are short and transmission rates are high. Consequently, during the reception of a frame—and for a fixed set of interferers—the bit-to-bit variations that may occur in $\mathrm{SINR}_i^r$ results from RF propagation effects only. Typically, the received signal powers $P_i^r$ are subject to large-scale path loss, shadowing, and small-scaling multipath fading.

Given the previous considerations, the probability $s_i^r$ *that a frame transmitted by* $i$ *is successfully received at* $r$ can be obtained by considering the set $\{c_{ik}^r\}_{k=1,\ldots,2^{n-2}}$ of all possible combinations of active nodes in $V - \{i, r\}$, as follows:

$$
\begin{aligned}
s_i^r &= P\{\text{successful frame reception}\} = \sum_k P\{\text{successful frame reception} \cap \mathcal{C}_i^r = c_{ik}^r\} \\
&= \sum_k P\{\text{succ. frame reception} \,|\, \mathcal{C}_i^r = c_{ik}^r\} P\{\mathcal{C}_i^r = c_{ik}^r\} \\
&= \sum_k f(c_{ik}^r) P\{\mathcal{C}_i^r = c_{ik}^r\}, \qquad (5.4)
\end{aligned}
$$

where we wrote $f(c_{ik}^r)$ to emphasize the fact that $P\{\text{succ. frame reception} \mid \mathcal{C}_i^r = c_{ik}^r\}$ is a function of the specific combination $c_{ik}^r$ of interferers. Its functional form will depend on

the specific choice of radio channel model and such PHY-layer aspects as modulation and demodulation schemes, channel coding, receiver design, and the like.

The above formalism allows the consideration of *any* radio channel model and PHY-layer aspect for computation of the probability $f(c_{ik}^r)$ of successful frame reception conditioned on a certain MAI level. For instance, one could choose to model the impact of a specific modulation scheme under correlated bit errors during frame reception.

Therefore, depending on which nodes are active at the time node $i$ transmits a frame to node $r$, there can be different values for the SINR and, consequently, different bit-error probabilities. Hence, from Eq. (5.4), one needs to know the frame error probabilities for all $2^{n-2}$ possible combinations $\{c_{ik}^r\}$, which depends on the *joint probabilities* of occurrence of all the combinations $\{c_{ik}^r\}_{k=1,\ldots,2^{n-2}}$. The exact functional form of the joint probabilities depends on the specific MAC protocol in use.

### 5.3.2 The Successful Handshake Probability

Previously, we have considered the successful frame reception probability. From the point of view of a reliable delivery service at the MAC layer, a frame is considered to be successfully transmitted at the intended receiver if a successful *acknowledgment* is received in response to the frame that was previously sent. Therefore, we need to consider the *successful handshake probability*, which we define as the joint probability that both the transmitted frame and its respective acknowledgment are received successfully. More specifically, two events need to happen for a node $i \in V$ to consider its frame successfully transmitted to a node $r \in V$: the successful reception of $i$'s frame at $r$, and the successful reception of $r$'s

acknowledgment at $i$. Therefore, if we denote by $q_i^r$ the probability of a successful handshake between nodes $i$ and $r$, and if we take into account all possible combinations of interferers at nodes $i$ and $r$ (indicated by the random variables $\mathcal{C}_r^i$ and $\mathcal{C}_i^r$, respectively), we have that

$$
\begin{aligned}
q_i^r &= P\{\text{DATA successful}, \text{ACK successful}\} \\
&= \sum_k \sum_l P\{\text{DATA suc.}, \mathcal{C}_i^r = c_{ik}^r, \text{ACK suc.}, \mathcal{C}_r^i = c_{rl}^i\} \\
&= \sum_k \sum_l P\{\text{ACK suc.}|\mathcal{C}_r^i = c_{rl}^i, \text{DATA suc.}, \mathcal{C}_i^r = c_{ik}^r\} P\{\mathcal{C}_r^i = c_{rl}^i|\text{DATA suc.}, \mathcal{C}_i^r = c_{ik}^r\} \\
&\quad P\{\text{DATA suc.}|\mathcal{C}_i^r = c_{ik}^r\} P\{\mathcal{C}_i^r = c_{ik}^r\} \\
&= \sum_l \sum_k f(c_{rl}^i) f(c_{ik}^r) P\{\mathcal{C}_r^i = c_{rl}^i|\text{DATA succ.}, \mathcal{C}_i^r = c_{ik}^r\} P\{\mathcal{C}_i^r = c_{ik}^r\}. \qquad (5.5)
\end{aligned}
$$

In Eq. (5.5), the probability that the set of active interferers $\mathcal{C}_r^i$ at node $i$ is $c_{rl}^i,\ l \in V$, is conditioned on the fact that the set of active interferers $\mathcal{C}_i^r$ at node $r$ is $c_{ik}^r,\ k \in V$. This is because, in general, the set of active interferers at node $i$ may not necessarily be the same as the set of interferers at node $r$. Moreover, the likelihood that a node is active when $r$ sends its ACK back to $i$ can change if it knows, somehow, that some specific set of nodes has already become active during the transmission of $i$'s DATA frame to $r$. Such dependencies will rely, among other things, on the MAC protocol in place, the size of DATA frames, etc.. For instance, on one hand, we could have a contention-based MAC protocol (e.g., ALOHA) where nodes would attempt to transmit packets independently of each other without listening to the channel (carrier sensing). In this case, the fact that some nodes have already become active during the transmission of the DATA frame will not prevent other inactive nodes to become active during the ACK transmission. On the other hand, in a carrier-sensing-type of MAC protocol, the nodes that have detected the transmission of the DATA frame in the

channel will defer their transmission to a future time that will probably not coincide with the transmission of the subsequent ACK frame (in general, ACK frames are very short).

The previous development considered the case where both DATA and ACK frames were of fixed size. However, if both (or any) of the DATA and ACK frames are of variable size, and their size distributions are known, Eq. (5.5) can be easily modified to include such cases. More specifically, if the DATA frame size is $B$ bytes long, with probability mass function $P\{B = b\}$, and the ACK frames are assumed to be of fixed size (which is generally the case), Eq. (5.5) modifies to

$$
\begin{aligned}
q_i^r &= P\{\text{DATA successful, ACK successful}\} \\
&= \sum_k \sum_l \sum_b P\{\text{DATA suc.}, B = b, \mathcal{C}_i^r = c_{ik}^r, \text{ACK suc.}, \mathcal{C}_r^i = c_{rl}^i\} \\
&= \sum_k \sum_l \sum_b f(c_{rl}^i) f(c_{ik}^r) P\{\mathcal{C}_r^i = c_{rl}^i | \text{DATA suc.}, B = b, \mathcal{C}_i^r = c_{ik}^r\} P\{\mathcal{C}_i^r = c_{ik}^r | B = b\} \\
&\quad P\{B = b\}, \qquad (5.6)
\end{aligned}
$$

where now $f(c_{rl}^i) = P\{\text{ACK suc.} \,|\, \mathcal{C}_r^i = c_{rl}^i, \text{DATA suc.}, B = b, \mathcal{C}_i^r = c_{ik}^r\}$ and $f(c_{ik}^r) = P\{\text{DATA succ.} | B = b, \mathcal{C}_i^r = c_{ik}^r\}$. In other words, the probability of having the set of interferers $\mathcal{C}_i^r = c_{ik}^r$ is conditioned on the DATA frame size $B = b$. For instance, in the ALOHA protocol, the bigger the DATA frame, the higher the probability that more nodes will be transmitting at about the same time that the DATA frame is being received. On the other hand, in other protocols, it might happen that the probability of having a specific set of interferers could be considered independent of the DATA frame size, i.e., $P\{\mathcal{C}_i^r = c_{ik}^r | B = b\} = P\{\mathcal{C}_i^r = c_{ik}^r\}$.

We just showed how to compute the successful handshake probability when the handshake involves the exchange of two frames only: a DATA frame and an ACK frame. Some

classes of MAC protocols use a four-way handshake mechanism. In those cases, the previous development can be easily extended, and one will need to know the four successful frame reception probabilites with respect to the four frames that were exchanged (as represented by the functions $f(\cdot)$ in Eq. (5.6)). Finally, it may happen that one needs to know the probability of *unsuccessful* handshake due to errors in one of the four frames. In that case, one needs to know the probability of unsuccessful reception of a particular frame, which is simply $1 - f(\cdot)$. Based on that, one can compute the probability of unsuccessful handshake due to an error in one of the frames. For instance, if the error was on the third frame, the first two are transmitted correctly and the third is not (and the fourth is not considered because it will not be sent).

### 5.3.3 The Case of Carrier Sense-Based MAC Protocols

In the specific case of carrier sense-based MAC protocols, a fundamental feedback information needed by every node in the network is the probability that the channel is perceived "busy" while a node is trying to transmit its own frame. At the PHY layer, the events that are related to the occurrence of a "busy channel" are different from the events involved with a "successful frame reception". The goal of the carrier sense activity is to detect if the signal power captured by a node's antenna(s) is above some particular power threshold, whereas the reception of a frame deals with the ability of a node's receiver to successfully decode a frame, which depends on many PHY-layer aspects such as modulation/demodulation scheme and receiver design.

Because the carrier sense activity depends on the amount of signal power captured by a node's antenna(s), the *probability that the channel is busy* depends, fundamentally, on

which nodes in the network are transmitting simultaneously, at a given time instant, and their respective contribution to the aggregate signal power captured by the antenna(s) of a node that is listening to the channel (including any background and/or thermal noise). It is important to mention that, depending on PHY-layer aspects such as antenna reception mode (e.g., omni-directional or directional) or channel used during carrier sense, the impact of the activity of other nodes can be significant different from that when the node is actually receiving a frame.

Let $P_{cs}^{i}$ denote the perceived signal power at node $i \in V$ when node $i$ is performing carrier sensing of the channel, and let $\gamma$ denote the signal power threshold above which the channel is considered to be "busy". As mentioned before, the perceived signal power $P_{cs}^{i}$ depends on which nodes $k \in V$ transmit simultaneously at a given time instant, and their respective contribution to the perceived signal power $P_{cs}^{i}$. Therefore, the probability that the channel is detected busy depends on which nodes $k \in V$ are active at the time node $i$ is performing the carrier sense in the channel. Consequently, we need to know which combinations of active nodes $k \in V$ lead to a perceived signal power $P_{cs}^{i}$ greater than the threshold $\gamma$. If $\mathcal{S}_{i}^{r}$ denotes the set of all possible combinations of active nodes $k \in V$ such that $P_{cs}^{i} \geq \gamma$ then, the probability that node $i$ perceives that the channel is busy is given by the probability of occurrence of any of the combinations in $\mathcal{S}_{i}^{r}$. We use the superscript $r$ to indicate that node $i$ senses the channel before transmitting to a node $r$. This is to allow the treatment of different carrier sensing mechanisms that condition the sensing activity on the target receiver $r$ (e.g., the directional virtual carrier sensing protocol [114]). If $c_{i}^{r}$ denotes each of the combinations in $\mathcal{S}_{i}^{r}$, and $\mathcal{C}_{i}^{r}$ is a random variable that indicates the occurrence of a specific combination

$c_i^r \in \mathcal{S}_i^r$, then, from the exclusiveness of the events $\mathcal{C}_i^r = c_i^r \in \mathcal{S}_i^r$, we have

$$P\left\{\text{channel is busy for node } i\right\} = P\left\{P_{cs}^i \geq \gamma\right\} = P\left\{\bigcup_{c_i^r \in \mathcal{S}_i^r} \left\{\mathcal{C}_i^r = c_i^r\right\}\right\}$$

$$= \sum_{c_i^r \in \mathcal{S}_i^r} P\left\{\mathcal{C}_i^r = c_i^r\right\}, \tag{5.7}$$

which is nothing but the sum of the probabilities of the occurrence of all possible combinations of active nodes $k \in V$ such that the perceived signal power $P_{cs}^i$ at node $i$ is greater than the threshold $\gamma$.

## 5.4 Impact of Flow Distribution

So far, we have only considered the computation of the successful handshake probability when a node has a packet to transmit to a *specific receiver*, i.e., the computation of the successful handshake probability *conditioned* on a specific target receiver $r \in V$. In reality, however, each packet that arrives at a node's input queue(s) may be potentially addressed to a distinct receiver within the node's one-hop neighborhood, as specified by the packet's header (in the case of unicast traffic, in particular). Each time this node attempts to transmit a frame, the conditions for having a successful handshake will depend on the selected target receiver, since its location will determine the impact of potential interferers. In addition, each packet may be assigned a different priority, depending on its target destination, data content, or if some sort of per-flow bandwidth allocation scheme is used, with packets being served distinctly according to some queueing scheduling discipline, for example. In fact, even if a single FIFO queue is used, the steady-state distribution of the aggregate flow at a node's input queue may depend on how traffic multiplexing occurs within a certain time period. Therefore,

within a time interval long enough, every time a node $i \in V$ decides to transmit a frame, it will do so by selecting a target receiver according to some probability that will be a function of the factors just considered.

Now, let us denote $\mathcal{R}_i$ the set of nodes to which node $i$ has a packet to transmit during the course of some observation time interval long enough, and let $\rho_i^r$ be the probability that node $r \in \mathcal{R}_i$ is the intended receiver of $i$ at any instant within this time interval. Given that, the steady-state probability $q_i$ that node $i$ has a successful handshake will be given by

$$\begin{aligned} q_i &= P\{\text{successful exchange}\} = \sum_{r \in \mathcal{R}_i} P\{\text{successful exchange} \cap\ r \text{ is the receiver}\} \\ &= \sum_{r \in \mathcal{R}_i} P\{\text{successful exchange} \mid r\} P\{r \text{ is the receiver}\} \\ &= \sum_{r \in \mathcal{R}_i} q_i^r \rho_i^r . \end{aligned} \tag{5.8}$$

## 5.5 Inter-Layer Dependence: The Nonlinear Multivariate System

At the core of the computation of the probability of successful frame reception in Eq. (5.4), the probability of successful handshake in Eqs. (5.5), (5.6), and (5.8), and the busy channel probability in Eq. (5.7), is the computation of the probabilities of possible combinations of active nodes (interferers) in the network at a given time instant. These probabilities are, in effect, probabilities of joint events related to the transmission probabilities (scheduling rates) of all nodes in the network. Therefore, all the aforementioned feedback probabilities depend, fundamentally, *on the transmission probabilities of every node in the network*.

Indeed, such fundamental dependence on the nodes' schedule discipline is a direct consequence of the inherent broadcast nature of the radio channels in ad hoc networks.

Consequently, it is reasonable to expect that many (or all) of the PHY-related input/feedback probabilities contained in the vector $\boldsymbol{\varphi}_i$ of node $i \in V$ depend, fundamentally, on the underlying scheduling discipline of every node in $V$, i.e., on the vector of transmission probabilities $\boldsymbol{\tau} = [\tau_1\, \tau_2\, \cdots\, \tau_n]^T$. In other words, many of the input/feedback information conveyed to the MAC protocol at each node can be affected by *the scheduling discipline imposed by the MAC protocol itself*. Such observation clearly shows that the dynamics of the MAC layer is tightly connected to the dynamics of the PHY layer (and vice-versa).

Because not all input/feedback probabilities contained in $\boldsymbol{\varphi}_i$ will be dependent on $\boldsymbol{\tau}$, we divide the variables in $\boldsymbol{\varphi}_i$ in two sets: the variables that *fundamentally depend* on the transmission probability vector $\boldsymbol{\tau}$, and the ones that do not. Let the $l$-tuple $\boldsymbol{\nu}_i = [\nu_{i1}\, \nu_{i2}\, \ldots\, \nu_{il}]^T$ be a vector containing the $l$ entries of $\boldsymbol{\varphi}_i$ that depend on $\boldsymbol{\tau}$, and $\boldsymbol{\omega}_i = [\omega_{i1}\, \omega_{i2}\, \ldots\, \omega_{im}]^T$ be an $m$-tuple with the remaining entries of $\boldsymbol{\varphi}_i$ (where $\boldsymbol{\varphi}_i$ is an $(l+m)$-tuple). For the vector $\boldsymbol{\omega}_i$, we assume that all the input/feedback information it contains is *known* and characterized *a priori*. On the other hand, for each $\nu_{ik} \in \boldsymbol{\nu}_i \subseteq \boldsymbol{\varphi}_i,\ k = 1, \ldots, l$, we postulate that there exists some (linear or non-linear) function $g_{ik}(\cdot)$ such that

$$\nu_{ik} = g_{ik}(\boldsymbol{\tau}), \quad k = 1, 2, \ldots, l, \quad \forall\, i \in V. \tag{5.9}$$

Equation (5.9) represents the mapping that is performed on the scheduling rates $\boldsymbol{\tau}$ to generate the input/feedback information $\nu_{ik}$ needed by the MAC layer at node $i$. Essentially, Eqs. (5.1) and (5.9) form a *coupled nonlinear multivariate system* on the variables $\tau_i$ and $\nu_{ik}$, $k = 1, \ldots, l,\ \forall\, i \in V$, (the $\boldsymbol{\omega}_i$'s, are assumed to be known *a priori*). Together, they allows us to consider not only the interdependencies between the PHY and MAC layers, but also the interdependencies among *all nodes* in the network. Nevertheless, solving such a

nonlinear system in arbitrary topologies constitutes an extremely complex task if we consider the number of possibilities for the network sizes and the functional forms for $h_i(\cdot)$ and $g_{ik}(\cdot)$. Furthermore, checking for the existence of a solution for the system can be very cumbersome, if not impossible. Hence, to simplify our modeling problem and to better understand the effects of different protocol parameters on the probabilities $\tau_i$ and $\nu_{ik}$, we *linearize* the above nonlinear system. Next section we present our approach to this problem.

## 5.6 Making the Model Tractable: The Interference Matrices

In this section, we present a linear approximation to the coupled nonlinear multivariate system formed by Eqs. (5.1) and (5.9), which will lead us to the introduction of the concept of *interference matrices*. To begin with, we present linear approximations to the successful handshake probability in Eq. (5.6), and the probability that the channel is sensed busy in Eq. (5.7).

### 5.6.1 Linear Approximation to the Successful Handshake Probability

Let us consider the computation of the probability $q_i^r$ that node $i$ has a successful handshake with node $r$. From Eqs. (5.5) and (5.6), one of the key problems in computing $q_i^r$ is the knowledge of the probabilities of the combinations $\{c_{ik}^r\}_{k=1,\ldots,2^{n-2}}$ of active interferers, as opposed to the successful reception probability $f(\cdot)$, which is known for any given MAI level. The exact functional form of the joint probabilities depends on the specific MAC protocol in use. However, finding an exact functional forms is inherently a difficult task, given the complexity of the interactions among the nodes, specially under multihop scenarios.

Moreover, because the number of possible combinations of active interferers increases exponentially with the number of nodes, computing the probabilities of all combinations becomes prohibitive with just a few tens of nodes. Fortunately, we can attain a linear approximation to the computation of $q_i^r$ for *any* multihop ad hoc network by taking advantage of the *necessary* behavior of *any* MAC protocol. More specifically, we exploit the following three considerations:

C1) **High contention**: When contention among nodes is high, the probability $\tau_k$ that node $k \in V$ attempts to transmit a frame, at any time, is expected to be arbitrarily small.

C2) **MAC efficiency**: If nodes $j$ and $k$ can interfere with each other's frame exchanges *significantly*—directly or indirectly—e.g., they are located up to two hops away from each other, it is expected that the MAC protocol operates in a way that the *probability that node $j$ schedules a transmission at a particular time instant, given that node $k$ has already scheduled a transmission at the same time instant, is arbitrarily small*. This is what the desired operation of *any* MAC protocol should be: to prevent interfering nodes from scheduling transmissions at about the same time, "clearing the floor," and guaranteeing that a successful handshake occurs. The more efficient the MAC protocol is, the smaller this conditional probability becomes.

C3) **Impact of "Cascade Effect"**: If two nodes $j$ and $k$ are very distant from each other, such that their signal powers cannot interfere significantly with each other's frame exchanges (or have their signal powers blocked somehow), their *decisions* to initiate a frame transmission at any time are considered to be independent of each other. In reality, though, two nodes very distant from each other can still have an *indirect* impact on each other's trans-

mission due to a "cascade effect": a node's decision to transmit a frame depends on its neighbors' decisions to transmit, which, in turn, depends on their neighbor's neighbors decisions to transmit, and so on. However, for all practical purposes, transmission decisions can be considered independent if nodes are sufficiently distant from each other (e.g., more than two hops away). Otherwise, consideration C2 applies.

Given the above considerations, we can now focus on the computation of the probabilities of the joint events contained in the combinations $\{c_{ik}^r\}_{k=1,\ldots,2^{n-2}}$. Among all possible combinations, we are particularly interested in two cases: (1) the combination corresponding to the event where "*no node transmits at the given time instant*," and (2) the combinations corresponding to the events where "*only node $k \in V$ transmits at the given time instant*." If the event "*no node transmits at the given time instant*" occurs, the MAI level at node $r$ is null and, consequently, the $\text{SINR}_i^r$ is the highest possible, maximizing the conditional probability $f(\cdot)$ of a successful frame reception at $r$. In the second case, where "*only node $k \in V$ transmits at the given time instant*," the impact of node $k$ alone is taken into account on the degradation of $\text{SINR}_i^r$ during a frame reception at node $r$, i.e., the "weight" of the interference caused by node $k$ at node $r$ is evaluated.

Let $A_i,\ i \in V$, represent the event that "node $i$ transmits a frame at the given time instant". Hence, $P\{A_i\} = \tau_i$. Now, the event "no node transmits at the given time instant" is represented by the joint event $\bigcap_{i=1}^{n} \overline{A_i}$, where $\overline{A_i}$ is the complement set of $A_i$. From DeMorgan's rules,

$$P\left\{\bigcap_{i=1}^{n} \overline{A_i}\right\} = P\left\{\overline{\bigcup_{i=1}^{n} A_i}\right\} = 1 - P\left\{\bigcup_{i=1}^{n} A_i\right\}. \tag{5.10}$$

where

$$P\left\{\bigcup_{i=1}^{n} A_i\right\} = \sum_{i=1}^{n} P\left\{A_i\right\} - \sum_{j}\sum_{k} P\{A_j \cap A_k\} + \sum_{j}\sum_{k}\sum_{l} P\left\{A_j \cap A_k \cap A_l\right\} + \cdots$$
$$\cdots + (-1)^{n+1} P\left\{\bigcap_{i=1}^{n} A_i\right\}. \tag{5.11}$$

Therefore, the computation of $P\left\{\bigcup_{i=1}^{n} A_i\right\}$ in Eq. (5.11) requires the knowledge of the probabilities of simultaneous transmissions from all possible subsets of nodes. However, according to consideration C2, if nodes $j$ and $k$ can interfere to each other's frame exchanges significantly, it is expected that the MAC protocol will do its best to prohibit both nodes from transmitting at about the same time, i.e., we should expect that $P\{A_j|A_k\} \ll 1$. In addition, because $P\{A_k\} \ll 1$ under high contention (from consideration C1), for any two nodes $j$ and $k$ we should have

$$P\{A_j \cap A_k\} = P\{A_j \mid A_k\}P\{A_k\} \approx 0. \tag{5.12}$$

On the other hand, from consideration C3, if nodes $j$ and $k$ are very distant (or physically blocked) from each other, their schedulings can be considered practically independent. In such cases, and under high contention,

$$P\left\{A_j \cap A_k\right\} = P\{A_j\}P\{A_k\} = \tau_j\tau_k \approx 0. \tag{5.13}$$

Extending our reasoning to the probabilities of the joint events that three or more nodes transmit at the same time in Eq. (5.11), we can approximate Eq. (5.10) by

$$P\left\{\bigcap_{i=1}^{n} \overline{A_i}\right\} \approx 1 - \sum_{i=1}^{n} P\left\{A_i\right\}. \tag{5.14}$$

Note that, if nodes are allowed to transmit independently of each other, regardless of the state of their neighbors (e.g., ALOHA), all the joint probabilities in Eq. (5.11) reduce

to product forms like in Eq. (5.13) and, under high contention, Eq. (5.14) approaches equality. In the other extreme case, if the MAC protocol is scheduled-based and can guarantee that one and only one node transmits at any given time, i.e., $A_i \cap A_j = \emptyset$ for all $i \neq j$, we simply have[1]

$$P\left\{\bigcup_{i=1}^{n} A_i\right\} = \sum_{i=1}^{n} P\left\{A_i\right\}, \tag{5.15}$$

and, in this case, Eq. (5.14) holds with equality. Such a situation should be expected from an efficient MAC protocol operating in a single-channel fully-connected network, for example. Indeed, such exclusiveness of events is what is generally aimed in the operation of an efficient MAC protocol with respect to nodes within some neighborhood sharing the same channel in a wireless multihop ad hoc network.

Now, let us consider the events where "just one node transmits at the given time instant". For the sake of argument, let us assume that node 1 is the transmitting node. Therefore, we are interested in computing the probability of the event $\left(\bigcap_{i=2}^{n} \overline{A_i}\right) \bigcap A_1$, which is

$$\begin{aligned} P\left\{\left(\bigcap_{i=2}^{n} \overline{A_i}\right) \bigcap A_1\right\} &= P\left\{\bigcap_{i=2}^{n} \overline{A_i} \,\middle|\, A_1\right\} P\{A_1\} = \left[1 - P\left\{\bigcup_{i=2}^{n} A_i \,\middle|\, A_1\right\}\right] P\{A_1\} \\ &= P\{A_1\} - P\left\{\bigcup_{i=2}^{n} A_i \,\middle|\, A_1\right\} P\{A_1\}. \end{aligned} \tag{5.16}$$

where

$$\begin{aligned} P\left\{\bigcup_{i=2}^{n} A_i \middle| A_1\right\} = \sum_{i=1}^{n} P\left\{A_i|A_1\right\} - \sum_{j,k} P\{A_j \cap A_k|A_1\} + \cdots \\ \cdots + (-1)^{n+1} P\left\{\bigcap_{i=2}^{n} A_i \middle| A_1\right\}. \end{aligned} \tag{5.17}$$

Using the same arguments based on considerations C1 to C3, and observing that all

[1] This is a corollary of the axioms of probability.

terms in Eq. (5.17) are multiplied by $P\{A_1\} \ll 1$ in Eq. (5.16), we obtain

$$P\left\{\left(\bigcap_{i=2}^{n}\overline{A_i}\right)\bigcap A_1\right\} \approx P\{A_1\}. \tag{5.18}$$

Having considered approximations to the probabilities of some of the events $c_{ik}^r, k = 1, \ldots, 2^{n-2}$, we need to look at the computation of the conditional probabilities relating the two sets of active interferers $\mathcal{C}_r^i$ and $\mathcal{C}_i^r$ in Eqs. (5.5) or (5.6). As mentioned in Section 5.3.2, the set of active interferers during the reception of an ACK may be dependent on which nodes were active during the transmission of the previous DATA frame. Again, such dependencies are intrinsically related to the MAC protocol in use and, for this reason, we will focus on two cases that represent the two extreme behaviors observed in the operation of a MAC protocol. In the first case, we assume that the set of active nodes $\mathcal{C}_r^i$ during the reception of an ACK is the same as the set $\mathcal{C}_i^r$ of active nodes during reception of the DATA frame. The rationale for this assumption is that ACK frames are usually of fixed size and much smaller than DATA frames. Therefore, during the reception of an ACK, it is very likely that the nodes that were active during the DATA frame transmission may still be active during the subsequent ACK transmission (specially if DATA frames are of variable sizes). In this case, we have

$$P\left\{\mathcal{C}_r^i = c_{ik}^r | \text{ DATA suc.}, \mathcal{C}_i^r = c_{ik}^r\right\} = 1. \tag{5.19}$$

Even in the case when DATA frames are of fixed size, nodes may become active at slightly different times from the instant that a node started transmitting a DATA frame. This could happen because of the delays generally incurred when switching among modes (receive/transmit, idle/transmit, etc.). In this case, interfering nodes could become active when a DATA frame was already being transmitted in the channel, overlapping with both DATA

and subsequent ACK frames, specially if ACKs are sent back without much delay, almost immediately after receiving the DATA frame. In the other extreme case, both sets $\mathcal{C}_r^i$ and $\mathcal{C}_i^r$ can be considered independent of each other, i.e.,

$$P\left\{\mathcal{C}_r^i = c_{rl}^i \,|\, \text{DATA suc.}, \mathcal{C}_i^r = c_{ik}^r\right\} = P\left\{\mathcal{C}_r^i = c_{rl}^i\right\}, \tag{5.20}$$

in which case we have a scenario where interfering nodes can become active independently of what happened during the previous DATA frame transmission. This is likely the most aggressive scenario as far as interference is concerned, because it allows for the occurrence of sets of interferers that would not normally happen in the operation of many MAC protocols.

For the computation of $q_i^r$ to become complete, we need to treat the case when DATA frames are of variable size, as expressed in Eq. (5.6). Again, for tractability, we assume that the set of active interferers is independent of the frame size, i.e.,

$$P\left\{\mathcal{C}_i^r = c_{ik}^r | B = b\right\} = P\left\{\mathcal{C}_i^r = c_{ik}^r\right\}. \tag{5.21}$$

Given all previous considerations, we can now compute an approximation for $q_i^r$. We will consider the case where the set $\mathcal{C}_r^i$ of active nodes during reception of an ACK is the same as the set $\mathcal{C}_i^r$ of active nodes during reception of the DATA frame. From Eq. (5.6),

$$\begin{aligned} q_i^r &= \sum_k \sum_l \sum_b f\left(c_{rl}^i\right) f\left(c_{ik}^r\right) P\left\{\mathcal{C}_r^i = c_{rl}^i | \text{DATA suc.}, B = b, \mathcal{C}_i^r = c_{ik}^r\right\} \times \\ &\quad \times P\{\mathcal{C}_i^r = c_{ik}^r | B = b\} P\{B = b\} \\ &= \sum_k \sum_b f\left(c_{rk}^i\right) f\left(c_{ik}^r\right) P\{\mathcal{C}_i^r = c_{ik}^r\} P\{B = b\} \\ &= \sum_k \overline{f\left(c_{rk}^i\right) f\left(c_{ik}^r\right)} P\left\{\mathcal{C}_i^r = c_{ik}^r\right\}, \end{aligned} \tag{5.22}$$

where $\overline{f(\cdot)}$ indicates the average of $f(\cdot)$ with respect to the frame size $B$. If we take just the two sets of events previously considered, $q_i^r$ is approximated by

$$q_i^r \approx \overline{f\left(c_{io}^r\right)f\left(c_{ro}^i\right)}P\left\{\text{no node transmits}\right\} + \sum_k \overline{f\left(c_{rk}^i\right)f\left(c_{ik}^r\right)}P\left\{\text{only } k \text{ transmits}\right\} \quad (5.23)$$

The probability of the events above are given by Eqs. (5.14) and (5.18) respectively, where $P\{A_k\} = \tau_k,\ \forall\, k \in V$. Hence,

$$q_i^r \approx \pi_i^r \left(1 - \sum_{k\in V} \tau_k\right) + \sum_{k\in V} \pi_{ik}^r \tau_k, \quad (5.24)$$

where $\pi_i^r = \overline{f(c_{i0}^r)f(c_{r0}^i)}$, and $\pi_{ik}^r = \overline{f(c_{rk}^i)f(c_{ik}^r)}$. Collecting the terms in $\tau_k$, we have

$$\begin{aligned} q_i^r &\approx \pi_i^r - \sum_{k\in V} \pi_i^r \tau_k + \sum_{k\in V} \pi_{ik}^r \tau_k = \pi_i^r - \sum_{k\in V} \left(\pi_i^r - \pi_{ik}^r\right)\tau_k \\ &= \pi_i^r - \sum_{k\in V} c_{ik}^r \tau_k, \end{aligned} \quad (5.25)$$

where $c_{ik}^r = (\pi_i^r - \pi_{ik}^r)$. It is interesting to observe that $c_{ik}^r$ in Eq. (5.25) provides the "weight" of node $k \in V$ with respect to its impact on the successful handshake probability between nodes $i$ and $r$. More specifically, in the event that "no node transmits," the product of probabilities of successful frame reception $f(\cdot)$ attains its maximum, $\pi_i^r$, because there is no MAI. If the potential interferer $k$ is far from both nodes $i$ and $r$, the contribution of its signal power to the MAI level will be practically null and, in this case, $\pi_{ik}^r \to \pi_i^r$, i.e., $c_{ik}^r \to 0$, canceling the impact of node $k$ in the successful handshake probability $q_i^r$. On the other hand, if node $k \in V$ is very close to both (or either) nodes $i$ and $r$, its signal power can be sufficiently high to deteriorate the SINR at both (or either) nodes, compromising their handshake. In that case, $\pi_{ik}^r \to 0$, i.e., $c_{ik}^r \to \pi_i^r$, and the "weight" of node $k$ is equivalent to saying that "node $k$ should not transmit when nodes $i$ and $r$ are attempting to establish a handshake."

Finally, let us consider the impact of the flow distribution, as described in Section 5.4. For that, we take the probability of successful handshake to a specific receiver, as computed in Eq. (5.25), and substitute into Eq. (5.8), which gives the overall steady-state probability $q_i$ that node $i$ has a successful handshake with the nodes $r \in \mathcal{R}_i$. Hence,

$$\begin{aligned} q_i &= \sum_{r \in \mathcal{R}_i} \left( \pi_i^r - \sum_{k \in V} c_{ik}^r \tau_k \right) \rho_i^r = \sum_{r \in \mathcal{R}_i} \pi_i^r \rho_i^r - \sum_{r \in \mathcal{R}_i} \sum_{k \in V} c_{ik}^r \tau_k \rho_i^r \\ &= \pi_i - \sum_{k \in V} c_{ik} \tau_k, \end{aligned} \tag{5.26}$$

where $\pi_i = \sum_{r \in \mathcal{R}_i} \pi_i^r \rho_i^r$ and $c_{ik} = \sum_{r \in \mathcal{R}_i} c_{ik}^r \rho_i^r$.

### 5.6.2 Linear Approximation to the Busy Channel Probability

In this Section, we obtain a linear approximation to the *busy channel probability* introduced in Section 5.3.3. For this purpose, we use similar arguments as the ones used previously to obtain a linear approximation to the successful handshake probability. From our remarks in Section 5.3.3, if a node $i \in V$ is in carrier-sense mode, the probability that node $i$ perceives that the channel is "busy" is the probability that $P_{cs}^i \geq \gamma$, where $P_{cs}^i$ is the aggregate signal power captured by the antenna(s) of node $i$, and $\gamma$ is the signal power threshold above which the channel is considered to be "busy". As we noticed before, such probability depends on which nodes in $V$ transmit simultaneously over the channel at a given time instant, and what is their contribution to the aggregate signal power captured by the antenna(s) of node $i$ (including any background and/or thermal noise). So, if $\mathcal{S}_i^r$ denotes the set of all possible combinations of active nodes $k \in V$ such that $P_{cs}^i \geq \gamma$, then the probability that node $i$ perceives that the channel is busy is given by the probability that any of the combinations

of active nodes in $\mathcal{S}_i^r$ occurs. If $c_i^r$ denotes each of the combinations in $\mathcal{S}_i^r$, and $\mathcal{C}_i^r$ is a random variable indicating the occurrence of a specific combination $c_i^r \in \mathcal{S}_i^r$, then, from the exclusiveness of the events $\mathcal{C}_i^r = c_i^r \in \mathcal{S}_i^r$, we showed in Eq. (5.7) that

$$P\left\{\text{channel is busy for node } i\right\} = P\left\{P_{cs}^i \geq \gamma\right\} = P\left\{\bigcup_{c_i^r \in \mathcal{S}_i^r} \left\{\mathcal{C}_i^r = c_i^r\right\}\right\}$$

$$= \sum_{c_i^r \in \mathcal{S}_i^r} P\left\{\mathcal{C}_i^r = c_i^r\right\},$$

Hence, to obtain a linear approximation, we pick all combinations $c_i^r \in \mathcal{S}_i^r$ in which "only node $k$ transmits and its individual contribution to the aggregate signal power $P_{cs}^i$ is greater than or equal to $\gamma$ (including background and/or thermal noise)." In other words, we approximate Eq. (5.18) by

$$P\left\{\text{channel is busy for node } i\right\} \approx \sum_{c_i^r \in \mathcal{S}_i^r} P\left\{\mathcal{C}_i^r = c_i^r \text{ where only one node transmits}\right\}, \tag{5.27}$$

From arguments similar to the ones used Section 5.6.1, and from Eq. (5.16), we have

$$P\left\{\text{channel is busy for node } i\right\} \approx \sum_{k \in \mathcal{S}_i^r} \tau_k = \sum_{k \in V} d_{ik}^r \tau_k, \tag{5.28}$$

where

$$d_{ik}^r = \begin{cases} 1, & \text{if } k \in \mathcal{S}_i^r \subseteq V \\ 0, & \text{otherwise.} \end{cases} \tag{5.29}$$

Now, taking into account all nodes to which node $i$ has a packet to deliver, i.e., taking into account the impact of flow distribution, we have

$$g_i = \sum_{r \in \mathcal{R}_i} \left( \sum_{k \in V} d_{ik}^r \tau_k \right) \rho_i^r = \sum_{k \in V} \left( \sum_{r \in \mathcal{R}_i} d_{ik}^r \rho_i^r \right) \tau_k = \sum_{k \in V} d_{ik} \tau_k, \tag{5.30}$$

Observe that, if node $k \in V$ is such that $d_{ik}^r = 1,\ \forall\, r \in \mathcal{R}_i$, then $\sum_{r\in\mathcal{R}_i} d_{ik}^r \rho_i^r = 1$, indicating that node $k$ has a direct impact on the carrier sensing mechanism when $i$ attempts to transmit a frame to all of its potential receivers in $\mathcal{S}_i^r$.

### 5.6.3 The Interference Matrices

Now that we have shown how to obtain a linear approximation to two examples of feedback probabilities, we will proceed in this section with the linear approximation of the general problem stated in Eqs. (5.1) and (5.9). As defined in Section 5.5, the vector $\boldsymbol{\varphi}_i$ of input/feedback probabilities is a vector containing all entries of $\boldsymbol{\nu}_i$ and $\boldsymbol{\omega}_i$, i.e., $\boldsymbol{\varphi}_i$ is the $(m+l)$-tuple $\boldsymbol{\varphi}_i = [\nu_{i1}\ \nu_{i2}\ \ldots\ \nu_{il}\,\omega_{i1}\ \omega_{i2}\ \ldots\ \omega_{im}]^T$. If $h_i(\boldsymbol{\varphi}_i)$ is an infinitely often differentiable function within a region around the point $\boldsymbol{\varphi}_i^o = [\nu_{i1}^o\ \nu_{i2}^o\ \ldots\ \nu_{il}^o\,\omega_{i1}^o\ \omega_{i2}^o\ \ldots\ \omega_{il}^o]^T$ in the $(m+l)$-dimensional space, then the Taylor series expansion of $h_i(\boldsymbol{\varphi}_i)$ around the point $\boldsymbol{\varphi}_i^o$ is given by [135]

$$h_i(\boldsymbol{\varphi}_i) = \sum_{j=0}^{\infty} \left\{ \frac{1}{j!} \left[ \sum_{k=1}^{n} (\varphi_{ik} - \varphi_{ik}^o) \frac{\partial}{\partial \varphi'_{ik}} \right]^j h(\boldsymbol{\varphi}'_i) \right\}_{\boldsymbol{\varphi}'_i = \boldsymbol{\varphi}_i^o}. \tag{5.31}$$

Hence, a first-order approximation of $\tau_i = h_i(\boldsymbol{\varphi}_i)$ around the point $\boldsymbol{\varphi}_i^o = [\nu_{i1}^o\ \nu_{i2}^o\ \ldots\ \nu_{il}^o\ \omega_{i1}^o\ \omega_{i2}^o\ \ldots\ \omega_{il}^o]^T$ is simply

$$\tau_i = h_i(\boldsymbol{\varphi}_i) \approx a_{i0} + \sum_{k=1}^{l} \alpha_{ik}\nu_{ik} + \sum_{k=1}^{m} \lambda_{ik}\omega_{ik}, \tag{5.32}$$

where

$$a_{i0} = h_i(\boldsymbol{\varphi}_i^o) - \sum_{k=1}^{l} \nu_{ik}^o \left.\frac{\partial h_i}{\partial \nu_{ik}}\right|_{\boldsymbol{\varphi}'_i = \boldsymbol{\varphi}_i^o} - \sum_{k=1}^{m} \omega_{ik}^o \left.\frac{\partial h_i}{\partial \omega_{ik}}\right|_{\boldsymbol{\varphi}'_i = \boldsymbol{\varphi}_i^o}, \tag{5.33}$$

and

$$\alpha_{ik} = \left.\frac{\partial h_i}{\partial \nu_{ik}}\right|_{\boldsymbol{\varphi}'_i = \boldsymbol{\varphi}_i^o}, \quad \lambda_{ik} = \left.\frac{\partial h_i}{\partial \omega_{ik}}\right|_{\boldsymbol{\varphi}'_i = \boldsymbol{\varphi}_i^o}. \tag{5.34}$$

The subscript $i$ in the MAC operation $h_i(\cdot)$ refers to node $i$'s own parameters and configuration of the MAC protocol in use. Usually, all nodes operate under the same MAC settings, under the same parameters. In this case, $h_i(\cdot) = h(\cdot),\ \forall\, i \in V$, and therefore, $\alpha_{ik} = \alpha_k$ and $\lambda_{ik} = \lambda_k,\ \forall\, i \in V$. Consequently, Eq. (5.32) simplifies to

$$\tau_i = h_i(\boldsymbol{\varphi}_i) \approx \alpha_0 + \sum_{k=1}^{l} \alpha_k \nu_{ik} + \sum_{k=1}^{m} \lambda_k \omega_{ik}, \tag{5.35}$$

which we will assume for the rest of our work.

The results obtained for the *successful handshake probability* and the *busy channel probability* in Eqs. (5.26) and Eq. (5.30), respectively, suggest the shape that we should expect for the linear approximations of the feedback probabilities $\nu_{ik}$ that depend on the transmission probabilities $\boldsymbol{\tau}$ in Eq. (5.9). In other words,

$$\nu_{ik} = g_{ik}(\boldsymbol{\tau}) \approx \mu^i_{k0} + \sum_{\substack{j \in V \\ j \neq i}} \mu^i_{kj} \tau_j, \quad k = 1, 2, \ldots, l, \tag{5.36}$$

where, as in Eqs. (5.26) and (5.30), the coefficients $\mu^i_{kj}$ are expected to satisfy $0 \leq \mu^i_{kj} \leq 1$, since they act as "weights" to the contribution of each $\tau_j$ to the overall probability $\nu_{ik}$. Hence, substituting Eq. (5.36) back into Eq. (5.35), we have

$$\tau_i = a_0 + \sum_{k=1}^{l} \alpha_k \left( \mu^i_{k0} + \sum_{\substack{j \in V \\ j \neq i}} \mu^i_{kj} \tau_j \right) + \sum_{k=1}^{m} \lambda_k \omega_{ik} = \pi_i + \sum_{\substack{j \in V \\ j \neq i}} \phi_{ij} \tau_j + \sum_{k=1}^{m} \lambda_k \omega_{ik}, \tag{5.37}$$

where

$$\pi_i = a_0 + \sum_{k=1}^{l} \alpha_k \mu^i_{k0}, \tag{5.38}$$

and

$$\phi_{ij} = \sum_{k=1}^{l} \alpha_k \mu^i_{kj}. \tag{5.39}$$

In matrix notation, we have

$$\boldsymbol{\tau} = \boldsymbol{\pi} + \boldsymbol{\Phi}\boldsymbol{\tau} + \boldsymbol{\Omega}\boldsymbol{\lambda}, \tag{5.40}$$

where $\boldsymbol{\pi} = [\pi_1\, \pi_2 \ldots \pi_n]^T$, $\boldsymbol{\Phi}$ is the $n \times n$ matrix with elements $\phi_{ij}$, $\boldsymbol{\Omega}$ is the $n \times m$ matrix with elements $\omega_{ij}$, and $\boldsymbol{\lambda} = [\lambda_1\, \lambda_2\, \ldots\, \lambda_m]^T$. By rearranging the terms in Eq. (5.40), we obtain the linear system

$$(\mathbf{I} - \boldsymbol{\Phi})\boldsymbol{\tau} = \boldsymbol{\pi} + \boldsymbol{\Omega}\boldsymbol{\lambda}, \tag{5.41}$$

where $\mathbf{I}$ is the $n \times n$ identity matrix. In its essence, the matrix $\boldsymbol{\Phi}$ conveys all the information about how each node interferes with every other node in the network based on the effect of the PHY and MAC layers. For this reason, we refer to $\boldsymbol{\Phi}$ as the **interference matrix**.

The linear system in Eq. (5.41) has a solution if and only if, the vector $\boldsymbol{\pi} + \boldsymbol{\Omega}\boldsymbol{\lambda}$ is in the column space of the matrix $\boldsymbol{\Gamma} = \mathbf{I} - \boldsymbol{\Phi}$, i.e., it is a linear combination of the columns of $\boldsymbol{\Gamma}$. Given the generality of the matrix $\boldsymbol{\Gamma}$, which can change every time we consider a different network topology (through the interference matrix $\boldsymbol{\Phi}$), we need to find out which matrices $\boldsymbol{\Gamma}$ allow the linear system in Eq. (5.41) to have a solution. In fact, we will aim higher and ask, ultimately, if the linear system in Eq. (5.41) has a solution *regardless of network topology*. Indeed, the answer to this question is *yes* and is a consequence of Theorem 1 below.

**Definition 1** *A square matrix* $\mathbf{A}$ *is* **strictly diagonally dominant** *if the absolute value of each diagonal element is greater than the sum of the absolute values of the non-diagonal elements in its row. That is,*

$$\sum_{j \neq i} |a(i,j)| < |a(i,i)|.$$

**Property 1** *Every strictly diagonally dominant matrix in nonsingular [62].*

**Theorem 1** *The matrix $\mathbf{\Gamma} = \mathbf{I} - \mathbf{\Phi}$ is nonsingular if*

$$\sum_{j \neq i} \left| \sum_{k=1}^{l} -\alpha_k \mu_{kj}^i \right| < 1.$$

**Proof**: By construction, the diagonal elements of matrix $\mathbf{\Gamma}$ are all positive and equal to one, whereas its off-diagonal elements $\phi_{ij}$ are given by Eq. (5.39). Hence, from Definition 1, the matrix $\mathbf{\Gamma}$ is strictly diagonally dominant if and only if

$$\sum_{j \neq i} |-\phi_{ij}| = \sum_{j \neq i} \left| \sum_{k=1}^{l} -\alpha_k \mu_{kj}^i \right| < 1, \quad \forall\, i \in V. \tag{5.42}$$

If the matrix $\mathbf{\Gamma}$ satisfies the condition above, it is nonsingular according to Property 1. □

**Corollary 1** *Given $n > 1$, if*

$$\sum_{k=1}^{l} |-\alpha_k| < \frac{1}{(n-1)},$$

*the matrix $\mathbf{\Gamma} = \mathbf{I} - \mathbf{\Phi}$ is nonsingular regardless of network topology and physical layer parameters.*

**Proof**: From Theorem 1, the matrix $\mathbf{\Gamma}$ is nonsingular if

$$\sum_{j \neq i} \left| \sum_{k=1}^{l} -\alpha_k \mu_{kj}^i \right| < 1, \quad \forall\, i \in V. \tag{5.43}$$

But,

$$\sum_{j \neq i} \left| \sum_{k=1}^{l} -\alpha_k \mu_{kj}^i \right| \leq \sum_{j \neq i} \sum_{k=1}^{l} \left| -\alpha_k \mu_{kj}^i \right| = \sum_{j \neq i} \sum_{k=1}^{l} |-\alpha_k| \left| \mu_{kj}^i \right|. \tag{5.44}$$

From Eq. (5.36), the coefficients $\mu_{kj}^i$ reflect the impact of the topology and physical layer parameters and, from our earlier remarks, they satisfy $0 \leq \mu_{kj}^i \leq 1$. Therefore,

$$\sum_{j \neq i} \left| \sum_{k=1}^{l} -\alpha_k \mu_{kj}^i \right| \leq \sum_{j \neq i} \sum_{k=1}^{l} |-\alpha_k| \left| \mu_{kj}^i \right| \leq \sum_{j \neq i} \sum_{k=1}^{l} |-\alpha_k| = (n-1) \sum_{k=1}^{l} |-\alpha_k|. \tag{5.45}$$

If the upper bound satisfies the condition of strictly diagonally dominance, the sum $\sum_{j\neq i}\left|\sum_{k=1}^{l}-\alpha_k\mu_{kj}^{i}\right|$ will also do. Therefore, if we apply the condition of strictly diagonally dominance with respect to the diagonal elements of $\mathbf{\Gamma}$, we have

$$(n-1)\sum_{k=1}^{l}|-\alpha_k|<1\Rightarrow\sum_{k=1}^{l}|-\alpha_k|<\frac{1}{(n-1)}, \tag{5.46}$$

and we guarantee that $\mathbf{\Gamma}$ is nonsingular regardless of network topology and physical layer parameters. □

Theorem 1 and Corollary 1 provide sufficient conditions for the matrix $\mathbf{\Gamma}=\mathbf{I}-\mathbf{\Phi}$ to be nonsingular. Consequently, the linear system in Eq. (5.41) can be solved, and the transmission probability vector $\boldsymbol{\tau}$ is finally given by

$$\boldsymbol{\tau}=\mathbf{\Gamma}^{-1}\boldsymbol{\pi}+\mathbf{\Gamma}^{-1}\mathbf{\Omega}\boldsymbol{\lambda}. \tag{5.47}$$

**Note 1**: Considering the fact that the coefficients $\alpha_k$ are functions of the parameters of the underlying MAC protocol, and the $\mu_{kj}^{i}$ reflect the impact of the topology and the physical layer parameters, the condition stated in Theorem 1 provides, in fact, a *design rule* for choosing *feasible* PHY/MAC parameters for a given network. In other words, Theorem 1 works as a design tool for network dimensioning and optimization. To illustrate that, we give an example of the application of Theorem 1 in the design of feasible IEEE 802.11 networks in Chapter 6. By applying the condition stated in Theorem 1, we show that the networks become more fair regarding the sharing of channel access among competing nodes while the average network throughput is kept practically intact;

**Note 2**: Likewise, the condition stated in Corollary 1 suggests a design rule for choosing feasible MAC parameters for a given network of size $n$ independent of physical

layer parameters. In other words, depending on the size of the network, Corollary 1 imposes a condition for having a solvable system with respect to the parameters of the chosen MAC protocol.

**Note 3**: It is important to mention that, although we have provided only a *sufficient condition* in Theorem 1, we believe that such a condition is a *necessary* one in order to have a solvable system. In Chapter 6, we investigated simulation results for IEEE 802.11 networks and we found that, when topologies did not satisfy the sufficient condition, they would contain some nodes obtaining zero throughput. This is a clear indication that the network is not well-posed in terms of chosen PHY/MAC parameters. Likewise, for the same topologies, the linear system would provide inconsistent results, like the generation of small negative probabilities!

**Note 4**: In the worst case scenario, the linear system in Eq. (5.41) can be computed in up to $O(n^3)$ operations (where $n$ is the number of nodes). Depending on the symmetry of the problem, this complexity can be reduced to $O(n)$ [57]. In contrast, in the work by Boorstyn et al. [13], which aimed to obtain the scheduling rates of a CSMA network corresponding to given desired link traffic rates, the complexity of the algorithm is exponential in general, and it grows quadratically or cubically with the *number of links* for most networks on the order of 100 nodes. Therefore, our modeling framework is quite scalable with the number of nodes.

## 5.7 Conclusions

In this chapter, we introduced a new modeling framework for the analytical study of *any* medium access control (MAC) protocols operating in multihop ad hoc networks that focuses on the interactions between the PHY and the MAC layers. To account for the effects

of both cross-layer interactions and the interference among all nodes, a novel linear model was introduced with which topology and PHY/MAC-layer aspects are naturally incorporated in what we defined as *interference matrices*. A key feature of the model is that nodes can be modeled individually, i.e., it allows a per-node setup of many layer-specific parameters. Moreover, no spatial probability distribution or special arrangement of nodes is assumed; the model allows the computation of individual (per-node) performance metrics for any given network topology and radio channel model.

# Chapter 6

# IEEE 802.11 Ad Hoc Networks with Omni-Directional Antennas

In this chapter, we show how the analytical modeling framework developed in Chapter 5 can be applied to the study of realistic MAC protocols in ad hoc networks. To this end, we present the modeling and analysis of wireless ad hoc networks that operate according to the IEEE 802.11 distributed coordination function (DCF) [64].

## 6.1 Modeling the IEEE 802.11 DCF MAC

In the recent past, there has been a number of attempts to model the IEEE 802.11 DCF MAC [64]. One of the most prominent works is the one by Bianchi [12], who presented a way to evaluate the saturation throughput of fully-connected networks based on the modeling of the binary exponential backoff algorithm, heart of the IEEE 802.11 DCF MAC. Bianchi

modeled the backoff time counter operation as a bi-dimensional discrete-time Markov chain, assuming that each frame "collides" with a constant and independent probability $p$ at each transmission attempt, regardless of the number of retransmissions already undertaken. This probability was named the *conditional collision probability*, meaning the probability of a collision experienced by a frame being transmitted on the channel. From the Markov chain, one can obtain the steady-state probability $\tau$ that a node transmits a frame at any time as a function of the conditional collision probability $p$ and some parameters of the IEEE 802.11 DCF backoff algorithm.

Building upon Bianchi's model, some works have tried to deal with other aspects of the IEEE 802.11 DCF not previously considered. Ziouva and Antonakopoulos [150] provided a general model for CSMA/CA protocols based on Bianchi's model. They assumed a backoff algorithm close to the one in the 802.11, and included the "freezing" activity of the 802.11 backoff algorithm, defining the probability of *detecting the channel busy*. Because their model targeted general CSMA/CA protocols, their Markov chain does not accurately reflects the IEEE 802.11 DCF operation. Ergen and Varaiya [38] followed Ziouva's approach with respect to the impact of the carrier sensing mechanism, and focused on the IEEE 802.11 itself. In their model, however, they make the very simplifying assumption that the conditional collision probability is *equal* to the probability of detecting the channel busy. In practice, the model by Ziouva and Antonakopoulos [150] makes this same simplifying assumption, particularly when the number of nodes in the network is large.

One drawback of these models (including Bianchi's) is the fact that they do not consider the finite retry limits of the IEEE 802.11 DCF, which proposes that DATA and RTS

frames must be retransmitted a finite number of times. Instead, they all assume that frames are retransmitted *infinitely* in time, until they are successfully transmitted. Wu et. al. [138] incorporated the finite retry limit into Bianchi's model. On the other hand, Wu's model did not attempt to model the impact of the carrier sense mechanism.

A major limitation of all the aforementioned models is the fact that they implicitly assume a fully-connected segment of network under perfect channel conditions (i.e., no hidden terminal problems, no PHY-layer aspects, etc.). Consequently, by defining a "collision probability," they assume that all frames received at the same time "collide" and, therefore, they are all lost. By doing so, they assume that all "collisions" are restricted to RTS frames only, disregarding thus, the possibility of errors in the CTS, DATA and/or ACK frames. In fact, by its very definition, all the previous models mistakenly define $p$, which should actually be referred as the *probability of a failed handshake*, since a sender's frame could still be correctly received at the receiver's side, but not its acknowledgment. In addition, it is not true, for instance, that the probability of a failed handshake is the same (or similar) to the probability of detecting the channel busy. Each of these probabilities reflect totally different phenomena at the PHY layer. Detecting that a channel is busy only requires that some energy level be perceived at a node (as a result of some transmission(s)). On the other hand, transmission errors are related to a more complex process, and deals with the ability of the nodes to correctly receive a frame, which depends on many PHY-layer parameters such as the modulation/demodulation scheme, receiver design, etc.

If errors in both control and data frames are to be considered, then the modeling of the IEEE 802.11 backoff operation needs to be modified. This is because all previous

work has disregarded the *two retry counters* defined by the standard [64]: the STA long retry counter (SLRC) and the STA short retry counter (SSRC). The SSRC is associated with the RTS frame, and the SLRC is associated with the DATA frame[1]. The SSRC (SLRC) is incremented whenever an RTS (DATA) frame is unsuccessfully transmitted. The SSRC (SLRC) is reset to 0 whenever a CTS (ACK) frame is received in response to an RTS (DATA) frame. Therefore, even though the SRRC may be reset after a successful RTS transmission, the subsequent DATA frame transmission may be unsuccessful, leading, instead, to an *increment* of the SLRC.

According to the standard, the contention window size is reset to its minimum value only after a successful DATA frame transmission occur or when the SLRC or SSRC reach their maximum values—*but never after a successful RTS transmission*. In previous models, the CTS, DATA, and ACK frames were all assumed to be error-free after a successful RTS transmission, implying that a reset of SRRC would necessarily lead to a reset of the contention window size (since the SLRC would never be incremented). Therefore, in previous works, the contention window size was solely controlled by the number of unsuccessful RTS transmissions.

For a faithful modeling of the IEEE 802.11 DCF MAC, one needs to consider both SSRC and SLRC retry counters. Unfortunately, if we choose to follow the modeling approach used by Bianchi, it is not hard to realize that we will need a four-dimensional Markov chain to cover all possible states of the binary exponential backoff algorithm. To make things simpler—while still considering the impact of errors in both control and data frames—we consider a small simplification of the original IEEE 802.11 DCF MAC by defining a *single* retry

[1] If this frame is bigger than a certain user-defined threshold.

counter RC. The RC will be incremented every time an RTS or DATA frame is unsuccessfully transmitted, i.e., when the CTS/ACK are not received within a timeout or when they are received with errors. Likewise, the RC and the contention window size will be reset only when either a DATA frame is successfully transmitted or when RC reaches its maximum value. As in the standard, we allow the contention window to increment up to a maximum value, after which it remains at this value until it is reset. With this small simplification, we are able to model the IEEE 802.11 DCF MAC using only a two-dimensional Markov chain, as described next.

Let $b_j(t)$ be the stochastic process representing the backoff time counter for a node $j \in V$ at a time $t$, and $s_j(t)$ be the stochastic process representing $j$'s backoff stage at time $t$, where $s_j(t) \in [0, M]$, and $M$ is the maximum backoff stage (i.e., the maximum value the retry counter RC can assume). Hence, $b_j(t) \in [0, W_{s_j(t)} - 1]$, where

$$W_{s_j(t)} = \begin{cases} 2^{s_j(t)} W_{\min} & \text{if} \quad 0 \leq s_j(t) < m \\ 2^m W_{\min} & \text{if} \quad m \leq s_j(t) \leq M. \end{cases} \tag{6.1}$$

Let us assume that the RTS/CTS handshake fails with a constant and independent probability $p_j$, and that the DATA/ACK handshake fails with a constant and independent probability $d_j$, both regardless of the number of retransmissions experienced. Also, let us assume that a node detects that the channel is busy with a constant and independent probability $g_j$. Note that these independence assumptions are with respect to the *number of retransmissions*, but $p_j$, $d_j$, and $g_j$ are *dependent on PHY-layer aspects*, and are computed according to the developments in Section **??**. Under these conditions, the process $\{s_j(t), b_j(t)\}$ can be modeled with the discrete-time Markov chain depicted in Fig. 6.1. As in [12], let us adopt the notation

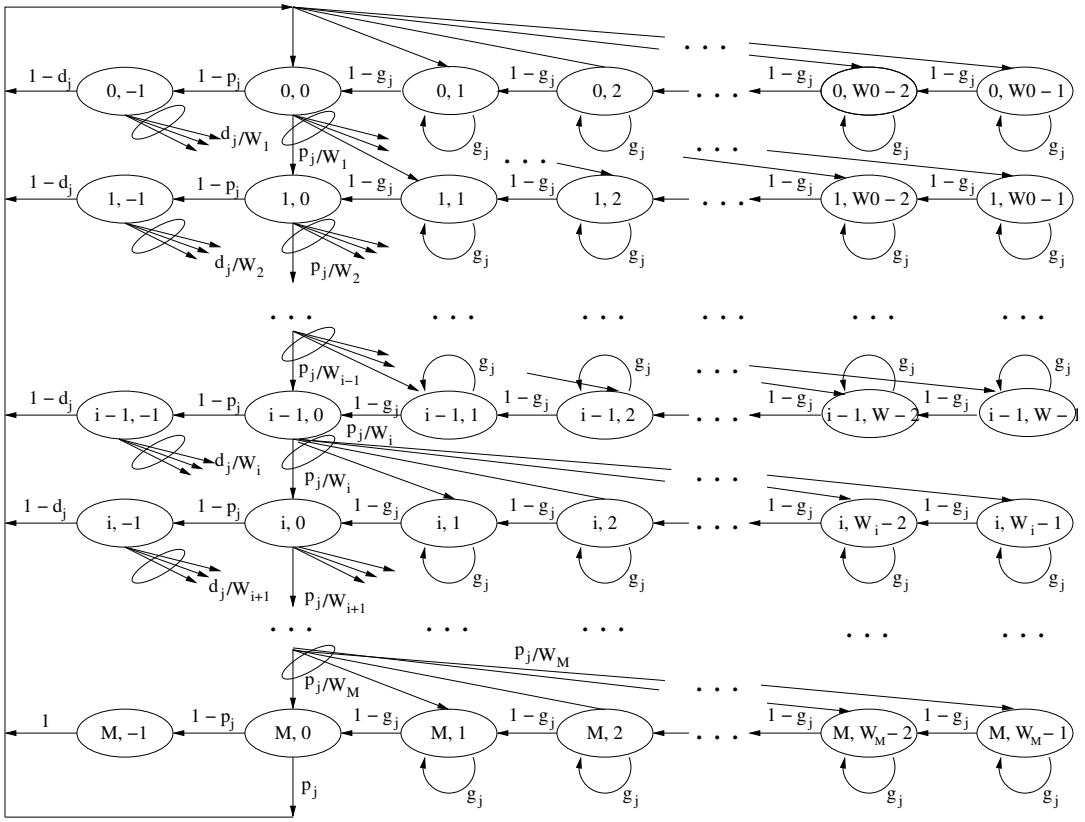


**Figure 6.1**: Markov model for the *modified* binary exponential backoff algorithm based on the IEEE 802.11 DCF MAC. Losses in both control and data frames taken into account.

$P\{i_1, k_1|i_0, k_0\} = P\{s(t+1) = i_1, b(t+1) = k_1|s(t) = i_0, b(t) = k_0\}$. From the above Markov chain, the only non-null one-step transition probabilities are

$$P\{i, k|i, k+1\} = 1 - g_j, \qquad k \in [0, W_i - 2], \qquad i \in [0, M] \tag{6.2}$$

$$P\{i, k|i, k\} = g_j, \qquad k \in [1, W_i - 1], \qquad i \in [0, M] \tag{6.3}$$

$$P\{i, -1|i, 0\} = 1 - p_j, \qquad i \in [0, M] \tag{6.4}$$

$$P\{i, k|i-1, 0\} = \frac{p_j}{W_i}, \qquad k \in [0, W_i - 1], \qquad i \in [1, M] \tag{6.5}$$

$$P\{i, k|i-1, -1\} = \frac{d_j}{W_i}, \qquad k \in [0, W_i - 1], \qquad i \in [1, M] \tag{6.6}$$

$$P\{0, k|i, -1\} = \frac{(1-d_j)}{W_0}, \qquad k \in [0, W_0 - 1], \qquad i \in [0, M-1] \tag{6.7}$$

$$P\{0,k|M,0\} = \frac{p_j}{W_0}, \qquad k \in [0, W_0 - 1] \tag{6.8}$$

$$P\{0,k|M,-1\} = \frac{1}{W_0}, \qquad k \in [0, W_0 - 1]. \tag{6.9}$$

The first and second equations indicate that the backoff counter is decremented if the channel is sensed idle (with probability $1 - g_j$), and frozen if the channel is sensed busy (with probability $g_j$). The third equation indicates that a successful handshake of control frames took place and the node is ready to send its DATA frame. The next equation indicates that, after an unsuccessful handshake of control frames (RTS/CTS) at stage $i-1$, a backoff interval is uniformly chosen within the interval $[0, W_i - 1]$ for the next stage $i$. The fourth equation indicates that the transmission of DATA frame failed at stage $i - 1$, and a backoff interval is uniformly chosen within the interval $[0, W_i - 1]$. The fifth equation indicates that a DATA frame was transmitted successfully and a new frame transmission starts at backoff stage 0 with a backoff window uniformly chosen within the interval $[0, W_0-1]$. The next equation indicates that a handshake of control packets failed and the number of allowed retransmissions reached its maximum. Hence, the DATA frame is discarded and a new one is picked at the head of the node's queue. A new frame transmission starts at backoff stage 0 with a backoff window uniformly chosen within the interval $[0, W_0 - 1]$. The last equation describes that either a DATA frame transmission was successful or it it failed. In either case, a new frame starts at backoff stage 0 with a backoff window uniformly chosen within the interval $[0, W_0 - 1]$.

Let $b_{i,k} = \lim_{t\to\infty} P\{s(t) = i, b(t) = k\}, i \in [0, M], k \in [0, W_i - 1]$ be the stationary distribution of the Markov chain. First, we note that

$$b_{i,0} = p_j\, b_{i-1,0} + d_j\, b_{i-1,-1}, \quad 1 \le i \le M. \tag{6.10}$$

But, because $b_{i-1,-1} = (1-p_j)b_{i-1,0}$, we have

$$b_{i,0} = [p_j + d_j(1-p_j)]\, b_{i-1,0}, \tag{6.11}$$

which leads to

$$b_{i,0} = [p_j + d_j(1-p_j)]^i\, b_{0,0}, \quad 0 \le i \le M. \tag{6.12}$$

For $i = 0$ and $k \in [1, W_0 - 1]$,

$$b_{0,k} = \frac{W_0 - k}{(1-g_j)W_0} \sum_{l=0}^{M-1} (1-p_j)(1-d_j)b_{l,0} + b_{M,0}, \tag{6.13}$$

whereas for $i \neq 0$ and $k \in [1, W_i - 1]$,

$$b_{i,k} = \frac{W_i - k}{(1-g_j)W_i} \left[p_j + d_j(1-p_j)\right]\, b_{i-1,0}, \quad i \in [1, M]. \tag{6.14}$$

From Eq. (6.11), and by noting that $b_{0,0} = \sum_{l=0}^{M-1}(1-p_j)(1-d_j)b_{l,0} + b_{M,0}$, Eqs. (6.13) and (6.14) can be rewritten as

$$b_{i,k} = \frac{W_i - k}{(1-g_j)W_i} \left[p_j + d_j(1-p_j)\right]^i\, b_{0,0}, \tag{6.15}$$

for $i \in [0, M]$ and $k \in [1, W_i - 1]$. Therefore, all values of $b_{i,k}$ can be expressed as functions of $b_{0,0}$, whose value can be found from the normalization condition $\sum_{i=0}^{M} \sum_{k=0}^{W_i - 1} b_{i,k} = 1$, yielding

$$b_{0,0} = \frac{2(1-g_j)(1-a_j)(1-2a_j)}{(1-a_j^{M+1})(1-2a_j)(1-2g_j) + \kappa W}, \tag{6.16}$$

where $a_j = p_j + d_j(1-p_j)$, and $\kappa = (1-a_j)\left[1 - (2a_j)^{M+1}\right]$ if $m = M$, and $\kappa = 1 - a_j\{1 + (2a_j)^m[1 + a_j^{M-m}(1-2a_j)]\}$ if $m < M$.

A node initiates a handshake when it attempts to send an RTS, i.e., when it reaches the states $b_{i,0},\ i \in [0, M]$. Therefore, the probability $\tau_j$ that node $j$ attempts to initiate a

handshake is obtained by taking $\tau_j = \sum_{i=0}^{M} b_{i,0}$, which is given by

$$\tau_j = \frac{2(1-g_j)(1-a_j^{M+1})(1-2a_j)}{(1-a_j^{M+1})(1-2a_j)(1-2g_j)+\kappa W}, \tag{6.17}$$

with $\kappa$ assuming the same values as before depending on whether $m \leq M$. It is interesting to note that, if $M \to \infty$, then $g_j = 0$, $d_j = 0$, and the Markov chain in Fig. 6.1 reduces to the one used by Bianchi [12] for the case when $m < M$. Accordingly, by making $M \to \infty$, we have $g_j = 0$ and $d_j = 0$ in Eq. (6.17), and the same expression as the one derived by Bianchi [12] is obtained.

## 6.2 Building the Interference Matrix

In this section, we show how to obtain the interference matrix of an ad hoc network that operates according to the IEEE 802.11 DCF MAC. To accomplish that, we follow the developments introduced in Chapter 5 and derive linear approximations to the operation of the IEEE 802.11 DCF MAC and to the impact of the feedback information it uses. After that, we investigate the conditions for the linear system to be solvable, according to Theorem 1 and Corollary 1 in Chapter 5. Finally, we investigate the relationship between system solvability and issues pertinent to network dimensioning and fairness of the IEEE 802.11 DCF MAC.

### 6.2.1 The Linear Approximation

Equation (6.17) contains exactly what we need to apply the analytical modeling framework introduced in Chapter 5: it provides the functional form $\tau_j = h_j(\boldsymbol{\varphi}_j)$ by which the IEEE 802.11 DCF MAC relates the steady-state transmission probability (scheduling rate)

$\tau_j$ with a vector of feedback probabilities $\boldsymbol{\varphi}_j$. In the specific case of the Markov model we developed for the IEEE 802.11 DCF MAC, the feedback variables are $p_j$, $q_j$, and $g_j$. But, because $p_j$ and $q_j$ denote probabilities of *unsuccessful* handshakes, we define the corresponding probabilities of *successful* handshakes $q_j^{rts} = 1 - p_j$, and $q_j^{dat} = 1 - d_j$, in order to be coherent with the framework developed in Chapter 5. Hence, the vector $\boldsymbol{\varphi}_j$ of feedback probabilities will be given by $\boldsymbol{\varphi}_j = [q_j^{rts}\, q_j^{dat}\, g_j]^T$. Following the steps presented in Section 5.6, a first-order approximation of $\tau_j$ can be easily obtained, and it is given by

$$\tau_j = \frac{2(1-W)}{(W+1)^2} + \frac{2W}{(W+1)^2}\, q_j^{rts} + \frac{2W}{(W+1)^2}\, q_j^{dat} - \frac{2(W-1)}{(W+1)^2}\, g_j, \tag{6.18}$$

with linear coefficients $\alpha_0 = 2(1-W)/(W+1)^2, \alpha_1 = \alpha_2 = 2W/(W+1)^2$, and $\alpha_3 = 2(W-1)/(W+1)^2$, according to the notation used in Eq. (5.35) in Chapter 5.

The computation of the feedback probabilities $q_j^{rts}$, $q_j^{dat}$, and $g_j$ follow the developments in Sections 5.6.1 and 5.6.2, and their linear approximations are functions of the transmission probabilities of all nodes in the network, as given by Eqs. (5.26), (5.30), i.e.,

$$\begin{aligned}\tau_j &= \alpha_0 + \alpha_1 \left( \pi_j^{rts} - \sum_{k \in V} c_{jk}^{rts} \tau_k \right) + \alpha_2 \left( \pi_j^{dat} - \sum_{k \in V} c_{jk}^{dat} \tau_k \right) - \alpha_3 \sum_{k \in V} d_{jk} \tau_k, \\ &= \pi_j + \sum_{\substack{j \in V \\ j \neq i}} \phi_{jk} \tau_k, \end{aligned} \tag{6.19}$$

where

$$\pi_j = \alpha_0 + \alpha_1 \pi_j^{rts} + \alpha_2 \pi_j^{dat}, \quad \forall\, j \in V, \tag{6.20}$$

and

$$\phi_{jk} = \begin{cases} -\alpha_1 c_{jk}^{rts} - \alpha_2 c_{jk}^{dat} - \alpha_3 d_{jk}, & \text{if } j \neq k \\ 0, & \text{otherwise.} \end{cases} \tag{6.21}$$

Therefore, we have obtained a linear system of equations relating the transmission probabilities of all nodes in the network, which is given by (in matrix notation)

$$(\mathbf{I} - \mathbf{\Phi})\,\boldsymbol{\tau} = \boldsymbol{\pi}, \tag{6.22}$$

where $\boldsymbol{\pi} = [\pi_1\ \pi_2\ \ldots\ \pi_n]^T$, and $\mathbf{\Phi}$ is the *interference matrix* whose elements are given by Eq. (6.21). As a final note, we observe that because the Markov model developed for the IEEE 802.11 DCF MAC does not contain any *a priori* feedback variables, Eq. (6.22) is, in fact, a simplified version of the more general case introduced in the modeling framework in Chapter 5, as expressed by Eq. (5.41).

### 6.2.2 Making the Linear System Solvable

In Chapter 5, we provided sufficient conditions for the linear system of transmission probabilities to have a solution. According to Theorem 1, the linear system of Eq. (6.22) has a solution if all of its rows satisfy

$$\sum_{j \neq k} \left| \alpha_1 c_{jk}^{rts} + \alpha_2 c_{jk}^{dat} + \alpha_3 d_{jk} \right| < 1, \quad \forall\, j \in V. \tag{6.23}$$

Thus, depending on the location of nodes, the parameters of the MAC layer (represented by the coefficients $\alpha_i, i = 1, 2, 3$), and/or the parameters of the PHY layer (which have their impact expressed through the coefficients $c_{ik}^{rts}$, $c_{ik}^{dat}$, and $d_{ik}$), the linear system of Eq. (6.22) has a solution. Consequently, given the location of the nodes and the characterization of the radio channel, one can choose appropriate PHY/MAC layer parameters to satisfy the above condition in order to have a solvable linear system.

On the other hand, if one wants to obtain a solvable system regardless of physical

layer parameters, Corollary 1 in Chapter 5 provides the answer. In this case, a sufficient condition for the linear system of Eq. (6.22) to have a solution is simply given by

$$\sum_{i=1}^{3} |\alpha_i| < \frac{1}{n-1}, \tag{6.24}$$

which, from the definition of the coefficients $\alpha_i$, reduces to

$$\frac{6W_{\min} - 2}{(W_{\min} + 1)^2} < \frac{1}{n-1}, \tag{6.25}$$

i.e., given the number $n$ of nodes in the network, the minimum contention window size $W_{\min}$ of the IEEE 802.11 DCF MAC must be chosen in such a way that the inequality in Eq. (6.25) is satisfied. Likewise, if we rearrange the terms in Eq. (6.25), we obtain an upper bound on the maximum number $n$ of nodes allowed in the network for a given minimum contention window size $W_{\min}$, i.e.,

$$n < \frac{(W_{\min} + 1)^2}{6W_{\min} - 2} + 1. \tag{6.26}$$

Therefore, Eq. (6.26) provides an upper bound on the maximum number of nodes allowed in the network so that a solution to the linear system is possible *regardless of physical layer aspects*. Figure 6.2 shows the maximum number of nodes allowed in the network as a function of the minimum contention window size $W_{\min}$, as provided by Eq. (6.26). As we can see, the maximum number of nodes allowed in the network increases *linearly* with the minimum contention window size $W_{\min}$. To understand this linear increase, we can make an approximation to the upper bound of Eq. (6.26) when $W_{\min} \gg 1$. In this case,

$$\frac{(W_{\min} + 1)^2}{6W_{\min} - 2} + 1 \approx \frac{W_{\min}^2}{6W_{\min}} = \frac{1}{6} W_{\min}, \tag{6.27}$$

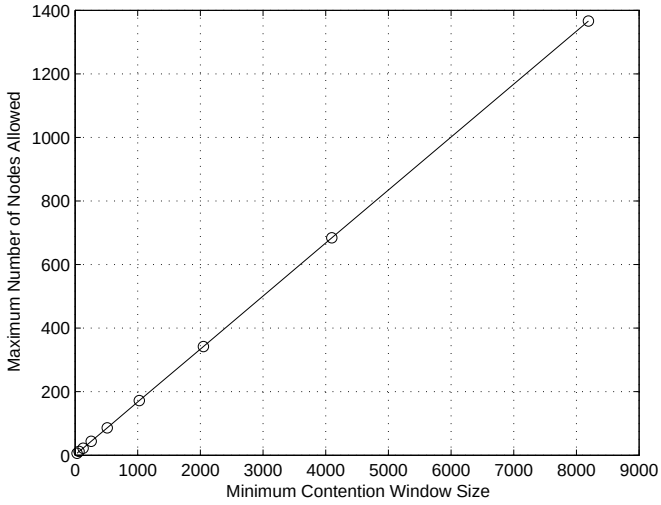


**Figure 6.2**: Maximum number of nodes allowed in the network versus the minimum contention window size.

which is exactly the relation we obtain if we adjust a linear function of the form $y = ax$ to the curve in Fig. 6.2. Likewise, because the minimum contention window size $W_{\min}$ of the IEEE 802.11 DCF MAC is specified as a power $m$ of the base 2, i.e., $W_{\min} = 2^m$, the maximum number of nodes allowed in the network increases exponentially with the power $m$ of the base 2 according to $\frac{1}{6} \times 2^m$, as shown in Figure 6.3. Consequently, from Eq. (6.27), the following practical rule of thumb can be postulated about the maximum number of nodes allowed in a saturated IEEE 802.11 network so that we have a solvable linear system regardless of physical layer aspects:

**Rule of Thumb (Maximum Number of Nodes):***In order to have a solvable linear system that corresponds to a saturated IEEE 802.11 network independent of physical layer aspects, the maximum number of nodes allowed in the network must be around a sixth of the minimum contention window size.*

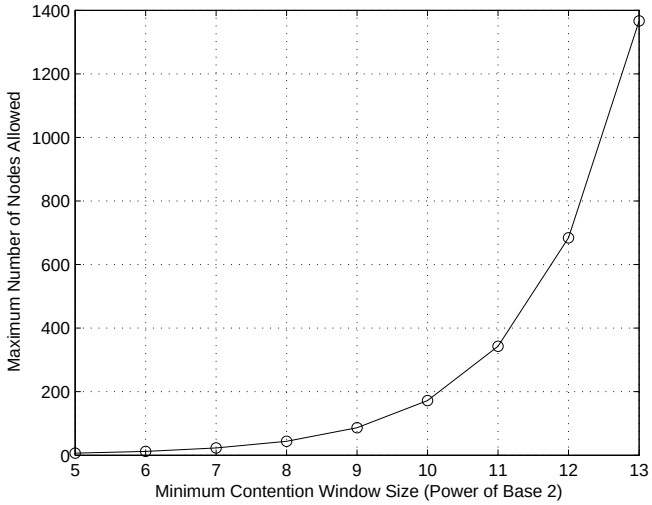


**Figure 6.3**: Maximum number of nodes allowed in the network versus the minimum contention window size expressed in terms of powers of the base 2.

It is interesting to observe that our rule of thumb is actually related to aspects of network performance and dimensioning. For instance, if we look at the results obtained in Chapter 2 about the average service time and jitter with respect to the minimum contention window size, we will see that a higher minimum contention window size is necessary as the number of nodes increases, as shown in Figures 2.7(a), (b), (c), (d), (e), (f), (g), and (h). For example, the rule of thumb says that the value of $W_{\min}$ necessary for a network with 50 nodes must be $50 \times 6 = 300$. Surprisingly, we can observe in Figure 2.7(e) that the average service time for a network of 50 nodes only attains reasonable values after the minimum contention window size increases above 256.

When physical layer aspects are in place, the rule of thumb does not apply. However, the relation between the sufficient condition of Theorem 1 and network dimensioning/performance can still be observed, as discussed next.

### 6.2.3 Network Fairness and the Suffi ciency Conditions

An important aspect related to the sufficiency conditions provided by Theorem 1 and Corollary 1 is regarding network *fairness*, i.e., the fair share of channel access among competing nodes, leading to overall throughput values much higher across all nodes. The IEEE 802.11 DCF MAC, in particular, is well-known for presenting serious fairness problems []. The fairness problem of the IEEE 802.11 DCF MAC is directly related to its binary exponential backoff algorithm and, consequently, to the selection of the minimum contention window size as well.

Interestingly, to make the linear system to become"solvable" seems to be directly related to make the system more fair as well (in the particular case of the IEEE 802.11 DCF MAC). To investigate this, we applied the sufficiency condition of Theorem 1 on 10 random topologies with 100 nodes each, using fixed PHY-layer parameters and a given radio channel model (described in more detail in Section 7.5). By varying only the minimum contention window size, we found that the system becomes solvable for the 10 selected topologies if $W_{\min} = 256$, as opposed to the default value of $W_{\min} = 32$. Given that, we computed the fairness of the 10 topologies for the two values of $W_{\min}$ using throughput results derived from discrete-event simulations using Qualnet [105]. To compute the level of *fairness*, we use *Jain's fairness index* [68], which is defined as

$$\text{Fairness Index } = \frac{1}{n}\frac{\left(\sum_{i=1}^{n} S_i\right)^2}{\sum_{i=1}^{n} S_i^2}, \tag{6.28}$$

where $S_i$ is the throughput of each node in the network, and $n$ is the number of nodes. Regarding the fairness index, the smaller the value is, the more fair the network becomes. Figure 6.4

shows the fairness index calculated for the 10 topologies using the two sizes of minimum contention window: $W_{\min} = 32$ and $W_{\min} = 256$. As we can see, the topologies with

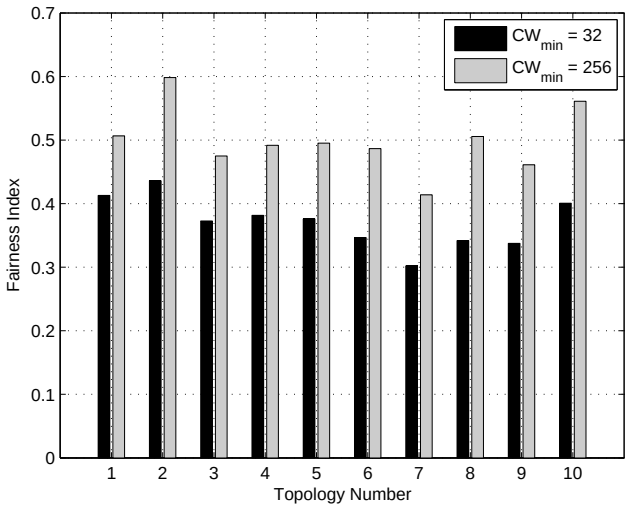


**Figure 6.4**: Fairness index of 10 topologies with 100 nodes each. Results correspond to discrete-event simulations of the IEEE 802.11 DCF MAC operating with minimum contention window sizes equal to $W_{\min} = 32$ and $W_{\min} = 256$.

$W_{\min} = 256$ are more "fair" compared to the ones with $W_{\min} = 32$. Furthermore, if we look at the average network throughput in Figure 6.5, we will see that for an overall decay in average throughput of only 8.8% for networks with $W_{\min} = 256$, we have an average increase in throughput fairness of 35% for the same networks, as observed in Figure 6.4. Lastly, it is interesting to observe the effect that fairness has on network throughput. In Figure 6.6, we show the *minimum throughput value* observed in each of the 10 topologies (of a given node in the network). As we can see, the minimum throughput value is much higher in the topologies with $W_{\min} = 256$, showing how much fair the networks become.

Given the above considerations, we can observe that by making the linear system *solvable*, we are actually also dealing with the *feasibility* of the network scenarios we want to

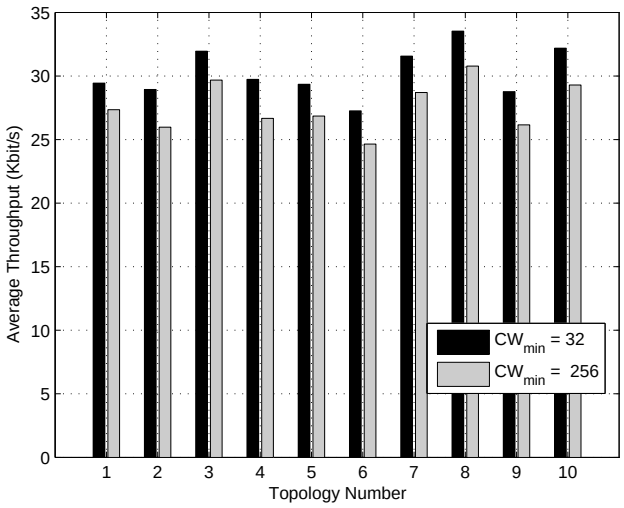


**Figure 6.5**: Average throughput for 10 topologies with 100 nodes each. Results correspond to discrete-event simulations of the IEEE 802.11 DCF MAC operating with minimum contention window sizes of $W_{\min} = 32$ and $W_{\min} = 256$.

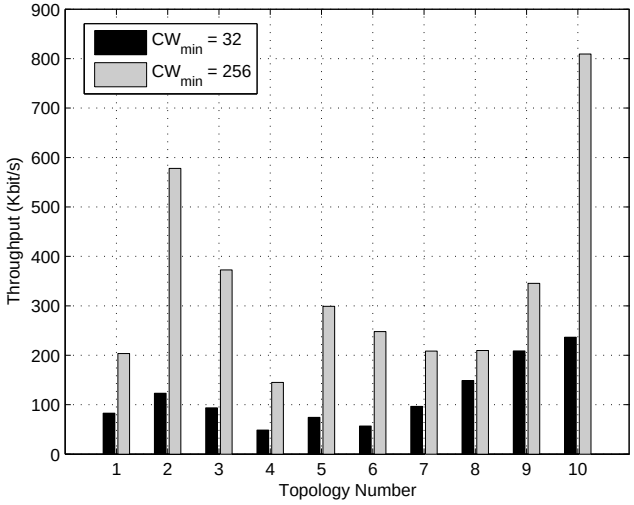


**Figure 6.6**: Minimum throughput observed in each of the 10 topologies with 100 nodes. Results correspond to discrete-event simulations of the IEEE 802.11 DCF MAC operating with minimum contention window sizes equal $W_{\min} = 32$ and $W_{\min} = 256$.

study. Therefore, the sufficiency conditions provided by Theorem 1 and Corollary 1 serve, in fact, as powerful tools for network dimensioning and design.

## 6.3 Performance Metrics

The scheduling rate $\tau_i$ of every node $i \in V$ constitutes the fundamental piece of information that we need to obtain the performance metrics of interest. In fact, many network performance metrics such as throughput and average service time depend, ultimately, on how frequent the nodes schedule their transmissions, how successful they are, and their impact on the transmission rate of every other node in the network—all intrinsically dependent on the underlying physical layer aspects and network topology. Therefore, it becomes apparent that a bottom-up modeling approach is needed in order to derive the performance metrics of interest.

In Chapter 2, we introduced a bottom-up modeling approach to compute the first two moments of the service time of the IEEE 802.11 DCF MAC. This model was used in Chapter 3 and further extended in Chapter 4. In all previous chapters, however, we used the simple Markov model proposed by Bianchi [12] to model the operation of the IEEE 802.11 DCF MAC. In Section 6.1, we introduced a more realistic Markov model for the operation of the IEEE 802.11 DCF MAC that considers the impact of physical layer aspects and the carrier sense activity of nodes.

Using the core of the developments and results introduced in Chapters 2 and 4, we can derive the performance metrics relative to the new Markov model for the IEEE 802.11 DCF MAC introduced in Section 6.1. This time, however, we treat nodes *individually*, and performance metrics are developed in a way that the impact of the physical layer and network

radio-based topology are taken into account on the performance of every node in the network.

In the sequel, we start with the derivation of the channel state probabilities as perceived individually by each node in the network. Following that, we proceed with the derivation of the main performance metrics of interest.

### 6.3.1 Channel State Probabilities

In Chapter 2, we derived closed-form expressions for the first two moments of a node's service time in saturated IEEE 802.11 DCF networks under perfect channel conditions (i.e., no physical layer aspects and no hidden terminals). To obtain the model, we identified three mutually exclusive events that dominate the behavior of the binary exponential backoff algorithm of the IEEE 802.11 DCF MAC. These events correspond to the possible channel states a node can sense when it is contending for channel access. Therefore, the first two moments of a node's service time are functions of the channel state as perceived by each node, and this channel state is conveyed in the form of *channel state probabilities*.

From the standpoint of a node that is in backoff mode, the channel can be sensed as *idle* or *busy*. If the channel is sensed *busy*, we argue in Chapter 2 that it is because either a successful frame transmission occurs over the channel or a "frame collision" happens. Based on these observations, the three mutually exclusive events defined earlier were $E_s = \{\text{successful transmission}\}$, $E_i = \{\text{idle channel}\}$, and $E_c = \{\text{collision}\}$. But, if physical layer aspects are to be taken into account, we need to consider a more realistic event than the simpler "collision" event defined previously. As it was pointed out in Section 6.1, instead of dealing with the event "collision," we need to consider the more gen-

eral event "unsuccessful handshake," and its opposite event, i.e., the "successful handshake," in order to be more faithful to the real operation of the IEEE 802.11 DCF MAC. Consequently, the three mutually exclusive events are now defined as $E_i^{idle} = \{\text{idle channel}\}$, $E_i^{suc} = \{\text{successful handshake}\}$, and $E_i^{uns} = \{\text{unsuccessful handshake}\}$, with probabilities $p_i^{idle} = P\{E_i^{idle}\}$, $p_i^{suc} = P\{E_i^{suc}\}$, and $p_i^{uns} = P\{E_i^{uns}\}$, respectively.

Because of the impact of topology and physical layer aspects, nodes no longer experience the same channel conditions, as it was assumed in Chapter 2. For this reason, from now on, we use the subscript $i$ to refer to each node $i \in V$. Given that, we can now proceed with the computation of the channel state probabilities $p_i^{idle}$, $p_i^{suc}$, and $p_i^{uns}$. From Section 5.6.2, the probability that a node in backoff mode senses that the channel is busy is given by Eq. (5.30). Consequently, the probability $p_i^{idle}$ that a node $i \in V$ in backoff mode senses that the channel is idle is simply

$$p_i^{idle} = 1 - g_i = 1 - \sum_{k \in V} d_{ik}\tau_k, \tag{6.29}$$

where $d_{ik}^r$ is defined as in Eq. (5.29).

For the probability $p_i^{suc}$ that a node $i \in V$ in backoff mode perceives that a successful handshake occurs over the channel, we need to consider the event that *at least one node transmits over the channel and it has a successful handshake that is perceived by node* $i$. Therefore, we need to consider all possible combinations of active nodes in $V$ that satisfy such constraint. If we denote by $\{c_{ik}^{suc}\}_{k=1,\ldots,l}$ the set of all $l \leq 2^{n-1}$ such combinations, and $\mathcal{C}_i^{suc}$ a random variable that indicates the occurrence of each of these combinations, we have

$$p_i^{suc} = P\left\{\bigcup_{k=1}^{l}\{\mathcal{C}_i^{suc} = c_i^{suc}\}\right\}. \tag{6.30}$$

Based on considerations C1, C2, and C3 from Section 5.6 about the nodes' transmission probabilities (which are related to the nodes' attempts to establish a handshake), we can obtain an approximation by taking only the combinations $c_{ik}^{suc}$ where *only node $k$ transmits and it is successful*

$$\begin{aligned} p_i^{suc} &\approx \sum_{k \in S_i} P\{k \text{ transmits } \cap \ k \text{ has successful handshake}\} \\ &= \sum_{k \in S_i} P\{k \text{ has successful handshake} \,|\, k \text{ transmits}\} P\{k \text{ transmits}\} \\ &= \sum_{k \in S_i} q_k \tau_k, \end{aligned} \tag{6.31}$$

where $S_i \subseteq V$ is the set of nodes within the carrier sense range of node $i$ (the signal has to be perceived by node $i$), and $q_k$ is the probability that node $k \in V$ executes a successful handshake given that it has attempted one. From the Marvov model in Section 6.1, this probability is simply

$$q_k = q_k^{rts} q_k^{dat} = (1 - p_k)(1 - d_k), \quad \forall\, k \in V. \tag{6.32}$$

Following similar arguments, the probability $p_i^{uns}$ that node $i$ perceives an *unsuccessful handshake occurring in the channel* can be approximated by

$$p_i^{uns} \approx \sum_{k \in S_i} (1 - q_k)\tau_k. \tag{6.33}$$

### 6.3.2 Average Backoff Time

Given the computation of the channel state probabilities, we can now find the average backoff time experienced at each node $i \in V$ based on the results obtained in Chapter 2 and Chapter 4, where the finite-retry limit mechanism of the IEEE 802.11 DCF MAC was

incorporated into the model. As a consequence of the fact that nodes are now treated individually, the many parameters that form the average backoff time need to be computed with respect to each node's own perception of the channel under the underlying radio-based topology and physical layer aspects. Therefore, if we use the subscript $i$ to indicate the parameters of the backoff time corresponding to node $i \in V$, the average backoff time $\overline{T}_{B_i}$ experienced at each node $i \in V$ will be given by (from the results in Chapter 2 and Chapter 4),

$$\overline{T}_{B_i} = \frac{\alpha_i(W_{\min}\beta_{1i} - \beta_{2i})}{2} + \beta_{3i}\, t_i^{res}, \quad \forall\, i \in V, \tag{6.34}$$

where $\alpha_i$ is the average backoff "step size", $W_{\min}$ is the minimum contention window size, $\beta_{1i}$, $\beta_{2i}$, and $\beta_{3i}$ are given in Eqs. (4.3)–(4.8), and $t_i^{res}$ is the average time spent in collision resolution.

Regarding the parameters $\beta_{1i}$, $\beta_{2i}$, and $\beta_{3i}$, they still follow Eqs. (4.3)–(4.8), except for the fact that they are now functions of the individual successful handshake probabilities $q_i, \forall\, i \in V$, given in Eq. (6.32). Because of physical layer aspects and network topology, the parameters $\alpha_i$ and $t_i^{res}$ need to be defined accordingly. First, let us consider the parameter $\alpha_i$. From Eq. (2.5), the parameter $\alpha_i$ depends on the channel state probabilities and the average time duration of each state. Using the channel state probabilities derived in Eqs. (6.29), (6.31), and (6.33), and denoting the average time duration of each state by $\sigma$, $t_i^{suc}$, and $t_i^{uns}$, the expression for the average step size $\alpha_i$ is now given by

$$\alpha_i = \sigma p_i^{idle} + t_i^{uns} p_i^{uns} + t_i^{suc} p_i^{suc}, \quad \forall\, i \in V. \tag{6.35}$$

As before, the value of the slot size $\sigma$ is fixed and defined by the IEEE 802.11 standard [64], and it will depend on the physical layer of choice (direct sequence spread spectrum

(DSSS) or frequency-hoping spread spectrum (FHSS)). For the case of the average time $t_i^{uns}$ the channel is perceived busy due to an *unsuccessful handshake*, we need to look at the reasons why the handshake may fail. A handshake will fail if any of the four events happen:

1. The RTS is not successfully received at the intended receiver;

2. The RTS is successfully received, but the CTS is not;

3. Both RTS and CTS are received successfully, but the DATA frame is not;

4. The RTS, CTS, and DATA frames are received successfully, but the ACK is not.

Each of the four events listed above lead to different durations of the time intervals in which the channel can be perceived busy from the standpoint of a node in carrier sense mode. For example, in the first case, if a transmitted RTS is not successfully received by its intended receiver, none of the subsequent frames following the RTS in the four-way handshake mechanism will be sent over the channel. Consequently, the time the channel is perceived busy by other nodes will be shorter than the time the channel is perceived busy when, for example, an RTS, CTS, and DATA frames are sent successfully over the channel (Case 4). In each case, the time duration depends on which frames were transmitted over the channel, the incurred propagation delays, and the extra time intervals specified by the standard, like the IFS and DIFS time intervals mentioned in Chapter 2.

When physical layer aspects are taken into account, we need to consider another time interval specified by the standard: the *extended interframe space* (EIFS) [64]. The EIFS should be used whenever the PHY indicates to the MAC that a frame transmission was begun that did not result in the correct reception of a complete MAC frame with a correct FCS value.

The EIFS interval should begin following indication by the PHY that the medium is idle after detection of the erroneous frame, without regard to the virtual carrier-sense mechanism. The EIFS is defined to provide enough time for another node to acknowledge what was, to this node, an incorrectly received frame before this node commences transmission. The duration of an EIFS is defined as

$$\text{EIFS} = \text{SIFS} + \text{ACK} + \text{PreambleLength} + \text{PLCPHeaderLength} + \text{DIFS}, \tag{6.36}$$

where the term (ACK + PreambleLength + PLCPHeaderLength) is expressed in microseconds required to transmit at the PHY's lowest mandatory rate. In other words, during backoff, if the node cannot successfully detect the MAC frame being transmitted over the channel, and, as a result, it is unable to set up its network allocation vector (NAV) appropriately (or respond to the MAC frame in case it is the target receiver), then, once the channel is detected to be idle again, the node does not wait for a DIFS interval before resuming its backoff time counter. Instead, it will wait for an EIFS time interval.

Ideally, we should distinguish in our analytical model the cases when a node in carrier sense mode correctly detects a MAC frame from the cases when it does not. But, considering that (a) the probability $p_i^{uns}$ of detecting an unsuccessful transmission over the channel is an approximation to a probability that encompasses many other possible events (Eq. (6.33)); and that (b) frame errors will happen due to channel impairments and multiple access interference, then, we will assume that the likelihood with which nodes will be able to correctly detect the MAC frames being transmitted over the channel (while in carrier sense mode) will be low. Consequently, in the long run, nodes will mostly need to apply the EIFS interval as soon as the channel is detected idle and before resuming their backoff time counter.

Given this assumption, if we let $\tilde{t}^{\text{rts}}$, $\tilde{t}^{\text{cts}}$, $\tilde{t}^{\text{dat}}$, and $\tilde{t}^{\text{ack}}$ denote the time durations corresponding to the four events listed above, we will have that

$$\tilde{t}^{\text{rts}} = \text{RTS} + \delta + \text{EIFS} \tag{6.37}$$

$$\tilde{t}^{\text{cts}} = \text{RTS} + \delta + \text{SIFS} + \text{CTS} + \delta + \text{EIFS}, \tag{6.38}$$

$$\tilde{t}^{\text{dat}} = \text{RTS} + \delta + \text{SIFS} + \text{CTS} + \delta + \text{SIFS} + \text{DATA} + \delta + \text{EIFS} \tag{6.39}$$

$$\tilde{t}^{\text{ack}} = \text{RTS} + \delta + \text{SIFS} + \text{CTS} + \delta + \text{SIFS} + \text{DATA} + \delta + \text{SIFS} + \text{ACK} + \delta + \text{EIFS}. \tag{6.40}$$

Now, if $\tilde{q}_k^{\text{rts}}$, $\tilde{q}_k^{\text{cts}}$, $\tilde{q}_k^{\text{data}}$, and $\tilde{q}_k^{\text{ack}}$ denote the probabilities that each node $k \in S_i$ has an unsuccessful handshake due to any of the four events listed above, and $\tilde{q}_{S_i}^{\text{rts}}$, $\tilde{q}_{S_i}^{\text{cts}}$, $\tilde{q}_{S_i}^{\text{data}}$, and $\tilde{q}_{S_i}^{\text{ack}}$ denote the probabilities that node $i \in V$ perceives each of these four events happening over the channel, then, over all nodes $k \in S_i$, we have

$$\tilde{q}_{S_i}^{\text{rts}} = \sum_{k \in S_i} \tilde{q}_k^{\text{rts}} \tau_k, \tag{6.41}$$

$$\tilde{q}_{S_i}^{\text{cts}} = \sum_{k \in S_i} \tilde{q}_k^{\text{cts}} \tau_k, \tag{6.42}$$

$$\tilde{q}_{S_i}^{\text{data}} = \sum_{k \in S_i} \tilde{q}_k^{\text{data}} \tau_k, \tag{6.43}$$

$$\tilde{q}_{S_i}^{\text{ack}} = \sum_{k \in S_i} \tilde{q}_k^{\text{ack}} \tau_k, \tag{6.44}$$

where the computation of the individual probabilities $\tilde{q}_k^{\text{rts}}$, $\tilde{q}_k^{\text{cts}}$, $\tilde{q}_k^{\text{data}}$, and $\tilde{q}_k^{\text{ack}}$ should follow the same developments as for the computation of the successful handshake probability $q_k$ in Section 5.6. Hence, the average time $t_i^{uns}$ the channel is perceived busy by a node $i \in V$ due to an *unsuccessful handshake* over the channel (in Eq. (6.35)) is finally given by

$$t_i^{uns} = \tilde{t}^{\text{rts}} \tilde{q}_{S_i}^{\text{rts}} + \tilde{t}^{\text{cts}} \tilde{q}_{S_i}^{\text{cts}} + \tilde{t}^{\text{data}} \tilde{q}_{S_i}^{\text{data}} + \tilde{t}^{\text{ack}} \tilde{q}_{S_i}^{\text{data}}. \tag{6.45}$$

Finally, for the average time $t_i^{suc}$ the channel is perceived busy due to a *successful handshake*, we have

$$t_i^{suc} = \text{RTS} + \text{SIFS} + \delta + \text{CTS} + \text{SIFS} + \delta + \text{H} + E\{P\} + \text{ SIFS} + \delta + \\ + \text{ACK} + \delta + \text{EIFS}, \tag{6.46}$$

where $H$ and $E\{P\}$ are the time to transmit the data frame header and an average payload size, respectively. Notice that $t_i^{suc}$ is equal to $\tilde{t}^{\text{ack}}$ in Eq. (6.40) because, although the ACK may not be received correctly, the time the channel is busy is basically the same.

To finish the computation of the backoff time in Eq. (6.34), we need to compute the average time $t_i^{res}$ a node $i \in V$ spends in collision resolution, as indicated in Eq. (6.34). In the standard, this means that a CTS is not received within a CTS_Timeout interval or an ACK is not received back within an ACK_Timeout interval. The length of these intervals, however, are not specified by the standard. Usually, such intervals are assumed to be equal to the time it lasts to receive the CTS (ACK) back after an RTS (DATA) is transmitted. Because the CTS and ACK frames have the same length in bytes, and they are transmitted with the same basic data rate, we define[2]

$$\text{CTS\_Timeout} = \text{ACK\_Timeout} = \text{SIFS} + \text{ACK} + 2\delta. \tag{6.47}$$

Finally, from the model in Section 6.1, the time spent in collision resolution depends on whether the failed handshake happened within a CTS timeout or an ACK timeout. In the case the handshake failed within a CTS timeout, the time spent on collision resolution is going to be equal to the CTS_Timeout value. Otherwise, it means that an RTS/CTS handshake was

[2]Simulators such as Qualnet and NS-2 use these same values.

successful, but the subsequent DATA/ACK handshake not. Therefore, by the time the node realizes that the DATA/ACK portion of the handshake failed, it has already spent the time on the first RTS/CTS handshake completion. Therefore, we time spent on collision resolution is conditioned on the reason for the failed handshake. In other words, by defining $t_i^{res}|_{rts/cts}$ as the time spent on collision resolution given that the handshake failed during the RTS/CTS portion of the handshake, and $t_i^{res}|_{dat/ack}$ as the time spent on collision resolution given that the handshake failed during the DATA/ACK portion of the handshake, we have

$$t_i^{res}|_{rts/cts} = \text{RTS} + \text{CTS\_Timeout} \tag{6.48}$$

$$t_i^{res}|_{dat/ack} = \text{RTS} + \delta + \text{SIFS} + \text{CTS} + \delta + \text{SIFS} + \text{H} + E\{P\} + \text{ACK\_Timeout}. \tag{6.49}$$

From Section 6.1, the probability that a failed RTS/CTS handshake occurs at the end of a backoff stage is given by $p_i, \forall i \in V$, whereas the probability that a failed DATA/ACK handshake fails is given by $d_i, \forall i \in V$. Hence, the average time $t_i^{res}$ a node $i \in V$ spends in collision resolution is given by

$$t_i^{res} = p_i t_i^{res}|_{rts/cts} + (1 - p_i) d_i t_i^{res}|_{dat/ack}, \quad \forall i \in V, \tag{6.50}$$

and the average backoff time in Eq. (6.34) can be finally computed for every node $i \in V$.

### 6.3.3 Average Service Time

Given the characterization of the average backoff time $\overline{T}_{B_i}$ of each node $i \in V$, we can proceed with the computation of the average time $\overline{T}_i^{ser}$ it takes for a node to serve data frames. By "average time to serve data frames" we refer to the average time interval that initiates at the moment a data frame is taken from the head of the output queue to the

moment the node decides that either the frame has been successfully transmitted or needs to be dropped after exceeding the maximum number of retransmissions (according to the IEEE 802.11 DCF MAC). Notice that, in Chapter 2, nodes were allowed to backoff *infinitely* in time. Consequently, data frames were assumed to be always transmitted successfully and, consequently, never dropped. Later, in Chapter 4, we introduced the finite-retry limit on the number of retransmissions into the analytical model. But, because of the assumption of perfect channel conditions, we restricted the impact of the finite-retry limit to the computation of the average backoff time only. Nevertheless, if physical layer aspects and network topology are taken into account, the computation of the average service time needs to be addressed more carefully.

Because each data frame is going to be either successfully transmitted or dropped, a key information to the computation of the average service time is the probability $p_i^{drop}$ *that a data frame is dropped (discarded)*. To compute this probability, we first note that the probability $q_i$ that a node $i \in V$ performs a successful handshake at the end of a backoff stage is given by Eq. (6.32). From the independence assumption adopted in Section 6.1 regarding the probability of successful handshake among backoff stages, and considering that each data frame is entitled to a maximum number $M$ of retransmissions, then, the probability that a data frame is dropped is simply given by

$$p_i^{drop} = (1 - q_{rts}q_{dat})^{M+1}, \quad \forall\, i \in V, \tag{6.51}$$

where the power of $M + 1$ stands for the $(M + 1)$-th attempt to transmit the data frame at the end of the $M$-th backoff stage (the counting of backoff stages starts at zero, and we need to count the first transmission attempt before the node starts making retransmissions (see

Figure 6.1)).

If the data frame is dropped, it means that it has already been retransmitted $M$ times. Therefore, if a data frame goes through all $M+1$ backoff stages, the average time $\overline{T}_{B_i}(M)$ spent in backoff is given by Eq. (2.9), which we repeat here for convenience:

$$\overline{T}_{B_i}(M) = \sum_{k=0}^{M} \overline{T}_{B_i}^{k} + M t_i^{res}, \tag{6.52}$$

where $\overline{T}_{B_i}^{k} = \alpha_i(W_k - 1)/2$ is the average time spent in backoff stage $k$, as introduced in Eq. (2.5), and $t_i^{res}$ is the average time the node $i \in V$ spends in collision resolution, as computed in Eq. (6.50) (note that backoff stages are numbered starting from zero in order to agree with the notation adopted in the Markov model). But, because

$$W_k = \begin{cases} 2^k W_{\min} & \text{if } 0 \leq k < m \\ 2^m W_{\min} & \text{if } m \leq k \leq M, \end{cases} \tag{6.53}$$

we have

$$\begin{aligned} \sum_{k=0}^{M} \overline{T}_{B_i}^{k} &= \sum_{k=0}^{m-1} \overline{T}_{B_i}^{k} + \sum_{k=m}^{M} \overline{T}_{B_i}^{k} = \sum_{k=0}^{m-1} \frac{\alpha_i \left(2^k W_{\min} - 1\right)}{2} + \sum_{k=m}^{M} \frac{\alpha_i \left(2^m W_{\min} - 1\right)}{2} \\ &= \sum_{k=0}^{m-1} \frac{\alpha_i \left(2^k W_{\min}\right)}{2} + \sum_{k=m}^{M} \frac{\alpha_i \left(2^m W_{\min}\right)}{2} - \sum_{k=0}^{M} \frac{\alpha_i}{2} \\ &= \frac{\alpha}{2} \left\{ W_{\min} \left[ 2^m (M - m + 2) - 1 \right] - M - 1 \right\}. \end{aligned} \tag{6.54}$$

Consequently, the average time $\overline{T}_{B_i}(M)$ spent in backoff until the end of the $M$-th backoff stage is given by

$$\overline{T}_{B_i}(M) = \frac{\alpha}{2} \left\{ W_{\min} \left[ 2^m (M - m + 2) - 1 \right] - M - 1 \right\} + M t_i^{res}. \tag{6.55}$$

To complete the computation of the average service time spent when a data frame is dropped, we need to take into account the final four-way handshake attempt at the end of

the $M$-th backoff stage. But, because this four-way handshake fails, the average time spent is given by $t_i^{res}$ in Eq. (6.50). Hence, the average service time $\overline{T}_i^{drop}$ spent when a data frame is dropped is given by

$$\overline{T}_i^{drop} = \overline{T}_{B_i}(M) + t_i^{res}. \tag{6.56}$$

On the other hand, if the data frame is transmitted successfully, it means that the successful transmission happens in any of the $M + 1$ transmission attempts. In this case, the average time spent in backoff is given by Eq. (6.34). But, again, the expression in Eq. (6.34) does not include the average time spent on the last four-way handshake attempt, in which case the data frame is successful, i.e., the total time spent in the successful four-way handshake at the end of the backoff stage. If $\overline{T}_i^{\text{4-way}}$ denotes the average time spent on a successful four-way handshake, than $\overline{T}_i^{\text{4-way}}$ will be given by

$$\overline{T}_i^{\text{4-way}} = \text{RTS} + \text{CTS} + H + E\{P\} + \text{ACK} + 3 \times \text{SIFS} + 4 \times \delta. \tag{6.57}$$

Therefore, the average service time $\overline{T}_i^{suc}$ spent when a data frame is successfully transmitted by a node $i \in V$ is given by

$$\overline{T}_i^{suc} = \overline{T}_{B_i} + \overline{T}_i^{\text{4-way}}, \quad \forall\, i \in V. \tag{6.58}$$

Finally, given that a data frame is dropped with probability $p_i^{drop}$, and it is transmitted successfully with probability $1 - p_i^{drop}$, the average service time $\overline{T}_i^{ser}$ observed at each node $i \in V$ will be given by

$$\overline{T}_i^{serv} = \left(1 - p_i^{drop}\right) \overline{T}_i^{suc} + p_i^{drop}\, \overline{T}_i^{drop}, \quad \forall i \in V. \tag{6.59}$$

### 6.3.4 Average Time Between Successful Data Frame Transmissions

Previously, we have computed the average time a node spends dealing with *each* data frame, i.e., the *average service time*. But, because data frames can be dropped, an important performance metric of interest is the *average time between the completion of two successful data frame transmissions*. It is expected that a random number of data frames are dropped right after completion of a successful four-way handshake and before the occurrence of the next successful data frame transmission.

Therefore, it is important to characterize the probability distribution of the number of dropped data frames between two consecutive successful data frame transmissions. Let $D$ be a random variable that indicates the number of dropped data frames right after completion of a successful four-way handshake and before the occurrence of the next successful data frame transmission. As a consequence of the independence assumption on the successful handshake between backoff stages, we have that the probability that a given data frame is dropped is independent of the event that any previous data frames were dropped, which is equal to $p_i^{drop}$ in Eq. (6.51) for a node $i \in V$. Consequently, $D$ is geometrically distributed with parameter $p_i^{drop}$. So, after completion of a successful four-way handshake, $D$ frames will be dropped before a successful data frame transmission occurs. The average service time for each of the $D$ drops is equal to $\overline{T}_i^{drop}$. After the $D$ frame are dropped, node $i$ succeeds in transmitting a data frame, which has an average service time equal to $\overline{T}_i^{suc}$. Consequently, the average time $\overline{T}_i$ between the completion of two successful data frame transmissions from

node $i \in V$ will be given by

$$\overline{T}_i = \sum_{d=0}^{\infty} \left( \overline{T}_i^{suc} + d\,\overline{T}_i^{drop} \right) P\{D = d\} = \sum_{d=0}^{\infty} \overline{T}_i^{suc} P\{D = d\} + \sum_{d=0}^{\infty} d\,\overline{T}_i^{drop} P\{D = d\}$$
$$= \overline{T}_i^{suc} \sum_{d=0}^{\infty} \left( p_i^{drop} \right)^d \left( 1 - p_i^{drop} \right) + \overline{T}_i^{drop} \sum_{d=0}^{\infty} d \left( p_i^{drop} \right)^d \left( 1 - p_i^{drop} \right), \tag{6.60}$$

which leads to

$$\overline{T}_i = \overline{T}_i^{suc} + \frac{p_i^{drop}}{1 - p_i^{drop}} \overline{T}_i^{drop}, \quad \forall\, i \in V. \tag{6.61}$$

### 6.3.5 Average Data Service Rate

Once the average service time is known, we can compute the average rate at which useful data is served by a node $i \in V$. This performance metric indicates how much useful data is served/processed per unit of time by a specific node in the network. For computation of this performance metric, we first observe that we are dealing with saturated networks, i.e., networks in which all nodes have always a data frame ready for transmission at the head of their output queues. Consequently, the *average data service rate* $G_i$ will be given by the ratio of the average data payload size $\overline{P}_i = E\{P_i\}$ that node $i$ transmits to the average service time $\overline{T}_i^{serv}$ per data frame, given by Eq. (6.59). In other words,

$$G_i = \frac{\overline{P}_i}{\left( 1 - p_i^{drop} \right) \overline{T}_i^{suc} + p_i^{drop}\, \overline{T}_i^{drop}}, \quad \forall\, i \in V. \tag{6.62}$$

### 6.3.6 Average Throughput

Finally, we compute the average throughput of each node $i \in V$, which is simply the average amount of useful data that node $i$ transmits successfully per unit of time. As before, we start from noticing that we are dealing with saturated networks. Therefore, the average

throughput $S_i$ of each node $i \in V$ will be given by the ratio of the average data payload size $\overline{P}_i$ that node $i$ transmits, to the the average time $\overline{T}_i$ between completion of two successful data frame transmissions, given by Eq. (6.61). Consequently,

$$S_i = \frac{\overline{P}_i}{\overline{T}_i^{suc} + \left(\frac{p_i^{drop}}{1-p_i^{drop}}\right)\overline{T}_i^{drop}}, \quad \forall\, i \in V. \tag{6.63}$$

As a final note, we can obtain a relationship between the average data service rate $G_i$ and the average throughput $S_i$. From Eqs. (6.62) and (6.63), it is easy to show that

$$S_i = \left(1 - p_i^{drop}\right) G_i, \quad \forall\, i \in V, \tag{6.64}$$

i.e., as expected, the average throughput $S_i$ is simply the fraction of the average data service rate $G_i$ corresponding to successful data frame transmissions.

## 6.4 Model Validation

In this section, we evaluate the accuracy of our analytical model in predicting the performance of nodes in multihop ad hoc networks that operate according to the IEEE 802.11 standard. We focus on ad hoc networks with static topologies under traffic saturation. Numerical results derived from the analytical model are compared with discrete-event simulations using the Qualnet Simulator v3.5 [105].

### 6.4.1 Scenarios Used for Comparison

#### Radio Channel Model

For the purposes of validation of our modeling framework, we consider a radio channel model with large-scale path loss propagation effects only. The path loss propagation

model we choose is the two-ray ground reflection model [111]. We choose a simpler channel model in order to focus on the model's ability to faithfully represent interdependencies among the nodes and the per-node performance metrics. Nonetheless, as discussed in Section 5.3.1, other signal propagation effects such as shadowing and small-scale multipath fading may be equally taken into consideration when computing the conditional probabilities $f(c_{ik}^r)$ of a successful frame reception. In Chapter 8, we study the impact of small-scale multipath fading channels on the performance of multihop ad hoc networks.

**IEEE 802.11 Parameters**

Regarding the IEEE 802.11 PHY layer, we use direct sequence spread spectrum (DSSS) with a raw bit rate of 1 Mbps with DBPSK modulation. Under this configuration, according to the standard, both preamble and MAC protocol data unit (MPDU) are transmitted at the same basic rate, under the same modulation scheme [64]. Without loss of generality, this is done just to ease the analysis and to avoid adding more complexity into the analytical model by treating each segment separately, with different modulation schemes.

Each node has the same transmit power and, for the given path loss propagation model, we select receive and carrier sensing thresholds in a way that the radio range is set to 200 m and carrier sensing range is set to 400 m. Table 7.5.1 summarizes the rest of the parameters used for PHY and MAC layers.

As in Qualnet, we treat bit errors independently. Hence, if we let $\gamma(c_{ik}^r)$ denote the SINR at node $r$ during reception of a bit that was transmitted by node *i*, and for which the combination of active interferers is $c_{ik}^r$ (as defined in Section 5.3.1), then, if $K$ is the length

**Table 6.1**: IEEE 802.11 Simulation Parameters.

| MAC | | PHY | |
|---|---|---|---|
| $W_{min}$ | 256 | Temperature (Kelvin) | 290 |
| $W_{max}$ | 1024 | Noise factor | 10 |
| MAC Header (bytes) | 34 | Transmission power (dBm) | 10 |
| ACK (bytes) | 38 | Sensitiviy of PHY (dBm) | -87.039 |
| CTS (bytes) | 38 | Minimum power for | |
| RTS (bytes) | 44 | received packet (dBm) | -76.067 |
| Slot Time ($\mu$sec) | 20 | Packet reception model | BER |
| SIFS ($\mu$sec) | 10 | | |
| DIFS ($\mu$sec) | 50 | | |

of the physical layer convergence protocol data unit (PPDU) defined by the IEEE 802.11 standard, and $P_b(\gamma)$ is the bit-error probability of DBPSK for a certain SINR level $\gamma$, the conditional probability $f(c_{ik}^r)$ of a successful frame reception (as used in Section (5.3.1)) will be given by

$$f(c_{ik}^r) = \{1 - P_b[\gamma(c_{ik}^r)]\}^K . \tag{6.65}$$

**Simulation Setup**

Because of the selected radio range, nodes are randomly placed in an area of $1000 \times 1000$ m, a size big enough to deploy a multihop network. The only constraint imposed is that the resulting graph is connected. This constraint is added simply to make sure that all nodes have at least one neighbor, and that considerable channel contention and hidden-terminal effects are present in the scenarios.

In simulations, each node chooses the same neighbor node (i.e., a node within its transmission range) for all its transmissions using the same CBR source rate. We pick source rates high enough to saturate all nodes in the network. Packet sizes are fixed to 1500 bytes (IP packet) and each simulation run corresponds to 5 minutes of data traffic. We repeat the

experiment for 50 seeds, with each trial corresponding to a different initial transmission times at each node. Initial transmission times are randomly chosen within the interval $[0,\ 0.01]$ s. This is done to allow the exponential backoff algorithm to be triggered at different instants in time, at each node, so that different state evolutions are taken into account for the same topology.

### 6.4.2 Accuracy of Models

Two aspects of interest in our modeling approach are *scalability* and *per-node* performance. To illustrate such aspects, let us consider two network topologies: one with 50 nodes and another with 100 nodes. Figures 6.7 and 6.8 show their respective topologies. In the figures, the numbers inside the areas indicate the node ID. To provide an idea of the density of nodes in each topology, a line between two nodes indicates that they are within 200 meters of one another. As it can be observed, the created topologies provide both highly-dense as well as poorly-connected areas. Needless to say, interference at a given receiver in the analytical model and simulations is not confined to only those sources shown directly "connected" in the figures.

Figure 6.9 shows the simulation and analytical results for the 50-node network. Figure 6.10 shows the results for the 100-node network. In the graphs, the $x$ axis contains the node ID, and the $y$ axis shows the respective throughput. As it can be seen, the predicted performance correlates very well with practically every node in the topology (in some cases, providing very close results). In the cases where the model is off by some factor, the predicted performance follows the observed pattern in the majority of the cases.

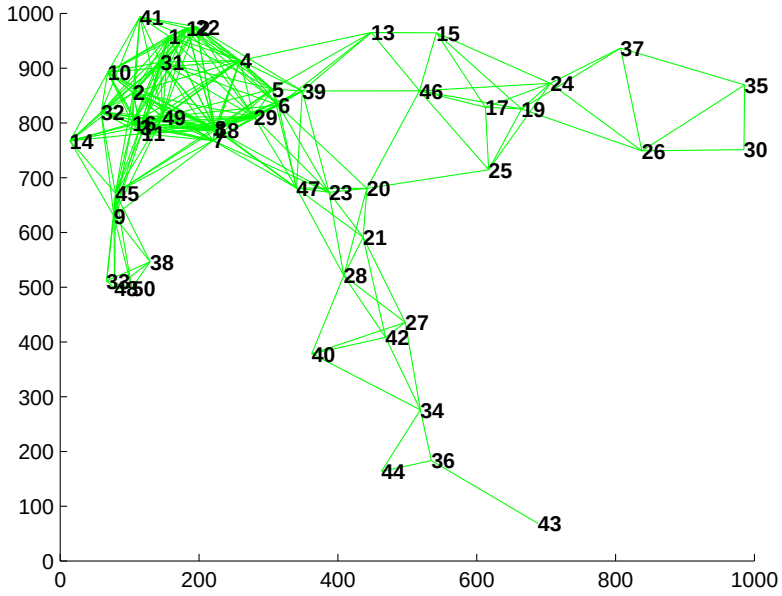


**Figure 6.7**: Network topology for the 50-node network.

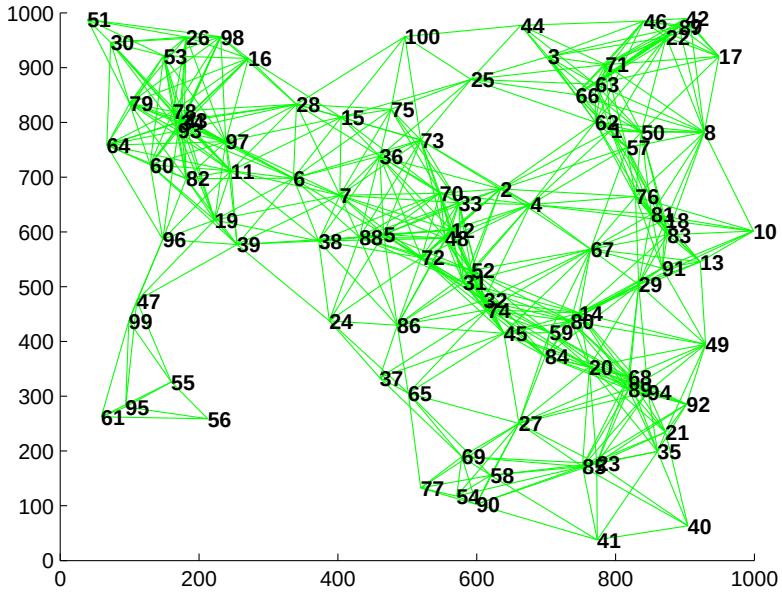


**Figure 6.8**: Network topology for the 100-node network.

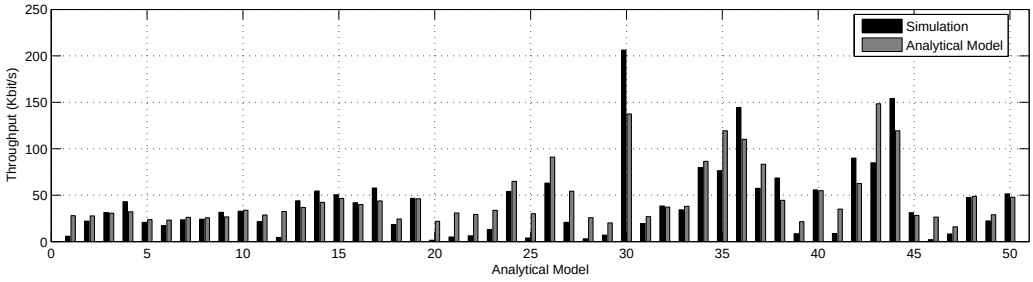


**Figure 6.9**: Throughput: simulations versus analytical model for the 50-node network.

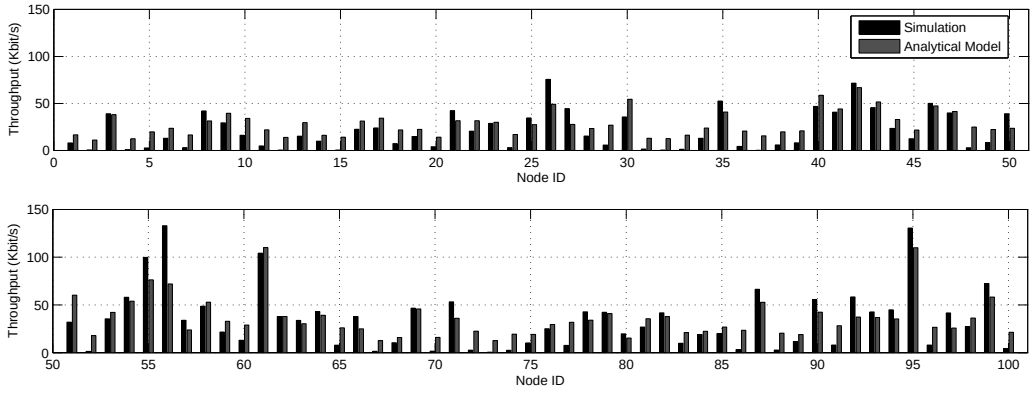


**Figure 6.10**: Throughput: simulations versus analytical model for the 100-node network.

A more statistically significant result is obtained if we evaluate the performance of our modeling approach over a number of different topologies. For this purpose, we considered 10 network topologies with 100 nodes each, all randomly generated as before. The topologies used for computating the histogram were similar to that shown in Figure 6.8. We compute the percentage prediction error with respect to the maximum range of throughput values observed in simulations (for that particular topology) for each node in each randomly generated topology. This way, we weigh the prediction error with respect to the dynamic range of throughput values obtained in simulations. We obtained a histogram for each topology by counting the number of nodes within a certain percentage prediction error, and we then averaged the histograms over all topologies. Figure 6.11 shows our results. As we can see, the percentage prediction error is within 20% in 93.5% of the nodes, showing how close our analytical model is in predicting the results obtained in discrete-event simulations.

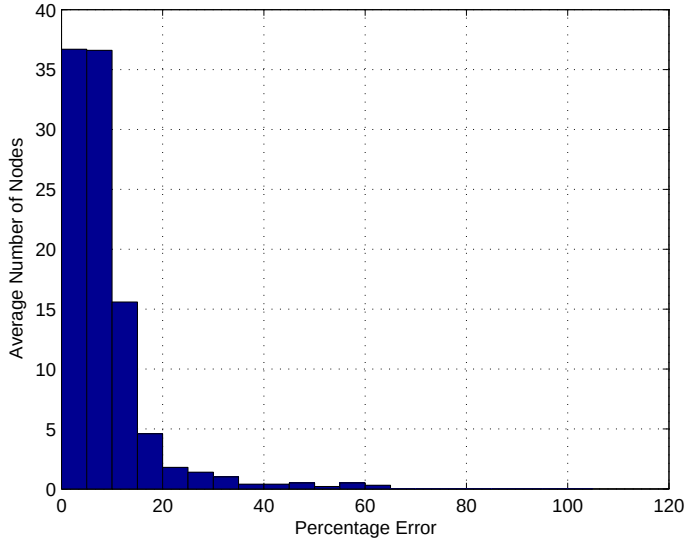


**Figure 6.11**: Percentage error prediction histogram over 10 random topologies.

Another important performance metric we can use to evaluate the accuracy of our analytical model in predicting the results obtained via discrete-event simulations with respect to per-node performance is the *normalized mean squared prediction error* (NMSPE). The NMSPE is defined as the ratio of the *mean squared prediction error* to the *variance* of the original data we want to predict. More specifically, if $\{X_i\}_{i=1}^{n}$ denotes the set of $n$ values of data we want to predict, with a sample mean value of $\overline{X} = \frac{1}{n}\sum_{i=1}^{n} X_i$, and $\{\widehat{X}_i\}_{i=1}^{n}$ is their corresponding predicted values, then, the NMSPE is given by

$$\text{NMSPE} = \frac{\sum_{i=1}^{n}(X_i - \widehat{X}_i)^2}{\sum_{i=1}^{n}(X_i - \overline{X})^2}. \tag{6.66}$$

The main advantage of the NMSPE is that it indicates how good the individual predictions are compared to the case where the best prediction we can make about each data value is equal to the *average* of the original data. In other words, if $\widehat{X}_i = \overline{X}$ for $i = 1, \ldots, n$, in Eq. (6.66), we have NMSPE $= 1$. Hence, the relative amount by which the mean squared prediction error is *less* than the variance of the original data reflects how much better we are from predicting the data by just their mean value. In the jargon of linear regression models, it is the fraction of the variance that is *explained by the model*.

Figure 6.12 shows the NMSPE computed for each of the 10 topologies with 100 nodes that we used before. As we can see, the analytical model performs quite well. The NMSPE is about 0.4 across all topologies investigated, which means that our predictions are 60% better than if we had predicted each node's throughput as equal to the average of the simulation data. Incidentally, it is important to mention that, so far in the literature, no other analytical model has ever attempted to predict *individual* throughput values. To date, all proposed analytical models have only attempted to predict the *average* throughput. Consequently, it means

that *we are, already, 60% better than any other analytical model that predicts each node's throughput only by the average throughput of the IEEE 802.11 ad hoc networks examined before*.

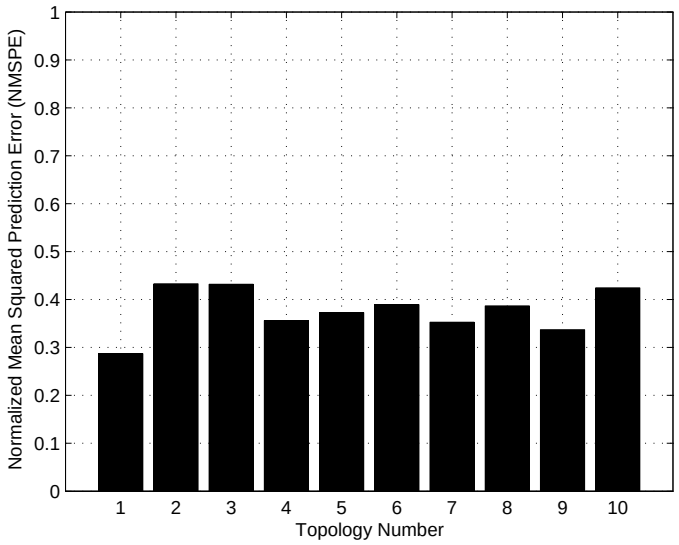


**Figure 6.12**: Normalized mean squared prediction error for 10 topologies with 100 nodes each.

Finally, we show the application of our model in predicting the *average* throughput for a given network topology. Figure 6.13 shows the comparison between the average throughput obtained in both simulations and analytical model. As we can see, the analytical model provides very accurate results compared to simulation results.

### 6.4.3 Modeling Time

The importance of the above results and the strength of our analytical model become apparent when we analyze the time required to obtain the above results through simulation and with our analytical model. In Qualnet, *each run* of the simulation for the 100-node scenario

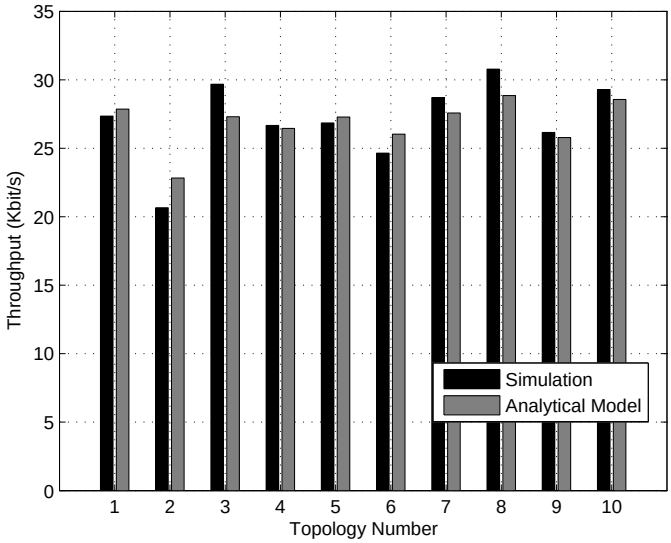


**Figure 6.13**: Average network throughput of 10 topologies with 100 nodes each.

(consisting of a 5-minute data traffic) takes about 1,118.4 seconds (19.69 minutes) in a Sun Blade 100 machine running Solaris 5.8. For the 50 seeds needed, this corresponds to 16.41 hours of simulation. In this same machine, our analytical model, implemented in Matlab 6.0, takes about 0.44 seconds. This corresponds to a time saving of more than 134,000 times. Clearly, this is a strong argument supporting the case for the need of powerful analytical models for multihop ad hoc networks, such as the one we are providing here.

### 6.4.4 Model Limitations

Despite the striking correlations of our analytical model with the results obtained via simulations, improvements in the model can still be done, especially regarding the modeling of the IEEE 802.11 itself.

As explained in Section 6.1, the Markov model we used to model the binary ex-

ponential backoff operation of the IEEE 802.11 DCF MAC has a small simplification with respect to the original specification. Instead of considering the two retry counters defined by the standard (the SLRC and the SSRC), we adopted a single retry counter, the RC, to be incremented whenever an RTS or DATA frame is unsuccessfully transmitted. Such simplification is likely to affect mostly the performance of nodes which are located in neighborhoods under heavy contention and/or nodes that are too distant of their intended receivers, in which case the frame losses tend to be more frequent, reflecting on the dynamics of the protocol with respect to the two retry counters.

In fact, related to the dynamics of the protocol operation is the issue of fairness of the IEEE 802.11 DCF MAC. As it is well known, the IEEE 802.11 DCF MAC tends to favor the nodes that have last acquired the channel with respect to a given time instant. This is because the nodes that succeeded in transmitting their frames reduce their contention window sizes, while the opposite happens to the nodes that failed to access the channel. Consequently, a biased behavior towards the nodes with smaller contention window sizes start happening: they have higher chances to find the channel free than the nodes which are backing off under bigger contention window sizes. Therefore, a more aggressive behavior is observed at nodes with smaller contention window sizes, which can obtain higher throughput values and can cause the "starvation" of the other competing nodes. Unfortunately, the model we introduced for the operation of the IEEE 802.11 DCF MAC does not attempt to capture the impact of the fairness problem. Therefore, a more accurate model of the operation of the IEEE 802.11 DCF MAC should be able to address these issues.

## 6.5 Conclusions

We have introduced a novel modeling framework for MAC protocols in multihop ad hoc networks. The model focuses on the interactions between the MAC layer and any layer(s) with which it exchanges information (directly or indirectly), and on the impact that each node has on the dynamics of every other node in the network—all conveniently conveyed through the use of *interference matrices*. A key feature of the model is that nodes can be modeled individually, i.e., it allows a per-node setup of many layer-specific parameters. Moreover, no spatial probability distribution or special arrangement of nodes is assumed. Instead, it allows the computation of individual (per-node) performance metrics for any given network topology and radio channel model. To show the applicability of the modeling framework, we modeled multihop ad hoc networks using a new analytical model for the IEEE 802.11 DCF.

Our analytical model constitutes a tool for a fast, accurate, and efficient evaluation of a node's performance for any system parameter value and topology of an ad hoc network. We have illustrated this using the IEEE 802.11 DCF as an example. Attempting to characterize a node's performance only by simulations would require considerable computational effort, specially when scalability is one of the main concerns. To be able to draw general conclusions, simulations would have to be run for a very large number of network sizes and topologies. Furthermore, if we are interested in evaluating the impact of a single parameter to a node's service time, for instance, simulations would have to be repeated for each parameter value of interest.

Our model was validated through discrete event simulations using the popular Qualnet tool, and the analytical results show a striking correlation with the results obtained via

simulation. The importance of the analytical model is that the time needed to obtain the desired results takes a very small fraction of the time required to obtain the same results via discrete-event simulations.

# Chapter 7

# Modeling Ad Hoc Networks that Utilize Directional Antennas

This chapter presents the first analytical modeling of wireless ad hoc networks that considers the impact of realistic antenna-gain patterns on network performance. As such, our modeling approach allows the study of ad hoc networks in which nodes are equipped with directional antennas. This modeling capability stands out from all previous analytical models, which have only dealt with omnidirectional or over-simplified antenna gain patterns, and which have not addressed the specific mechanisms of the medium access control (MAC) protocols used (e.g., the backoff mechanism). Our numerical results show that our analytical model predicts the results obtained via discrete-event simulations very accurately, and does it with a processing time that is orders of magnitude faster than the time required by simulations. Furthermore, we show that the simplistic "pie slices" used in prior analytical models for antenna patterns over-estimate the throughput of the protocols dramatically compared to the results obtained

using realistic antenna patterns.

## 7.1 Introduction

Directional antennas (antennas that are able to transmit/receive energy over intended directions) have a number of advantages over *omnidirectional* antennas, i.e., antennas that (ideally) radiate or absorb energy equally well along all directions. Among these advantages, directional antennas can increase the signaling range without spending extra power, reduce intersymbol interference (ISI) and flat-fading by canceling or attenuating interferences from giving directions, and suppress interference between users. In particular, directional antennas can increase the potential for spatial reuse, thereby increasing system capacity.

A number of protocols for wireless ad hoc networks with directional antennas have been proposed, mostly on the medium access control (MAC) layer (e.g., [74,75,86,145]). The vast majority of the performance-evaluation work on MAC protocols that exploit directional antennas has used discrete-event simulations to model protocol behavior. Only a few works have attempted to model ad hoc networks with directional antennas *analytically*. Section 8.2 summarizes this prior work, which has been very limited in that all the analytical models proposed to date have assumed (a) simplistic ways in which packets are offered to a shared channel, ignoring the specific mechanisms used in MAC protocols (e.g., backoff mechanisms), and (b) the use of over-simplified antenna gain patterns, like the "pie-slice" and "cone-plus-ball" antenna models [23,131,144,146]. In the simplistic antenna models used to date, all directions within a certain angle sector have constant gain, while no power is radiated/absorbed along the other directions ("pie-slice"), or a lower constant gain is assumed for the directions outside

the angle sector to represent the back and side lobes of the antenna pattern ("cone-plus-ball"). In reality, no physical antenna can provide such constant gain for a given angle sector, and real antenna patterns are far more complex than "pie-slices" or "cone-plus-ball" models. In fact, real antenna patterns have non-negligible gains in *all* directions, and often have significant side and back lobes that can contribute considerably to the amount of perceived noise, leading to performance degradations such as the ones observed by Ramanathan et al. [96] in a real-life ad hoc network testbed. Consequently, conclusions about capacity improvements based on such over-simplified antenna models (e.g., [144] and [95]), may not necessarily reflect the true potentials or limitations of the use of directional antennas in ad hoc networks.

In this chapter, we present the first analytical modeling of wireless ad hoc networks that considers the impact of realistic antenna gain patterns on network performance. In particular, we focus on the modeling of wireless ad hoc networks with directional antennas.

Section 7.3 summarizes the operation of the *directional virtual carrier sensing* (DVCS) protocol [114], which we use subsequently to show the accuracy of our analytical model compared to simulations. Section 7.4 outlines the main issues that arise in the analytical modeling of ad hoc networks in which nodes use directional antennas. Based on the analytical model of the IEEE 802.11 developed in chapter 6, we model the DVCS protocol and compare its accuracy against results obtained with discrete-event simulations using realistic antenna patterns. The numerical results presented in Section 7.5 indicate that our analytical model predicts simulation results very accurately, with processing times that are orders of magnitude faster than simulations. In addition, we show that "pie-slice" models of antenna patterns are extremely optimistic regarding the benefits of directional antennas. Because simplified an-

tenna patterns do not have side lobes, average throughputs are dramatically over-estimated. In the cases we modeled, "pie-slice" patterns renders 200% higher throughput than what is obtained using realistic antenna patterns. Section 8.5 summarizes our conclusions.

## 7.2 Related Analytical Work

Most of the work in ad hoc networks with directional antennas has used discrete-event simulations to model protocol operation and evaluate its performance (e.g., [30, 75] and references therein). As far as the analytical modeling is concerned, most of the previous work has concentrated on single-hop networks [76, 103, 132, 133]. To date, very few attempts have been done to the analytical modeling of multihop ad hoc networks with directional antennas. Chang and Chang [23] were arguably the first to analyze the use of directional antennas in slotted ALOHA and non-persistent CSMA. Their modeling approach closely follows the formalism used by Takagi and Kleinrock [113], in which nodes are spatially located according to a two-dimensional Poisson distribution, radio links are error-free (no physical layer aspects whatsoever), no acknowledgment traffic exists, and the transmitters have "instantaneous" knowledge of successful receptions. They use the "pie-slice" antenna gain model for the directional antennas. Later, Zander [146] proposed a slightly different approach to model slotted ALOHA, with the same antenna model and spatial distribution assumptions, but included a propagation model and treated packet receptions with a simple threshold model based on signal-to-noise ratio (SNR).

Wang and Garcia-Luna-Aceves [131] introduced the modeling of collision avoidance MAC protocols with directional antennas. Based on the IEEE 802.11 DCF MAC, they

modeled and analyzed many of its variants with respect to the directional transmission of control and data packets coupled with omnidirectional or directional receptions (and hybrid operations). Their modeling approach also follows the work by Takagi and Kleinrock [113] with respect to the spatial distribution of nodes and absence of physical layer aspects, and the approach of Wu and Varshney [139] for the modeling of the node activity with a Markov chain with only three states. The limitations of this effort is that it assumes the "pie-slice" antenna model, and that transmission probabilities are taken from a "range of small values", thereby disregarding the fact that transmission probabilities are protocol-dependent (i.e., they do not consider the binary exponential backoff operation of the IEEE 802.11 and such parameters as contention window size or retry limits).

## 7.3 The Directional Virtual Carrier Sensing (DVCS) Protocol

A number of MAC protocols for ad hoc networks with directional antennas have been proposed in the past few years. In many cases, however, the proposed protocols have failed to provide a new MAC protocol in its strict sense, i.e., no new paradigms or mechanisms at the MAC *level* were presented. Instead, they have essentially investigated how directional transmissions/receptions of control/data frames impact network performance under a given MAC protocol originally designed to work with omnidirectional antennas (e.g., IEEE 802.11). Examples of such proposals include [74], [86], [95], and [131]. Few works have tried to propose new MAC-level mechanisms that attempt to take full advantage of the capabilities provided by directional antennas. One of the first such attempts was the *directional virtual carrier sensing protocol* (DVCS) proposed by Takai et al. [114].

The main idea behind DVCS is to allow contention-based MAC protocols to determine direction-specific channel availability. For that, DVCS uses the *directional network allocation vector* (DNAV), a directional version of the network allocation vector (NAV) of the IEEE 802.11, which contains information about the total duration of a transaction that is about to happen over the channel. During this time, the node cannot transmit any frame to the channel, reserving it for others do it. In DVCS, the DNAV reserves the channel for others only in a *range of directions*. To accomplish this, DVCS requires minimal information from the underlying physical device, such as the angle of arrival (AOA) and the antenna gain for each signal, features that can be readily available at the physical layer.

Multiple DNAVs can be set for a node, and each DNAV is associated with a direction and a width. Every node using DVCS maintains a unique timer for each DNAV, and updates the direction, width, and expiration time of each DNAV every time the physical layer gives newer information on the corresponding ongoing transmission. DVCS determines that the channel is available for a specific direction when no DNAV covers that direction.

In DVCS, each node caches estimated AOAs from neighboring nodes every time it hears any signal, regardless of whether the signal is addressed to it. If a node has data to send, it first checks if AOA information for the particular neighbor has been cached. If yes, it beamforms the directional antenna towards the cached AOA direction to send an RTS frame. Otherwise, the frame is transmitted omnidirectionally. Updates are done every time the node receives a newer signal from the neighbor, and it invalidates the cache if it fails to get the CTS back from the neighbor after 4 failed directional transmissions of RTS frames. Subsequent RTS frames are sent omnnidirectionally.

When the node receives an RTS frame from a neighbor, it adapts its beam pattern to maximize the received power and locks the pattern for the CTS transmission. If the node transmitted an RTS frame to a neighbor, it locks the beam pattern after it receives the CTS frame from the neighbor. The beam patterns at both sides are used for both transmission and reception, and are unlocked after the ACK frame is transmitted. We refer the reader to [114] for more details.

## 7.4 Challenges in the Modeling of Wireless Ad Hoc Networks with Directional Antennas

Many issues arise in the modeling the behavior of an ad hoc network with directional antennas accurately. A good analytical model should be able to incorporate the impact of realistic antenna-gain patterns under specific radio channel models, which has *never* been done before, as well as include the intricate interactions between the MAC layer—designed to operate with directional antennas—and the many aspects of the underlying PHY layer. Most importantly, the model should capture each node's dynamics resulting from its interaction with *every other node in the network*, a core phenomenon within a wireless ad hoc network.

In the case of an ad hoc network using DVCS, for example, one needs to translate into the analytical model how the DNAV works, and which events at the PHY layer are critical at each step of the protocol operation. For instance, during a node's carrier sensing operation, only signal transmissions perceived within the *range of directions* of the target receiver can interfere with the node's backoff operation. In addition, because the node in backoff switches

to omnidirectional mode, the relative antenna gains between this node and all the other nodes will be different from the case when this node is actually transmitting/receiving a frame. In the latter case, the node selects/forms a directional beam pattern to transmit/receive a frame, which will lead to different relative antenna gains with respect to every other node in the network.

Because of the richness of the DVCS operation, and because it is built upon the IEEE 802.11 DCF MAC, we can use the model for the IEEE 802.11 DCF MAC we developed in Chapter 6 to capture the operation of the DVCS and its DNAV mechanism. Next section, we present the model validation of our analytical modeling.

## 7.5 Model Validation

In this Section, we evaluate the accuracy of the analytical model in predicting the performance of multihop ad hoc networks operating with directional antennas under the *directional virtual carrier sensing protocol* (DVCS) MAC protocol [114]. The DVCS allows contention-based MAC protocols to determine direction-specific channel availability. The DVCS uses the *directional network allocation vector* (DNAV), a directional version of the network allocation vector (NAV) of the IEEE 802.11, which contains information about the duration of a transaction that is about to happen on the channel. During this time, the node cannot transmit any frame to the channel, reserving it for others do it. In DVCS, the DNAV reserves the channel for others only in a *range of directions*, and determines that the channel is available for a specific direction when no DNAV covers that direction. We refer the reader to [114] for more details.

### 7.5.1 Simulation and Modeling Setup

We implement the analytical model in Matlab$^{TM}$ 7.0 [81], and conduct discrete-event simulations in Qualnet$^{TM}$ v3.5 [105]. For the directional antennas, we use a switched-beam antenna system with the default antenna gain pattern provided by Qualnet$^{TM}$, as shown in Figure 7.1. As in [114], we only focus on *interference reduction*, i.e., power control is

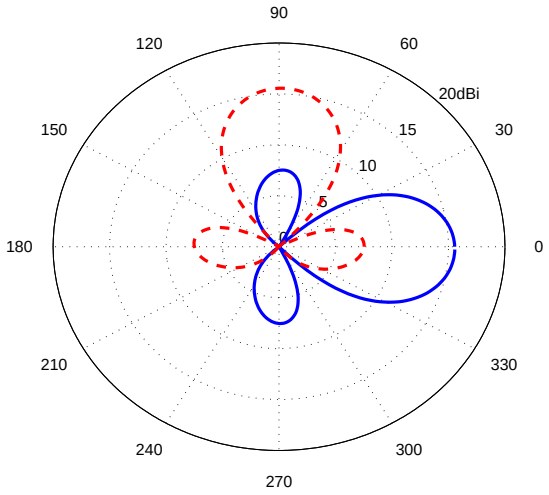


**Figure 7.1**: Antenna gain pattern used for simulations and the analytical model. The figure shows two antenna patterns with boresight angles at 0 and 90 degrees, respectively.

enforced at the transmitter, decreasing the transmit power to compensate for the gain yielded towards the antenna boresight (15 dBi). Consequently, no communication range extension is in place[1].

The selected path loss propagation model is the two-ray ground reflection model. No shadowing or small-scale multipath fading is considered, and bit errors are treated independently, as it is done in Qualnet$^{TM}$. Nodes are randomly placed in an area of $1500 \times 1500$ m.

[1] There is an inherent trade-off between communication range extension and interference reduction [95, 131].

**Table 7.1**: Simulation Parameters: MAC and PHY layers.

| MAC | | PHY | |
|---|---|---|---|
| $W_{\min}$ | 32 | Temperature (Kelvin) | 290 |
| $W_{\max}$ | 1024 | Noise factor | 10 |
| MAC Header (bytes) | 34 | Transmission power (dBm) | 15 |
| ACK (bytes) | 38 | Receive Sensitivity (dBm) | -91.0 |
| CTS (bytes) | 38 | Receive Threshold (dBm) | -81.0 |
| RTS (bytes) | 44 | Packet reception model | BER |
| Slot Time ($\mu$sec) | 20 | Directional Trans. Power (dBm) | 0.0 |
| SIFS ($\mu$sec) | 10 | RX Directional Sensitivity | -75.0 |
| DIFS ($\mu$sec) | 50 | DNAV delta angle (degrees) | 37.0 |

For the physical layer, we use the direct sequence spread spectrum (DSSS) IEEE 802.11 PHY, with a raw bit rate of 1 Mbps under DBPSK modulation. Table 7.5.1 summarizes the rest of the parameters used for the PHY and MAC layers.

The focus of this paper is on the modeling capability of dealing with directional antennas and on the modeling of DVCS itself. Therefore, although we have presented the formalism for dealing with multiple receivers and packet size distributions, these features will not be treated here, as their impact on network performance deserves an analysis on its own. Hence, each node has a single, one-hop receiver for its packets throughout the simulation time, to which it will send fixed-size packets of 1500 bytes (IP packet) generated from a CBR source. The source rate is high enough to saturate all nodes. Each simulation run corresponds to 5 minutes of data traffic, and the experiment is repeated for 20 seeds, with each trial corresponding to a different initial transmission time for each node. Initial transmission times are randomly chosen within the interval $[0,\ 0.01]$ s. This is done to allow the IEEE 802.11 exponential backoff algorithm to be triggered at different time instants at each node, so that different state evolutions occur within the same topology.

Because we analyze a static scenario, we let all RTS transmissions to be directional, as opposed to the default specification of DVCS, which proposes RTS to be transmitted omnidirectionally after 4 consecutive failed attempts, in which case it is assumed that the failure to get a CTS back is due to an inaccurate knowledge of the right direction to transmit (due to mobility).

### 7.5.2 Numerical Results

One of the advantages of our modeling approach is the ability to obtain *per node* performance metrics for a given network topology under a specific radio propagation model and detailed PHY/MAC layers [19]. The power of our modeling approach is best appreciated in the computation of the average throughput for a given network scenario. Figure 7.2 shows the average throughput results computed for 10 random topologies with 100 nodes each. As we can see, the model is able to predict the average throughput very accurately. Figure 7.3 contains a histogram for the average number of nodes within a certain percentage prediction error. The percentage prediction error is computed with respect to the maximum range of throughput values observed in simulations for each node in each randomly generated topology. The histogram is the average of the 10 histograms over all topologies. According to our results, the percentage prediction error is within 20% for about 82% of the nodes. As highlighted in [19], the strength of our analytical model become also apparent when we compare the time required to obtain the above results through simulations and with the analytical model. Each simulation run in Qualnet for the 100-node scenario corresponding to 5 min of data traffic takes about 3060 s (51 min) in a Sun Blade 100 machine running Solaris 5.9. For the 20 seeds

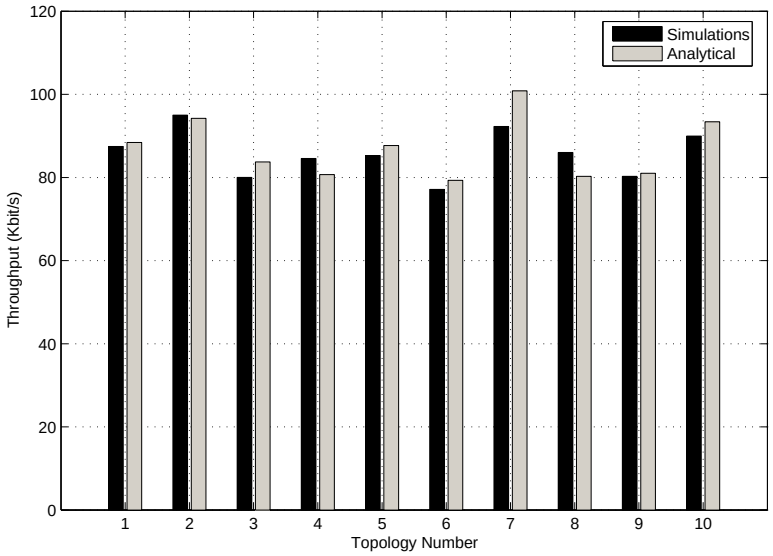


**Figure 7.2**: Average throughput for 10 random topologies with 100 nodes.

used, this corresponds to 17 hours of simulation. Using Matlab 7.0 in this same machine, our analytical model generates results in about 22 s. This corresponds to a time saving of 2800 times. The accuracy and speed attained by our analytical model compared to simulations enables the study of many physical-layer parameters associated with antenna-gain patterns on the performance of a MAC protocol.

## 7.6 Realistic versus Simplified Antenna-Gain Patterns

In this Section, we show how misleading it can be the modeling of ad hoc networks with directional antennas based on over-simplified antenna-gain patterns like, for instance, the "pie-slice" or the "cone-plus-ball" antenna models. For this purpose, we use the same switched-beam antenna system as before, but with antenna-gain patterns that follow a "pie-slice" antenna model, shown in Figure 7.4.

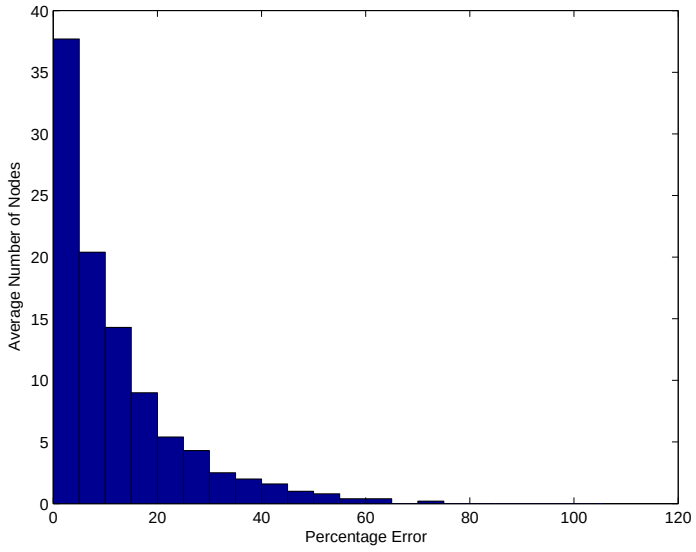


**Figure 7.3**: Percentage error prediction histogram over 10 random topologies with 100 nodes.

Because the previous switched-beam antenna system had 8 main patterns (from which the system selects the best pattern to transmit/receive), the pie-slice antenna model also has 8 patterns, each corresponding to a sector of 45 degrees. Inside each sector, the gain is $15$ dBi, whereas outside the sector the gain is $-41.84$ dBi, which is the minimum observed gain in the antenna-gain pattern of Figure 7.1.

Keeping the same MAC- and PHY-layer parameters as used in Section 7.5, we compute the average throughput for 10 random topologies with a 100 nodes each. The numerical results corresponding to both antenna-gain patterns are shown in Figure 7.5. As we can see, throughput results for ad hoc networks using over-simplified antenna gain patterns are too optimistic. The results suggest an increase in average throughput of more than 200% for the pie-slice antenna patterns. Obviously, such high average throughput is a direct consequence of the fact that no side lobes are present in the pie-slice model, and also non-negligible gains

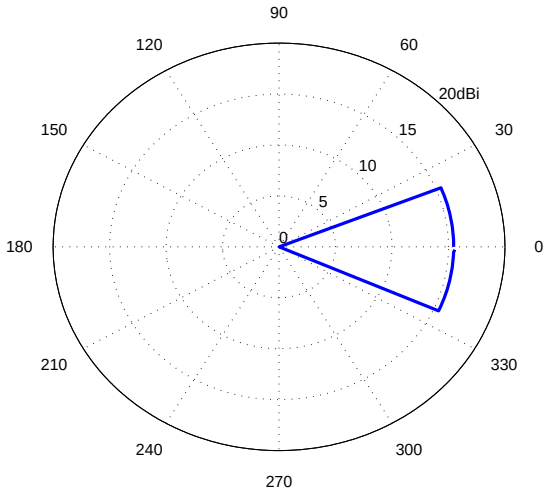


**Figure 7.4**: Pie-slice antenna-gain pattern used for comparison with the realistic antenna-gain model shown in Fig. 7.1.

are present at *all directions* in the realistic antenna gain pattern. Therefore, the use of over-simplified antenna gain patterns in the study of ad hoc networks with directional antennas do not reflect the true potentials and limitations that this technology can achieve.

## 7.7 Conclusions

This chapter presented the first analytical modeling of wireless ad hoc networks that considered the impact of realistic antenna gain patterns on network performance. As such, our modeling approach allows the study of ad hoc networks equipped with *directional antennas*, i.e., antenna systems that are able to transmit/receive energy over preferred directions. We validated our analytical model by comparing its predictions with results obtained through a state-of-the-art simulation package. The results obtained show that our analytical model

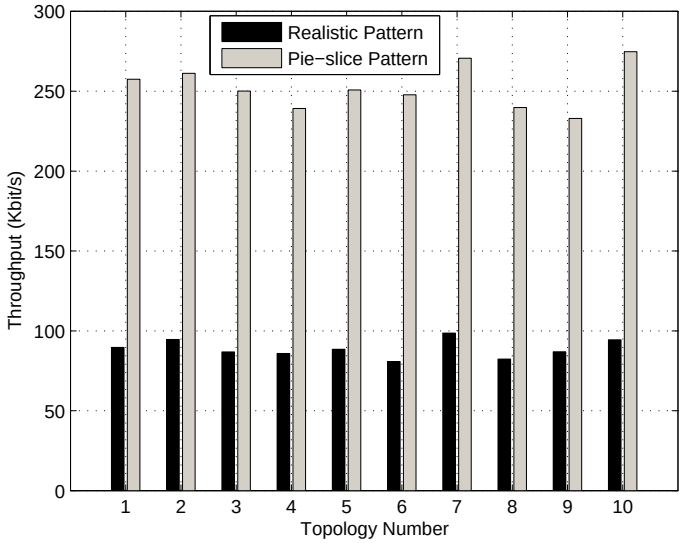


**Figure 7.5**: Average throughput results for 10 topologies with 100 nodes each comparing the predicted performance using the "pie-slice" antenna-gain pattern and a realistic one.

predicts simulation results very accurately, with a processing time that is orders of magnitude faster than simulations. Furthermore, we show that the "pie-slice" models for antenna patterns used in the past exaggerate the throughout attained in a network with directional antennas.

# Chapter 8

# Modeling Ad Hoc Networks that Utilize Space-Time Coding

This chapter presents the first analytical model for ad hoc networks equipped with multiple-input multiple-output (MIMO) radios using space-time coding (STC) that considers the impact of the underlying radio-based topology on network performance. In particular, we consider the space-time block coding (STBC) technique known as the "Alamouti scheme." We derive the effective signal-to-interference-plus-noise density ratio (SINR) of the Alamouti scheme under multiple access interference (MAI), and we propose the moment generating function (MGF) method to derive closed-form expressions for its symbol error probability under different modulation schemes when fading paths are independent but not necessarily identically distributed. The impact of the Alamouti scheme on IEEE 802.11 ad hoc networks is studied by taking into account the impact of errors in both control and data frames, the carrier-sensing activity, and the finite-retry limit of frame retransmissions as derived in Chapter 6. We apply the

Alamouti scheme to different antenna system configurations and compare their performance with respect to the basic single-input-single-output (SISO) IEEE 802.11 DCF MAC.

## 8.1 Introduction

Recent information-theoretic results [136], [43, 44], [119] have shown that large gains in communication capacity over wireless channels can be obtained if multiple antenna elements are used in both ends of the wireless link—the so-called *multiple-input multiple-output (MIMO) systems*. As a consequence, MIMO technology has emerged as one of the most promising fields in modern communications with a chance to resolve the bottleneck capacity of future high-demand wireless networks [53, 85].

In practice, however, achieving the high capacity gains promised by theory requires the development of algorithms and signal design/processing techniques that are able to trade off system complexity with performance (the theory only provides performance bounds based on algorithms/codes with unbounded complexity or latency [53]). One such set of practical signal design techniques is *space-time coding* (STC) [117], [129]. As the name suggests, STC exploits both temporal and spatial dimensions inherent in the use of multiple spatially-distributed antennas to design codes that aim to achieve the capacity limits of MIMO channels. In the *space-time encoder*, code symbols are generated and transmitted simultaneously from each antenna in a way that *diversity*, *array*, and/or *coding* gains can be obtained under high spectral efficiency with the use of appropriate signal processing and decoding procedures at the receiver.

Despite the enormous advantages envisaged with the use of MIMO technology, to

date, the majority of the work in ad hoc networks equipped with multiple antennas has focused on solutions in which the primary goal is to obtain a more reliable communication link by focusing energy into desired directions ("directional antennas"). So far, very few works have attempted to integrate MIMO systems into ad hoc networks, and little is known about the impact of such technology on the performance of ad hoc networks under specific medium access control (MAC) protocols. Section 8.2 reviews the prior work on MIMO ad hoc networks.

Although a cross-layer design approach to both physical (PHY) and MAC layers is likely to obtain the most benefit out of MIMO technology, it is important to know what is the impact of MIMO on the performance of ad hoc networks *if the MAC layer is kept intact*. In fact, such separation of roles may be unavoidable in many cases (e.g., the IEEE 802.11 standard states that [64, pp. 149] "the architecture of the IEEE 802.11 MAC is intended to be PHY independent."). Accordingly, this chapter attempts to address the following questions by introducing the first analytical model of MIMO ad hoc networks with *specific* PHY and MAC layers:

1. How do the PHY improvements provided by a *specific* MIMO technology reflect on overall network performance for a *given* MAC protocol?

2. Are the gains significant enough to justify the added complexity and processing cost incurred by the MIMO technology?

3. How do the performance gains obtained with *multiple-input single-output* (MISO) or MIMO systems compare to the simplest *single-input single-output* (SISO) case?

4. What are the relative gains in performance as the number of antenna elements increases?

We investigate the impact of *space-time block codes* (STBC) [118] in ad hoc networks operating with the IEEE 802.11 DCF MAC. For the STBC, we investigate the use of the Alamouti scheme [4], which is currently part of both W-CDMA and CDMA-2000 standards. Among its advantages, the Alamouti scheme supports maximum-likelihood detection based only on linear processing at the receiver and it does not require channel state information (CSI) at the transmitter. Section 8.3.1 describes the basics of the Alamouti scheme, with an example of a MIMO system with two transmit antennas and two receive antennas. Section 8.3.2 derives the effective signal-to-interference-plus-noise density ratio (SINR) of the Alamouti scheme under multiple access interference (MAI), which is key for the performance of Alamouti-enabled MIMO ad hoc networks. Also, Section 8.3.3 proposes the use of the moment generating function (MGF) method to derive closed-form expressions for the symbol error probability of the Alamouti scheme under different modulation schemes when fading paths are independent but not necessarily identically distributed.

In Section 8.4, we study the impact of the Alamouti scheme into IEEE 802.11 ad hoc networks. Because of its flexibility, we study the use of Alamouti scheme in MISO and MIMO ad hoc networks, comparing their relative performance with respect to SISO networks. Section 8.5 summarizes our conclusions.

## 8.2 Related Work

So far, not much work has been done on MIMO ad hoc networks. Sundaresan *et al.* [112] introduced a distributed MAC protocol for MIMO links based on a centralized MAC that applies spatial multiplexing assuming closed-loop MIMO and ideal interference

cancellation. Tang *et al.* [115] proposed the design of a new transceiver based on a space-time interference canceling technique for MIMO-OFDM, and a MAC protocol (MIMA-MAC) that takes advantage of their transceiver capability in demodulating multiple data streams. Park *et al.* [90] designed a MAC protocol (SPACE-MAC) for MIMO links based on MIMO *beamforming*, i.e., a MIMO technique by which the same symbol is transmitted from each antenna according to a pre-selected weighting scheme[1]. At demodulation, appropriate weights are selected at the receive antennas to recover the transmitted symbol. SPACE-MAC selects the weights in such a way that simultaneous transmissions may occur among nodes within range of each other, improving the spatial reuse.

Regarding the use of space-time coding in ad hoc networks, Stamoulis and Al-Dhahir [109] investigated the impact of space-time block codes on IEEE 802.11a wireless local area networks (WLANs) operating in ad hoc mode. They used simulations to assess the benefits of the Alamouti scheme on the performance of upper-layer protocols like TCP. Their work assumes fully-connected networks (i.e., no hidden terminals) and focuses on the simplest Alamouti scheme, i.e., a MISO system with two transmit antennas and one receive antenna.

Hu and Zhang [63] attempted to model MIMO ad hoc networks by focusing on IEEE 802.11 ad hoc networks operating with STBC. For the modeling of the IEEE 802.11 DCF MAC, they used the same Markov model as the one introduced by Bianchi [12], which does not include the impact of the finite-retry limits or the carrier-sensing activity of the nodes, and assumes that collisions occur only among RTS frames. In addition, they disregarded

[1]The term "beamforming" is also used in the context of smart antennas to describe the adjustment of the antenna weights to *direct* the antenna beam in a given direction.

the impact of the network topology, and assumed that "events experienced by one user are statistically the same as those of other users," stating that each node has the *same* average throughput. In fact, in their model, each node is surrounded by the same average number of nodes, and the multihop network simplifies, in practice, to many "single-hop" networks, where interactions happen only with *immediate* neighbors. Therefore, their model ignores the impact of the topology and the radio connectivity among all nodes in the network. Consequently, it does not capture the interactions between PHY and MAC layers, which is key for an accurate evaluation of the impact of any PHY-layer aspect on the performance of a multihop network.

## 8.3 Space-Time Coding (STC)

The fundamentals of space-time coding (STC) were first established by Tarokh *et al.* [117] who proposed *space-time trellis codes* (STTC). STTC is an extension of standard trellis codes to MIMO systems, with the difference that the decoding procedure of STTC requires multidimensional Viterbi algorithms at the receiver. They designed codes that attain a diversity order equal to the number of transmit antennas, and a coding gain that depends on the complexity of the code (i.e., number of states in the trellis) without incurring any loss in bandwidth efficiency. Unfortunately, a major drawback of STTC is the fact that the decoding complexity increases exponentially as a function of the diversity level and transmission rate.

Later, Alamouti [4] proposed a space-time block coding (STBC) scheme for transmission with two antennas that supports maximum-likelihood detection based only on linear processing at the receiver. In addition, the Alamouti scheme does not require any channel feedback from the receiver to the transmitter (the channel is unknown to the transmitter) and it

does not incur any bandwidth expansion. The basic Alamouti scheme consists of two transmit antennas and one receive antenna (MISO system), but it can be easily generalized to the case of two transmit antennas and $M$ receive antennas to provide a diversity order of $2M$. Tarokh *et al.* [118] generalized this scheme to an arbitrary number of transmit antennas. In this chapter, however, we focus on systems with two transmit antennas and $M$ receive antennas.

Next, we present a short overview of the basics of the Alamouti scheme applied to a MIMO system with two transmit antennas and two receive antennas. Following that, we compute the impact of multiple access interference (MAI) in an ad hoc network operating with the Alamouti scheme, and show a simple way to compute the symbol error probability of the Alamouti scheme under multipath fading.

### 8.3.1 Example: The 2 $\times$ 2 MIMO Alamouti Scheme

The Alamouti scheme [4] works over two symbol periods. Over the first symbol period, two different symbols $s_1$ and $s_2$ are transmitted simultaneously from antennas 1 and 2, respectively. During the next symbol period, symbol $-s_2^*$ is transmitted from antenna 1, and symbol $s_1^*$ is transmitted from antenna 2 (where * indicates the complex conjugate operation). At each symbol period, the energy $E_s$ available at the transmitter is equally divided between the two antennas, i.e., each symbol has energy $E_s/2$ (no extra power is needed). It is assumed that the channel remains constant over two consecutive symbol periods and it is frequency flat, with $h_{kl} = |h_{kl}|e^{j\theta_{kl}},\ k, l = 1, 2$, representing the complex channel gains between the $l$th transmit antenna and the $k$th receive antenna. Under such conditions, the $2 \times 2$ channel

matrix $\mathbf{H}$ is given by

$$\mathbf{H} = \begin{bmatrix} h_{11} & h_{12} \\ h_{21} & h_{22} \end{bmatrix}, \tag{8.1}$$

and the received signals $\mathbf{y}_1$ and $\mathbf{y}_2$ at the receive antenna array over consecutive symbol periods are given by

$$\mathbf{y}_1 = \begin{bmatrix} h_{11} & h_{12} \\ h_{21} & h_{22} \end{bmatrix} \begin{bmatrix} s_1 \\ s_2 \end{bmatrix} + \begin{bmatrix} n_1 \\ n_2 \end{bmatrix}, \tag{8.2}$$

$$\mathbf{y}_2 = \begin{bmatrix} h_{11} & h_{12} \\ h_{21} & h_{22} \end{bmatrix} \begin{bmatrix} -s_2^* \\ s_1^* \end{bmatrix} + \begin{bmatrix} n_3 \\ n_4 \end{bmatrix}, \tag{8.3}$$

where $n_1$, $n_2$, $n_3$, and $n_4$ are assumed to be uncorrelated AWGN samples with zero mean and power $N_0$.

The receiver uses the sequentially-received symbols $\mathbf{y}_1$ and $\mathbf{y}_2$ to form the vector $\mathbf{y} = [\mathbf{y}_1\, \mathbf{y}_2^*]^T$, given by

$$\begin{aligned} \mathbf{y} &= \begin{bmatrix} \mathbf{y}_1 \\ \mathbf{y}_2^* \end{bmatrix} = \begin{bmatrix} h_{11} & h_{12} \\ h_{21} & h_{22} \\ h_{12}^* & -h_{11}^* \\ h_{22}^* & -h_{21}^* \end{bmatrix} \begin{bmatrix} s_1 \\ s_2 \end{bmatrix} + \begin{bmatrix} n_1 \\ n_2 \\ n_3^* \\ n_4^* \end{bmatrix} \\ &= \mathbf{H}_{\mathrm{A}}\, \mathbf{s} + \mathbf{n}, \end{aligned} \tag{8.4}$$

where $\mathbf{s} = [s_1\ s_2]^T$ and $\mathbf{n} = [n_1\ n_2\ n_3^*\ n_4^*]^T$. By construction, $\mathbf{H}_{\mathrm{A}}$ is orthogonal *irrespective of the channel realization*, i.e., $\mathbf{H}_{\mathrm{A}}^H \mathbf{H}_{\mathrm{A}} = \|\mathbf{H}\|_F^2 \mathbf{I}_2$, where $\mathbf{I}_2$ is the $2 \times 2$ identity matrix and $\|\mathbf{H}\|_F^2$ is the *frobenius norm* of $\mathbf{H}$, i.e.,

$$\|\mathbf{H}\|_F^2 = \sum_i \sum_j |h_{ij}|^2. \tag{8.5}$$

By defining the new vector $\mathbf{z} = \mathbf{H}_{\mathrm{A}}^{H}\mathbf{y}$, one gets

$$\mathbf{z} = \|\mathbf{H}\|_F^2 \mathbf{I}_2\, \mathbf{s} + \tilde{\mathbf{n}}, \tag{8.6}$$

where $\tilde{\mathbf{n}} = \mathbf{H}_{\mathrm{A}}^{H}\mathbf{n}$ is a complex Gaussian noise vector with $E\{\tilde{\mathbf{n}}\} = \mathbf{0}$, and covariance matrix $E\{\tilde{\mathbf{n}}\tilde{\mathbf{n}}^H\} = \|\mathbf{H}\|_F^2 N_0 \mathbf{I}_2$. The diagonal nature of $\mathbf{z}$ effectively decouples the two symbol transmissions, so that each component of $\mathbf{z}$ corresponds to one of the transmitted symbols:

$$z_i = \|\mathbf{H}\|_F^2\, s_i + \tilde{n}_i, \;\; i = 1, 2. \tag{8.7}$$

Thus, the received SNR corresponds to the SNR for $z_i$, which is given by [56]

$$\text{SNR} = \frac{\|\mathbf{H}\|_F^2 E_s}{2N_0}, \tag{8.8}$$

where the factor of 2 comes from the fact that $s_i$ is transmitted using half of the total energy $E_s$.

### 8.3.2 Multiple Access Interference (MAI)

In order to model MIMO ad hoc networks properly, we need to characterize the impact of MAI on the signaling technique of choice, taking into account the MIMO nature of the channel. In this section, we consider the impact of MAI in ad hoc networks operating with the Alamouti scheme. Without loss of generality, we consider the simplest Alamouti scheme, which consists of two transmit antennas and one receive antenna (MISO channel). In this case, we assume that every node in the network has two antennas, but only the signals captured by one of the antennas are decoded/demodulated for signal reception.

Let $h_{1k}^{j}$ and $h_{2k}^{j}$ denote the complex channel gains between antennas 1 and 2 of node $k$ and the receive antenna of node $j$, respectively (notice that we have a $1 \times 2$ channel

matrix in the MISO case). Likewise, let $s_{1k}$ and $s_{2k}$ denote the two symbols transmitted from antennas 1 and 2 of node $k$. Now, let us assume that node $i$ transmits a signal to node $j$ and that other $K$ nodes are transmitting simultaneously over the channel (not necessarily to node $j$). Therefore, the signals $y_1^j$ and $y_2^j$ received by node $j$ over two consecutive symbol periods are given by

$$y_1^j = h_{1i}^j s_{1i} + h_{2i}^j s_{2i} + \underbrace{\sum_{k=1}^{K} \Big( h_{1k}^j s_{1k} + h_{2k}^j s_{2k} \Big)}_{\text{MAI}}, \tag{8.9}$$

$$y_2^j = -h_{1i}^j s_{2i}^* + h_{2i}^j s_{1i}^* + \underbrace{\sum_{k=1}^{K} \Big( -h_{1k}^j s_{2k}^* + h_{2k}^j s_{1k}^* \Big)}_{\text{MAI}}, \tag{8.10}$$

where, as indicated, the terms under summation form the multiple access interference (MAI) at node $j$. As explained before, node $j$ constructs the vector $\mathbf{y}_j = [y_1^j \; y_2^{j*}]^T$, leading to

$$\begin{aligned} \mathbf{y}_j &= \begin{bmatrix} h_{1i}^j & h_{2i}^j \\ h_{2i}^{j*} & -h_{1i}^{j*} \end{bmatrix} \begin{bmatrix} s_{1i} \\ s_{2i} \end{bmatrix} + \sum_{k=1}^{K} \begin{bmatrix} h_{1k}^j & h_{2k}^j \\ h_{2k}^{j*} & -h_{1k}^{j*} \end{bmatrix} \begin{bmatrix} s_{1k} \\ s_{2k} \end{bmatrix} \\ &= \mathbf{H}_i \, \mathbf{s}_i + \sum_{k=1}^{K} \mathbf{H}_k \, \mathbf{s}_k \end{aligned} \tag{8.11}$$

As in the previous section, it is assumed that node $j$ estimates the channel perfectly from the signals received by node $i$, i.e., node $j$ has accurate estimates of the channel gains $h_{1i}^j$ and $h_{2i}^j$. Therefore, node $j$ forms the new vector $\mathbf{z}_j = \mathbf{H}_i^H \mathbf{y}_j$ given by

$$\mathbf{z}_j = \mathbf{H}_i^H \mathbf{H}_i \, \mathbf{s}_i + \sum_{k=1}^{K} \mathbf{H}_i^H \mathbf{H}_k \, \mathbf{s}_k = \|\mathbf{H}_i\|_F^2 \mathbf{I}_2 \, \mathbf{s}_i + \mathbf{m}, \tag{8.12}$$

where $\mathbf{m}$ is the MAI term given by $\mathbf{m} = \sum_{k=1}^{K} \mathbf{H}_i^H \mathbf{H}_k \, \mathbf{s}_k$. Notice the resemblance between Eqs. (8.12) and (8.6). Assuming that the symbols are equally probable and drawn from a

symmetric constellation, then $E\{\mathbf{m}\} = \mathbf{0}$. For the covariance matrix $E\{\mathbf{m}\mathbf{m}^H\}$, we have

$$E\{\mathbf{m}\mathbf{m}^H\} = E\left\{\left(\sum_{k=1}^{K}\mathbf{H}_i^H\mathbf{H}_k\,\mathbf{s}_k\right)\left(\sum_{l=1}^{K}\mathbf{H}_i^H\mathbf{H}_l\,\mathbf{s}_l\right)^H\right\}$$
$$= \sum_{k=1}^{K}\sum_{l=1}^{K}\mathbf{H}_i^H\mathbf{H}_k\,E\{\mathbf{s}_k\mathbf{s}_l^H\}\mathbf{H}_l^H\mathbf{H}_i. \tag{8.13}$$

If we also make the common assumption that symbols are generated independently at each node, the double summation in Eq. (8.13) simplifies to

$$E\{\mathbf{m}\mathbf{m}^H\} = \sum_{k=1}^{K}\mathbf{H}_i^H\mathbf{H}_k\,E\{\mathbf{s}_k\mathbf{s}_k^H\}\mathbf{H}_k^H\mathbf{H}_i = \sum_{k=1}^{K}\mathbf{H}_i^H\mathbf{H}_k\,\sigma_s^2\mathbf{I}_2\mathbf{H}_k^H\mathbf{H}_i$$
$$= \sigma_s^2\|\mathbf{H}_i\|_F^2\sum_{k=1}^{K}\|\mathbf{H}_k\|_F^2\mathbf{I}_2, \tag{8.14}$$

where $\sigma_s^2 = E\{s_{1k}s_{1k}^*\} = E\{s_{2k}s_{2k}^*\}$ is the power of the transmitted symbols (remember that they are transmitted with the same power). Hence, as in the previous section, the signal-to-interference-ratio (SIR) for each received symbol corresponds to the SIR for $z_i$, which is given by

$$\text{SIR} = \frac{\|\mathbf{H}_i\|_F^2 E_s/2}{\sum_k \|\mathbf{H}_k\|_F^2 E_s/2} \tag{8.15}$$

This last expression tells us that the interference caused by all simultaneous transmissions is nothing but the sum of all the signal powers received by node $j$ from all possible transmit-receive antenna pairs formed between node $j$ and the transmitting nodes. Finally, if we consider both the additive background noise (from previous section) and the MAI, we have the signal-to-interference-plus-noise (SINR) ratio, given by

$$\text{SINR} = \frac{\|\mathbf{H}_i\|_F^2 E_s/2}{N_0 + \sum_k \|\mathbf{H}_k\|_F^2 E_s/2}. \tag{8.16}$$

### 8.3.3 Symbol Error Probability

The symbol error probability of the Alamouti scheme can be easily obtained if we notice that the received SNR is *the sum of the SNRs from each individual path*[2], i.e., from Eqs. (8.5) and (8.8),

$$\text{SNR} = \gamma = \sum_{i=1}^{2}\sum_{j=1}^{M_R}\gamma_{ij} = \sum_{i=1}^{2}\sum_{j=1}^{M_R}\frac{|h_{ij}|^2 E_s}{2N_0}, \tag{8.17}$$

where $M_R$ is the number of receive antennas. Such additive property of SNRs suggests the use of the *moment generating function* (MGF) method for computation of the symbol error probability of different modulation schemes [56]. The MGF for a nonnegative random variable $\gamma$ with pdf $p_\gamma(\gamma), \gamma \geq 0$, is defined as

$$\mathcal{M}(s) = \int_0^\infty p_\gamma(\gamma)e^{s\gamma}d\gamma. \tag{8.18}$$

The idea behind the MGF approach is to express the probability of error in AWGN for the modulation of interest as an exponential function of $\gamma$. For instance, let us suppose that the probability of symbol error $P_s$ in AWGN for the modulation of interest is expressed in the form

$$P_s(\gamma) = c_1 e^{-c_2\gamma}, \tag{8.19}$$

where $c_1$ and $c_2$ are constants. Hence, because the average probability of symbol error is computed by integrating the error probability in AWGN over the fading distribution [56], we have

$$\overline{P}_s = \int_0^\infty P_s(\gamma)p_\gamma(\gamma)d\gamma = \int_0^\infty c_1 e^{-c_2\gamma}p_\gamma(\gamma)d\gamma = c_1\mathcal{M}(-c_2),$$

[2]The same additive property of SNRs is observed in receiver diversity with maximal ratio combining (MRC) [56].

where $\mathcal{M}(-c_2)$ is the MGF of $\gamma$ evaluated at $-c_2$.

Given that, the symbol error probability of the Alamouti scheme becomes particularly simple if it is assumed that the fading paths are independent but not necessarily identically distributed. In this case, the branch SNRs are independent and the joint pdf of $\gamma$ becomes a product of the individual pdfs, i.e., $p_{\gamma_1,\ldots,\gamma_M}(\gamma_1,\ldots,\gamma_{2M}) = p_{\gamma_1}(\gamma_1)\cdots p_{\gamma_{2M}}(\gamma_{2M})$. Using this factorization and substituting $\gamma = \gamma_1 + \ldots + \gamma_{2M}$ in Eq. (8.20) yields

$$\begin{aligned}\overline{P}_s &= c_1 \int_0^{\infty} \cdots \int_0^{\infty} \exp\left[-c_2\left(\sum_{i=1}^{2M}\gamma_i\right)\right] \prod_{i=1}^{2M} p_{\gamma_i}(\gamma_i)d\gamma_i \\ &= c_1 \prod_{i=1}^{2M} \int_0^{\infty} e^{-c_2\gamma_i} p_{\gamma_i}(\gamma_i)d\gamma_i = c_1 \prod_{i=1}^{2M} \mathcal{M}_{\gamma_i}(-c_2) \end{aligned} \tag{8.20}$$

For instance, the symbol error probability for DBPSK under AWGN is $P_s = P_b(\gamma_b) = \exp(-\gamma_b)/2$, i.e., $c_1 = 0.5$ and $c_2 = 1$. Hence, the average probability of bit error under DBPSK is given by

$$\overline{P}_b = \frac{1}{2}\prod_{i=1}^{2M} \mathcal{M}_{\gamma_i}(-1). \tag{8.21}$$

For Rician fading, the moment generating function is given by [56]

$$\mathcal{M}_{\gamma}(s) = \frac{1+K}{1+K-s\overline{\gamma}} \exp\left[\frac{Ks\overline{\gamma}}{1+K-s\overline{\gamma}}\right]. \tag{8.22}$$

Substituting Eq. (8.22) into Eq. (8.21) we obtain the average probability of bit error for the Alamouti scheme with two transmit antennas and $M$ receive antennas in the case of DBPSK modulation under Rician fading, which is given by

$$\overline{P}_b = \frac{1}{2}\left[\frac{1+K}{1+K+\overline{\gamma}}\right]^{2M} \exp\left[\frac{-2MK\overline{\gamma}}{1+K+\overline{\gamma}}\right]. \tag{8.23}$$

Following the same approach, one can obtain average error probabilities for many other modulations schemes under multipath fading [56].

As a final note, the same development can be used when considering the SINR of Eq. (8.16). In this case, as usual, the aggregate MAI is assumed to be Gaussian-distributed, with the mean and covariance matrix as computed before, and assuming that the channel gains in the denominator of Eq. (8.16) correspond to *average channel gains*, which are nothing but, the channel gains due to path-loss propagation effects.

## 8.4 Performance of MIMO Ad Hoc Networks

In this Section, we evaluate the performance of ad hoc networks that employ the Alamouti scheme at the physical layer and operate with the modified IEEE 802.11 DCF MAC described before. We investigate both MISO and MIMO ad hoc networks by taking advantage of the flexibility of the Alamouti scheme (it works with any number $M$ of receive antennas, as explained in Section 8.3). Table II contains the configurations of the antenna systems we study. For the MISO case, we assume that all nodes are equipped with two antennas. In this case, both antennas are used during transmission (necessary for the Alamouti scheme) and, during reception, only the signals arriving at one of the antennas are conveyed to the appropriate decoding/demodulation stages. For the MIMO cases, the opposite applies, i.e., all nodes are equipped with $M \geq 2$ antennas, but only two of them are used during transmission, whereas all antennas are used during reception. The performance of both MISO and MIMO networks are compared with the basic SISO network (nodes equipped with a single antenna). In the following, we will refer to a network with $N$ transmit antennas and $M$ receive antennas as an $N \times M$ MISO/MIMO network (depending on the values of $N$ and $M$).

One of the advantages of MIMO systems is to combat time-varying multipath fad-

**Table 8.1**: Antenna Configurations used for Performance Evaluation

| System | N. of Transmit Antennas | N. of Receive Antennas |
|---|---|---|
| MISO | 2 | 1 |
| MIMO | 2 | 2 |
| MIMO | 2 | 4 |
| MIMO | 2 | 6 |

ing. For our study, we assume a multipath fading following a Rician model [56]. We choose the Rician model because it is appropriate for scenarios where there exists both line-of-sight (LOS) and non-line-of-sight (NLOS) signals. The key parameter of the Rician distribution is the $K$ parameter, which expresses the ratio of the power of the LOS signal to the power of the NLOS signals. A small value of $K$ indicates a rich scattering environment with a weak LOS signal (strong fading). A large value of $K$ indicates a decrease in multipath propagation and, therefore, weak fading. We assume that fading is frequency flat and independent at each path. Thus, we can use the bit-error computation procedures presented in Section 8.3.3.

For the numerical results, we use the same setup and PHY/MAC parameters as described in Section 7.5, with the exception of the inclusion of multipath fading. We compute the average network throughput over 10 random topologies with 100 nodes each, for different values of the Rician parameter $K$ and for the antenna systems indicated in Table II. Figure 8.1 shows the numerical results. The bars in the graph indicate the standard deviation of the computed averages. As we can see, the use of the Alamouti scheme does improve performance significantly, especially when fading is strong (small values of $K$). For instance, the gains in average throughput of the $2\times6$ MIMO over the simplest SISO network are almost 400% when $K = 5$. Improvements in throughput are perceived even for the basic MISO configuration, which improves throughput over SISO in more than 200% under strong fading, and about

125% without much fading (large $K$).

Another important aspect to observe it that, as the number of receive antennas increases ($M > 2$), the relative gains in average throughput diminishes with respect to the previous configuration. Therefore, we observe that adding more antennas at each node does not give a linear increase in performance. As the number of antennas increases, the errors in the channel are better combated, and throughput becomes basically bounded by the degree of contention in the network. In other words, it is the MAC layer that limits the achievable throughput once the PHY layer attains its best performance. Such results are expected, because the Alamouti scheme is a *transmitter diversity* scheme. In other words, it was not designed to provide data rate increases (*capacity gains*) through spatial multiplexing. Instead, it provides a more robust channel through *diversity* and *array* gains, as explained in Section 8.3.1.

The above results suggest that the use (or not) of more antennas depends on the amount of contention in place, which, in turn, depends on the total number of nodes, their distribution in the terrain, and the efficiency of the underlying MAC protocol in scheduling each node's transmissions. For the scenarios we studied, it seems that the best trade off that can achieved between the number of antennas and the system complexity is the 2×2 MIMO configuration. Using four or six antennas does increase throughput, but the relative gains are not significant enough to justify the added system complexity. At the same time, the MISO network already has 2 antennas at each node, and the cost to implement a 2×2 MIMO network is just the extra internal processing of the signals captured by the second antenna already in place.

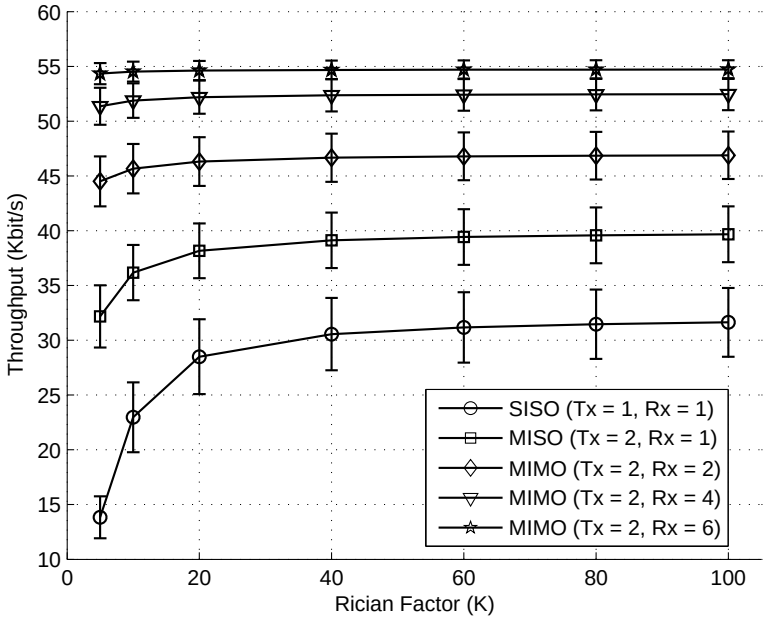


**Figure 8.1**: Average network throughput versus the value of the Rician parameter $K$ for different antenna systems. The results compare MISO and MIMO Alamouti-enabled 802.11 ad hoc networks with SISO 802.11 ad hoc networks.

## 8.5 Conclusions

In this chapter, presented the first analytical model for wireless ad hoc networks equipped with multiple-input multiple-output (MIMO) radios using space-time coding (STC) that considered the impact of the underlying radio-based topology on network performance. In particular, we considered the application of space-time block coding (STBC) in the form of a transmitter diversity technique known as the "Alamouti scheme." We derived the effective signal-to-interference-plus-noise density ratio (SINR) of the Alamouti scheme under multiple access interference (MAI), and we proposed the moment generating function (MGF) method to derive closed-form expressions for its symbol error probability under different modulation schemes when fading paths are independent but not necessarily identically distributed.

The impact of the Alamouti scheme on IEEE 802.11 DCF MAC was studied by taking into account the impact of errors in both control and data frames, the carrier-sensing activity, and the finite-retry limit of frame retransmissions, as derived in Chapter 6. We studied the performance of the Alamouti scheme in IEEE 802.11 ad hoc networks by comparing the relative gains in performance between SISO, MISO, and MIMO systems. From our results, we found that the Alamouti scheme does improve performance of IEEE 802.11 ad hoc networks, especially in environments where multipath fading effects are severe. In addition, we found that as the number of receive antennas increase, the relative gains in performance decrease, being limited by the degree of contention in the network. For this reason, there is an inherent trade-off between performance and system complexity when choosing the appropriate number of receive antennas.

# Chapter 9

# Conclusions and Future Work

## 9.1 Conclusions

In this dissertation, we have introduced a new modeling framework for the analytical study of MAC protocols in wireless ad hoc networks. The modeling framework focuses on the interactions between the PHY and the MAC layers, and on the impact that each node has on the dynamics of every other node in the network. To account for the effects of both cross-layer interactions and the interference among all nodes, a novel linear model is introduced with which topology and PHY/MAC-layer aspects are naturally incorporated in what we define as *interference matrices*. A key feature of the model is that nodes can be modeled individually, i.e., it allows a per-node setup of many layer-specific parameters. Moreover, no spatial probability distribution or special arrangement of nodes is assumed; the model allows the computation of individual (per-node) performance metrics for any given network topology and radio channel model.

Because of the importance of the IEEE 802.11 in the development of current and future wireless ad hoc networks, we illustrate the applicability of our analytical modeling framework through the modeling of wireless ad hoc networks that operate according to the IEEE 802.11 standard. To accomplish that, we presented a comprehensive analytical modeling of the operation of the IEEE 802.11 DCF MAC, for which we derived many performance metrics of interest, such as delay, throughput, and energy consumption.

The proposed modeling framework constitutes a tool for a fast, accurate, and efficient evaluation of a node's performance for any system parameter value and topology of an ad hoc network. Attempting to characterize a node's performance only by simulations would require considerable computational effort, specially when scalability is one of the main concerns. To be able to draw general conclusions, simulations would have to be run for a very large number of network sizes and topologies. Furthermore, if we are interested in evaluating the impact of a single parameter to a node's service time, for instance, simulations would have to be repeated for each parameter value of interest.

Our model was validated through discrete event simulations using the popular Qualnet tool, and the analytical results showed a striking correlation with the results obtained via simulation. The importance of the analytical model is that the time needed to obtain the desired results takes a very small fraction of the time required to obtain the same results via discrete-event simulations.

We applied our modeling framework to ad hoc networks in which systems of multiple antenna elements are used in both ends of the wireless links. We provided the first analytical modeling of wireless ad hoc networks that considers the impact of realistic antenna-gain

patterns on network performance. As such, our modeling approach allows the study of ad hoc networks in which nodes are equipped with *directional antennas*, i.e., systems of antennas that are able to transmit/receive energy over intended directions, as opposed to omnidirectional antennas, which (ideally) radiate or absorb energy equally well along all directions. This modeling capability stands out from all previous analytical models, which have only dealt with omnidirectional or over-simplified antenna gain patterns, and which have not addressed the specific mechanisms of the medium access control (MAC) protocols used (e.g., the backoff mechanism). We modeled the *directional virtual carrier sensing* (DVCS) [114] protocol to validate our analytical model and show its applicability. Our numerical results show that our new analytical model predicts the results obtained via discrete-event simulations very accurately, and does it with a processing time that us orders of magnitude faster than the time required by simulations. Furthermore, we show that the simplistic "pie slices" used in prior analytical models for antenna patterns over-estimate the throughput of the protocols dramatically compared to the results obtained using realistic antenna patterns.

In addition, we presented the first analytical model for wireless ad hoc networks in which nodes are equipped with multiple-input multiple-output (MIMO) radios and use space-time coding (STC). In particular, we considered the space-time block coding (STBC) technique known as the "Alamouti scheme." We derived the effective signal-to-interference-plus-noise density ratio (SINR) of the Alamouti scheme and closed-form expressions for its symbol error probability under different modulations. The impact of the Alamouti scheme on IEEE 802.11 ad hoc networks was studied using our analytical modeling framework and the new analytical model for the IEEE 802.11 DCF MAC we introduced in this thesis. We studied

the performance of the Alamouti scheme in IEEE 802.11 ad hoc networks by comparing the relative gains in performance between SISO, MISO, and MIMO systems. From our results, we found that the Alamouti scheme does improve performance of IEEE 802.11 ad hoc networks, especially in environments where multipath fading effects are severe. In addition, we found that as the number of receive antennas increase, the relative gains in performance decrease, being limited by the degree of contention in the network. For this reason, there is an inherent trade-off between performance and system complexity when choosing the appropriate number of receive antennas.

## 9.2 Future Work

The analytical modeling framework introduced in this dissertation can be extended in many ways to address important questions and aspects of wireless ad hoc networks.

In this dissertation, we focused on the interactions between the PHY and the MAC layers. Nevertheless, the introduced modeling framework can naturally accommodate the impact that other layers of the protocol stack may have on the behavior of a given MAC protocol. This is because we modeled the MAC behavior as a function of a vector $\boldsymbol{\varphi}_i$ used by a particular MAC protocol. According to our modeling framework, the entries in the vector $\boldsymbol{\varphi}_i$ represent probabilities of events "whose outcomes are important input and/or feedback information to the operation of the MAC protocol in place." Consequently, the impact of *any* layer of the protocol stack can be represented, in principle, by any entry in the vector $\boldsymbol{\varphi}_i$. In this case, the challenge in the modeling problem consists of choosing the appropriate functions that faithfully represent the behaviors of the protocol layers we are interested in investigat-

ing and, possibly, their dependencies on the scheduling rates of all nodes in the network, as represented by the functions $\nu_{ik}$ in Eq. (5.9). As future work, the modeling framework can be extended to incorporate the impact of network routing operations (network layer) or the impact of transport-layer protocols, such as the transport control protocol (TCP) used in the Internet and its variants designed for ad hoc networks.

Given that the PHY and the MAC layers play such a fundamental role in the performance of any wireless ad hoc network—and because all other layers in the protocol stack rely on the PHY/MAC performance—the focus on the modeling of PHY/MAC-layer interactions deserves a study on its own, and it should be fully exploited in the design and optimization of wireless ad hoc networks. In fact, contrary to wired networks and the Internet, it has become a common belief that cross-layer designs would largely benefit wireless networks, especially at the PHY and MAC layers [32,106,140]. In this respect, the modeling framework introduced in this dissertation constitutes a suitable platform for such studies, as it focuses on PHY/MAC-layer interactions and represents the PHY/MAC functionalities by taking into account the impact of all nodes in the network. Therefore, by using our analytical modeling framework, we can assess not only the performance of realistic PHY/MAC cross-layer designs, but also the impact that different PHY/MAC parameters have on network performance. Chapters 7 and 8 illustrate well the type of modeling and performance analysis that can be carried out with respect to different choices in the design of PHY and MAC layers.

Following a cross-layer design approach, an important direction for future work is the extension of the work on MIMO ad hoc networks presented in Chapter 8 to the modeling of ad hoc networks that utilize space-time coding techniques that exploit *spatial multiplexing* to

obtain *multiplexing gains* (also referred to as *capacity gains*). In this dissertation, we explored a space-time coding technique that is based on a *transmitter diversity* scheme, whose main goal is to combat multipath fading. As showed in Chapter 8, impressive gains in throughput can be achieved under severe multipath fading as we increase the number of receive antennas. Unfortunately, increasing the number of antennas does not lead to a linear increase in network throughput. The idea of using space-time coding techniques that explore spatial multiplexing is due to the fact that these techniques attempt to achieve the capacity gains promised in the theory of MIMO channels, i.e., capacity can increase *linearly with the number of antennas* [53, 56]. Therefore, an important extension of our modeling work is to incorporate the modeling of space-time coding techniques that exploit spatial multiplexing. In fact, a fundamental design question in MIMO systems is whether one should use multiple antennas to obtain diversity gain, multiplexing gain, or both [56]. The diversity/multiplexing tradeoff has been studied extensively in the literature [51, 142, 148], but not in the context of ad hoc networks and their interactions with different MAC protocols. Therefore, our analytical modeling framework can be used to investigatd the advantages and disadvantages in the choice of different space-time coding techniques when applied to ad hoc networks with specific MAC protocols under different radio-channel conditions.

Another important aspect that is related to the PHY layer is the investigation of radio-channel propagation models that allow the modeling of ad hoc networks under more realistic scenarios, such as the use of propagation models that take into account the 3-dimensional topology aspects of a terrain and their respective impact on symbol error probabilities of different modulation schemes.

In this dissertation, we showed the application of our analytical modeling framework in the modeling of IEEE 802.11 ad hoc networks. The IEEE 802.11 DCF MAC utilizes a variant of the popular carrier-sensing multiple access (CSMA) scheme [73], which is a *contention-based* MAC protocol. In contention-based MAC protocols, some *random access scheme* is employed as a mechanism to grant nodes access to the available channel(s). Hence, contention-based MAC protocols are, inherently, *probabilistic systems*. Consequently, we can use our modeling framework to model this class of MAC protocols and its variants. In addition, our modeling framework can also be used in the modeling of *scheduled-based* MAC protocols. Scheduled-based MAC protocols attempt to prearrange or negotiate a set of timetables for nodes to have access to the channel. As it is well-known, optimal solutions for channel access scheduling in ad hoc networks (in the sense of multihop networks) often results in NP-hard problems [37, 40, 98]. Consequently, proposed solutions to channel access scheduling must rely on some type of heuristic that leads to sub-optimal solutions. It turns out that many of the proposed solutions for scheduled-based MAC protocols are based on the assumption that ad hoc networks can be treated as simple graphs [28,37,97]. As we discussed in this dissertation, interference in ad hoc networks can happen from every node in the network and, consequently, the view of an ad hoc network as a "graph that interconnects neighbors" is misleading, and it does not reflect what really happens under a radio-based channel. Moreover, many of the proposed solutions for scheduled-based MAC protocols either employ some sort of "election scheme" based on some probabilistic function [7, 8], or employ the exchange of messages (handshakes) to resolve scheduling conflicts [116, 149]. Consequently, due to the random behavior of the proposed election schemes and the propagation effects of radio

channels, all such MAC protocols can be modeled according to a probabilistic framework. Last, but not least, even if optimal channel access scheduling was feasible, the radio channel propagation effects are random in nature and, consequently, unsuccessful frame receptions can happen at the intended receiver. Therefore, even under perfect channel access scheduling, acknowledgments (ACKs) are expected to be sent to guarantee that a frame is successfully received at the intended receiver (MAC-level reliable delivery service). In this case, again, we need to deal with probabilities of successful frame exchanges, which could be treated according to the framework introduced in this dissertation.

Based on previous considerations, an interesting venue for future work is the application of our modeling framework in the modeling of scheduled-based MAC protocols and their performance evaluation compared to the class of contention-based MAC protocols. It has been shown that scheduled-based MAC protocols perform generally better than contention-based MAC protocols. However, such performance comparisons have been done based on unrealistic assumptions regarding the PHY layer and other network aspects (e.g., assumptions on *accurate* knowledge of complete network topology or the two-hop neighborhood). To date, the literature still lacks a fair comparison between both class of protocols that takes into account the underlying radio channel propagation effects and the possible inaccuracies (and intrinsic delays) of scheduled-based MAC protocols on acquiring key information, such as (complete or partial) network topology, as an example. In this sense, our modeling framework could be used to assess the true advantages/disadvantages of both class of MAC protocols in ad hoc networks.

A characteristic of the modeling framework introduced in this dissertation is that

nodes are assumed to be *static* in the terrain, i.e., there is no *mobility*. In spite of this constraint, some of the most important applications envisaged for ad hoc networks deal with static networks. This is the case of many applications for sensor networks (which can be viewed as special types of ad hoc networks), and the so-called *wireless mesh networks*, which are a fast-growing emerging technology that is regarded as a flexible and low-cost extension to wired infrastructure networks [3, 14]. Therefore, our modeling framework can be used in the study of specific PHY/MAC-layer designs tailored to these types of networks. In particular, the sufficient conditions for feasible network configurations provided in Chapter 5 can be used in the dimensioning and optimization of network scenarios typical of these classes of wireless ad hoc networks.

Regarding the modeling of IEEE 802.11 ad hoc networks, some directions for future work include the design of an analytical model that is able to incorporate the two retry counters of the IEEE 802.11 DCF MAC. As discussed in Chapter 6, the dynamics of the two retry counters may have an impact on the fairness of the IEEE 802.11 DCF MAC and, consequently, on the accuracy of the analytical model. Hence, a faithful model of the IEEE 802.11 DCF MAC should contain both retry counters. Parallel to this, the modeling of the IEEE 802.11 DCF MAC can be improved if an investigation of the fundamental reasons for the fairness issues typical of the IEEE 802.11 DCF MAC can be incorporated directly into the analytical model.

Another topic that deserves special attention with respect to the IEEE 802.11 is the modeling of its energy consumption in multihop ad hoc networks when physical layer aspects are taken into account. In this dissertation, we only dealt with the modeling of en-

ergy consumption in single-hop networks under ideal conditions. The investigation of energy consumption in multihop scenarios may lead to a better understanding of the appropriate selections of power/rate settings under different channel conditions [91, 94], and may lead to innovative power-saving mechanisms for the IEEE 802.11 DCF MAC.

For completeness, a very challenge problem is that of modeling IEEE 802.11 ad hoc networks under non-saturation conditions. Real networks are generally expected to operate under non-saturation conditions (nodes may not always have packets to be sent). To accomplish that, we need to extend the modeling of the IEEE 802.11 DCF MAC to incorporate its behavior when no packet is available at the head of a node's input queue. In this case, we need to obtain not only the appropriate model for the IEEE 802.11 DCF MAC under non-saturation conditions, but also the development of the respective performance metrics, such as throughput and average delay.

Last, but not least, another important venue for future work is the study of *network capacity* under specific PHY/MAC layers. To date, the majority of the work on network capacity follows the seminal work by Gupta and Kumar [59], which makes rather general assumptions about the PHY and the MAC layers (especially the MAC layer). In spite of the importance of such studies, a gap still remains on the study of capacity of networks under specific PHY and MAC layers, and the impact that relevant PHY/MAC-layer parameters may have on network capacity. We believe that our modeling framework allows the study of not only network capacity under the perspective of scalability laws for specific PHY/MAC layers, but it also provides a framework for *network optimization* and *network dimensioning* based on the sufficient conditions for feasible network configurations provided in Chapter 5.

# Bibliography


[1] N. Abramson. The ALOHA system—another alternative for computer communications. In *AFIPS Conf. Proc.*, volume 37, pages 281–285. FJCC, 1970.

[2] N. Abramson. The throughput of packet broadcast channels. *IEEE Trans. on Communications*, COM-25(1):117–128, Jan 1977.

[3] I. Akyildiz, X. Wang, and W. Wang. Wireless mesh networks: A survey. *Computer Networks*, 47:445–487, 2005.

[4] S. Alamouti. A simple transmit diversity technique for wireless communications. *IEEE Journal on Selected Areas in Communications*, 16(8):1451–1458, October 1998.

[5] J. C. Arnbak and W. V. Blitterswijk. Capacity of slotted aloha in rayleigh-fading channels. *IEEE Journal on Selected Areas in Communications*, SAC-5(2):261–269, Feb 1987.

[6] T. Baicheva, S. Dodunekov, and P. Kazakov. Undetected error probability performance of cyclic redundancy-check codes of 16-bit redundancy. *IEEE Proceedings*, 147(5):253–256, Oct 2000.

[7] L. Bao and J. Garcia-Luna-Aceves. A new approach to channel access scheduling for ad hoc networks. In *Proc. of The Seventh ACM Annual International Conference on Mobile Computing and networking (MOBICOM)*, pages 210–220, Rome, Italy, July 2001.

[8] L. Bao and J. Garcia-Luna-Aceves. Transmission scheduling in ad hoc networks with directional antennas. In *Proc. of The Eighth ACM Annual International Conference on Mobile Computing and networking (MOBICOM)*, pages 48–58, Atlanta, USA, September 2002.

[9] V. Barghavan, A. Demers, S. Shenker, and L. Zhang. MACAW: A media access protocol for wireless LAN's. In *Proc. of ACM SIGCOMM '94*, pages 212–225, 1994.

[10] B. Bensaou, Y. Wang, and C. C. Ko. Fair medium access in 802.11 based wireless ad-hoc networks. In *First Annual IEEE and ACM International Workshop on Mobile Ad Hoc Networking and Computing*, Aug 2000.

[11] C. Bettstetter, G. Resta, and P. Santi. The node distribution of the random waypoint mobility model for wireless ad hoc networks. *IEEE Trans. on Mobile Computing*, 2(3):257–269, Jul 2003.

[12] G. Bianchi. Performance analysis of the IEEE 802.11 distributed coordination function. *IEEE Journal on Selected Areas in Communications*, 18(3):535–547, March 2000.

[13] R. R. Boorstyn, A. Kershenbaum, B. Maglaris, and V. Sahin. Throughput analysis in multihop CSMA packet radio networks. *IEEE Trans. on Communications*, COM-35(3):267–274, Mar 1987.

[14] R. Bruno, M. Conti, and E. Gregori. Mesh networks: Commodity multihop ad hoc networks. *IEEE Communications Magazine*, pages 123–131, March 2005.

[15] F. Cali, M. Conti, and E. Gregori. Dynamic tuning of the IEEE 802.11 protocol to achieve a theoretical throughput limit. *IEEE/ACM Tran. on Networking*, 8(6):785–799, Dec 2000.

[16] M. M. Carvalho and J. J. Garcia-Luna-Aceves. A packet delay analysis of IEEE 802.11 dcf in single-hop ad hoc networks. *Journal of the Brazilian Telecommunications Society*. To appear. (**Invited Paper**).

[17] M. M. Carvalho and J. J. Garcia-Luna-Aceves. Delay analysis of IEEE 802.11 in single-hop networks. In *Proc. 11th IEEE International Conference on Network Protocols (ICNP)*, pages 146–155, Atlanta, USA, November 2003.

[18] M. M. Carvalho and J. J. Garcia-Luna-Aceves. Modeling single-hop wireless networks under Rician fading channels. In *Proc. IEEE Wireless Communications and Networking Conference (WCNC)*, volume 1, pages 219–224, Atlanta, USA, March 2004.

[19] M. M. Carvalho and J. J. Garcia-Luna-Aceves. A scalable model for channel access protocols in multihop ad hoc networks. In *Proc. of the 10th Annual International Conference on Mobile Computing and Networking (MobiCom)*, pages 330–344, Philadelphia, USA, September 2004.

[20] M. M. Carvalho and J. J. Garcia-Luna-Aceves. Analytical modeling of ad hoc networks that utilize space-time coding. In *Proc. IEEE 4th Intl. Symposium on Modeling and Optimization in Mobile, Ad Hoc, and Wireless Networks (WiOpt)*, Boston, USA, April 2006.

[21] M. M. Carvalho and J. J. Garcia-Luna-Aceves. Modeling wireless ad hoc networks

with directional antennas. In *Proc. IEEE 25th Annual Joint Conference of the IEEE Computer and Communications Societies (INFOCOM)*, Barcelona, Spain, April 2006.

[22] M. M. Carvalho, C. B. Margi, K. Obraczka, and J. J. Garcia-Luna-Aceves. Modeling energy consumption in single-hop IEEE 802.11 ad hoc networks. In *Proc. IEEE 13th International Conference on Computer Communications and Networks (ICCCN)*, pages 367–372, Chicago, USA, October 2004. (**Best Paper Candidate**).

[23] C. Chang and J. Chang. Optimal design parameters in a multihop packet radio network using random access techniques. In *Proc. GLOBECOM*, pages 493–497, New York, USA, 1984.

[24] J. Chen, K. M. Sivalingam, and P. Agrawal. Performance comparison of battery power consumption in wireless multiple access protocols. *Wireless Networks*, 5(6):445–460, 1999.

[25] D. Cheung. A path loss comparison between the 5 GHz UNII band (802.11a) and the 2.4 GHz ISM band (802.11b). Technical report, Intel Labs, Intel Corporation, January 2002.

[26] H. Chhaya and S. Gupta. Performance modeling of asynchronous data transfer methods of IEEE 802.11 MAC protocol. *Wireless Networks*, 3:217–234, 1997.

[27] I. Chlamtac, M. Conti, and J. Liu. Mobile ad hoc networking: Imperatives and challenges. *Ad Hoc Networks*, 1(1):13–64, July 2003.

[28] I. Chlamtac and A. Faragó. Making transmission schedules immune to topology changes in multi-hop packet radio networks. *IEEE/ACM Transactions on Networking*, 2(1):23–29, February 1994.

[29] A. Chockalingam and M. Zorzi. Energy efficiency of media access protocols for mobile data networks. *IEEE Trans. on Communications*, 46(11):1418–1421, 1998.

[30] R. Choudhury and N. Vaidya. Deafness: A MAC problem in ad hoc networks when using directional antennas. In *Proc. ICNP*, pages 283–292, Berlin, Germany, Oct. 2005.

[31] A. Colvin. CSMA with collision avoidance. *Computer Commun.*, 6(5):227–235, 1983.

[32] M. Conti, G. Maselli, G. Turi, and S. Giordano. Cross layering in mobile ad hoc network design. *IEEE Computer*, 37(2):48–51, February 2004.

[33] D. H. Davis and S. A. Gronemeyer. Performance of slotted ALOHA random access with delay capture and randomized time of arrival. *IEEE Trans. Commun.*, COM-28(5):703–710, May 1980.

[34] J. Ebert, S. Aier, G. Kofahl, A. Becker, B. Burns, and A. Wolisz. Measurement and simulation of the energy consumption of an WLAN interface. Technical Report TKN-02-010, Technical University Berlin, Telecommunication Networks Group, Germany, June 2002.

[35] J. Ebert, B. Burns, and A. Wolisz. A trace-based approach for determining the energy consumption of a WLAN network interface. In *European Wireless Conference*, pages 230–236, February 2002.

[36] A. Ephremides and B. Hajeck. Information theory and communication networks: An unconsumated union. *IEEE Trans. Information Theory*, 44:2416–2434, Oct 1998.

[37] A. Ephremides and T. Truong. Scheduling broadcasts in multihop radio networks. *IEEE Trans. on Communications*, 36(4):450–460, April 1990.

[38] M. Ergen, B. Dunbar, and P. Varaiya. Throughput analysis of an extended service set in 802.11. In *Proc. GLOBECOM*, Dallas, USA, November 2004.

[39] D. Estrin, D. Culler, K. Pister, and G. Sukhatme. Connecting the physical world with pervasive networks. *IEEE Pervasive Computing*, 1(1):59–69, 2002.

[40] S. Even, O. Goldreich, S. Moran, and P. Tong. On the NP-completeness of certain network testing problems. *Networks*, 14(1):1–24, 1984.

[41] L. M. Feeney and M. Nilsson. Investigating the energy consumption of a wireless network interface in an ad hoc networking environment. In *Proc. IEEE INFOCOM*, 2001.

[42] C. Foh and M. Zukerman. Performance analysis of the IEEE 802.11 MAC protocol. In *Proc. of the European Wireless 2002 Conference*, pages 184–190, Florence, Italy, February 2002.

[43] G. Foschini. Layered space-time architecture for wireless communication in fading environments when using multi-element antennas. *Bell Labs Technical Journal*, pages 41–59, 1996.

[44] G. Foschini and M. Gans. On limits of wireless communications in a fading environment when using multiple antennas. *Wireless Personal Communications*, 6:311–355, 1998.

[45] J. Freebersyser and B. Leiner. A DoD perspective on mobile ad hoc networks. In C. Perkins, editor, *Ad Hoc Networking*, pages 29–51. Addison Wesley, 2001.

[46] A. Fu, E. Modiano, and J. Tsitsiklis. Transmission scheduling over a fading channel with energy and deadline constraints. In *Proc. Conference on Information Sciences and Systems*, Mar 2002.

[47] C. L. Fullmer and J. J. Garcia-Luna-Aceves. Floor acquisition multiple access (FAMA) for packet-radio networks. In *SIGCOMM '95*, pages 262–273, Cambridge, MA (USA), Aug 1995.

[48] C. L. Fullmer and J. J. Garcia-Luna-Aceves. Solutions to hidden terminal problems in wireless networks. In *Proc. ACM SIGCOMM 97*, Cannes, France, September 1997.

[49] R. Gallager. A perspective on multiaccess channels. *IEEE Trans. Information Theory*, IT-31:124–142, Mar 1985.

[50] A. E. Gamal, E. Uysal, and B. Prabhakar. Energy-efficient transmission over a wireless link via lazy packet scheduling. In *Proc. of IEEE INFOCOM*, volume 1, pages 386–394, Apr 2001.

[51] H. Gamal, G. Caire, and M. Damon. Lattice coding and decoding achieve the optimal diversity-multiplexing tradeoff of MIMO channels. *IEEE Trans. Information Theory*, 50:969–985, June 2004.

[52] M. Gastpar and M. Vetterli. On the capacity of mobile ad hoc networks with delay constraints. In *Proc. of IEEEINFOCOM*, volume 3, pages 1577–1586, Jun 2002.

[53] D. Gesbert, M. Shafi, D. Shiu, P. Smith, and A. Naguib. From theory to practice: An overview of MIMO space-time coded wireless systems. *IEEE Journal on Selected Areas in Communications*, 21(3):281–302, April 2003.

[54] I. Gitman. On the capacity of slotted ALOHA networks and some desigh problems. *IEEE Trans. on Communications*, COM-23(3):305–317, Mar 1975.

[55] S. Gobriel, R. Melhem, and D. Mossé. A unified interference/collision analysis for power-aware adhoc networks. In *Proc. IEEE INFOCOM*, Hong Kong, March 2004.

[56] A. Goldsmith. *Wireless Communications*. Cambridge University Press, 2005.

[57] G. H. Golub and C. F. V. Loan. *Matrix Computations*. The John Hopkins University Press, third edition, 1996.

[58] M. Grossglauser and D. Tse. Mobility increases the capacity of ad hoc wireless networks. *IEEE/ACM Trans. Networking*, 10(4):477–486, Aug 2002.

[59] P. Gupta and P. R. Kumar. The capacity of wireless networks. *IEEE Trans. on Information Theory*, 46(2):388–400, Mar 2000.

[60] Z. Hadzi-Velkov and B. Spasenovski. The influence of flat rayleigh fading channel with hidden terminals and capture over the IEEE 802.11 WLANs. In *Proc. 54th IEEE Vehicular Technology Conference*, volume 2, pages 972–976, 2001.

[61] Z. Hadzi-Velkov and B. Spasenovski. On the capacity of IEEE 802.11 DCF with capture in multipath-faded channels. *International Journal of Wireless Information Networks*, 9(3):191–199, July 2002.

[62] R. Horn and C. Johnson. *Matrix Analysis*. Cambridge University, 1990.

[63] M. Hu and J. Zhang. MIMO ad hoc networks: Medium access control, satuation throughput, and optimal hop distance. *Journal of Communications and Networks*, pages 317–330, December 2004.

[64] *IEEE Standard for Wireless LAN Medium Access Control (MAC) and Physical Layer (PHY) Specifications*, Nov 1997. P802.11.

[65] International Telecommunication Union. *World Telecommunication Development Report: Reinventing Telecoms*, March 2002. Executive Summary.

[66] International Telecommunication Union. *World Telecommunication Development Report: Access Indicators for the Information Society*, December 2003. Executive Summary.

[67] Intersil Corp. *Intersil HFA3861B Direct Sequence Sprad Spectrum Baseband Processor*, Feb 2002. Data Sheet FN4816.2.

[68] R. Jain. *The Art of Computer Systems Performance Analysis*. John Wiley & Sons, 1991.

[69] P. Karn. MACA - a new channel access method for packet radio. In *ARRL/CRRL Amateur Radio 9th Computer Networking Conference*, pages 134–140, 1990.

[70] H. Kim and J. C. Hou. Improving protocol capacity with model-based frame scheduling in IEEE 802.11-operated WLANs. In *Proc. of the 9th ACM International Conference on Mobile Computing and Networking (MOBICOM)*, pages 190–204, San Diego, CA, USA, September 2003.

[71] J. H. Kim and J. K. Lee. Capture effects of wireless csma/ca protocols in rayleigh and shadow fading channels. *IEEE Trans. Veh. Tech.*, 48(3):1277–1286, Mar 1999.

[72] L. Kleinrock and S. S. Lam. Packet switching in a multiaccess broadcast channel: Performance evaluation. *IEEE Trans. on Communications*, COM-23(4):410–423, Apr 1975.

[73] L. Kleinrock and F. A. Tobagi. Packet switching in radio channels: Part I - carrier sense multiple-access modes and their throughput-delay characteristics. *IEEE Trans. on Communications*, COM-23(12):1400–1416, 1975.

[74] Y. Ko, V. Shankarkumar, and N. Vaidya. Medium access control protocols using directional antennas in ad hoc networks. In *Proc. IEEE INFOCOM*, Tel-Aviv, Israel, Mar. 2000.

[75] T. Korakis, G. Jakllari, and L. Tassiulas. A MAC protocol for full exploitation of directional antennas in ad-hoc wireless networks. In *Proc. MobiHoc'03*, pages 98–107, Annapolis, USA, Oct. 2003.

[76] C. Lau and C. Leung. A slotted ALOHA packet radio system with multiple antennas and receivers. *IEEE Trans. on Vehicular Technology*, 39(3):218–226, August 1990.

[77] C. T. Lau and C. Leung. Capture models for mobile packet radio networks. *IEEE Trans. on Communications*, 40(5):917–925, May 1992.

[78] W. F. Lo and H. T. Mouftah. Carrier sense multiple access with collision detection for radio channels. In *IEEE 13th Int'l Commun. and Energy Conf.*, pages 244–247, 1984.

[79] A. Maharshi, L. Tong, and A. Swami. Cross-layer designs of multichannel reservation mac under rayleigh fading. *IEEE/ACM Trans. Signal Processing*, 51(8):2054–2067, Aug 2003.

[80] C. Margi and K. Obraczka. Instrumenting network simulators for evaluating energy consumption in power-aware ad-hoc network protocols. In *Proc. IEEE MASCOTS'04*, Volendam, The Netherlands, Oct. 2004.

[81] The MathWorks, Inc. *Matlab v.7.0*.

[82] R. Metcalfe and D. Boggs. Ethernet: Distributed packet switching for local computer networks. *Communications of the ACM*, 19(7):395–404, July 1976.

[83] R. Moraes, H. Sadjadpour, and J. J. Garcia-Luna-Aceves. Making ad-hoc networks scale using mobility and multi-copy forwarding. In *Proc. of IEEE Globecom*, Nov 2004. To appear.

[84] M. Musser and J. Daigle. Throughput analysis of an asynchronous code division multiple access (CDMA) system. In *Proc. ICC'82*, Philadelphia, PA, Jun 1982.

[85] A. Naguib, N. Seshadri, and A. Calderbank. Increasing data rate over wireless channels. *IEEE Signal Processing Magazine*, pages 76–92, May 2000.

[86] A. Nasipuri, S. Ye, J. You, and R. Hiromoto. A MAC protocol for mobile ad hoc networks using directional antennas. In *Proc. IEEE WCNC*, Chicago, USA, Sep. 2000.

[87] The network simulator - ns-2. http://www.isi.edu/nsnam/ns/.

[88] S. J. Oh and K. M. Wasserman. Dynamic spreading gain control in multiservice CDMA networks. *IEEE Journal on Selected Areas in Communications*, 17(5):918–927, 1999.

[89] A. Papoulis. *Probability, Random Variables, and Stochastic Processes*. McGraw-Hill, 3rd edition, 1991.

[90] J. Park, A. Nandan, M. Gerla, and H. Lee. SPACE-MAC: Enabling spatial reuse using MIMO channel-aware MAC. In *Proc. IEEE Int. Conf. Communications (ICC)*, Seoul, Korea, May 2005.

[91] J. Pavon and S. Choi. Link adaptation strategy for IEEE 802.11 WLAN via received signal strength measurement. In *Proc. IEEE ICC*, pages 1108–1113, Anchorage, USA, May 2003.

[92] C. Peraki and S. Servetto. On the maximum stable throughput problem in random networks with directional antennas. In *Proc. ACM MobiHoc*, pages 76–87, Annapolis, USA, Jun 2003.

[93] M. Pursley. Throughput of frequency-hopped spread spectrum communications for packet radio networks. In *Proc. 1983 CISS*, John Hopkins Univ., Baltimore, MD, USA, 1983.

[94] D. Qiao, S. Choi, A. Jain, and K. G. Shin. Miser: An optimal low-energy transmission strategy for IEEE 802.11a/h. In *Proc. of the 9th Annual International Conference on Mobile Computing and Networking (MOBICOM)*. ACM Press, September 2003.

[95] R. Ramanathan. On the performance of ad hoc networks with beamforming antennas. In *Proc. MobiHoc*, Long Beach, USA, June 2001.

[96] R. Ramanathan, J. Redi, C. Santivanez, D. Wiggins, and S. Polit. Ad hoc networking with directional antennas: A complete system solution. *IEEE Journal on Selected Areas in Communications*, 23(3):496–506, March 2005.

[97] S. Ramanathan. A unified framework and algorithm for channel assignment in wireless networks. *Wireless Networks*, 5(2):81–94, March 1999.

[98] R. Ramaswami and K. Parhi. Distributed scheduling of broadcasts in a radio network. In *IEEE INFOCOM*, volume 2, pages 497–504, Otawa, Canada, April 1989.

[99] T. S. Rappaport. *Wireless Communications: Principles and Practice*. Prentice-Hall, 1996.

[100] D. Raychauduri. Performance analysis of random access packet-switched code division multiple access systems. *IEEE Trans. Commun.*, COM-29(6):895–901, Jun 1981.

[101] L. G. Roberts. ALOHA packet system with and without slots and capture. *Comput. Commun. Rev.*, 5:28–42, Apr 1975.

[102] E. M. Royer, P. M. Melliar-Smith, and L. E. Moser. An analysis of the optimum node density for ad hoc mobile networks. In *Proc. of the IEEE International Conference on Communications (ICC)*, Helsinki, Finland, Jun 2001.

[103] C. Sakr and T. Todd. Carrier-sense protocols for packet-switched smart antenna basestations. In *Proc. ICNP*, pages 45–52, Oct. 1997.

[104] M. Satyanarayanan. Reaching for Weiser's vision. *IEEE Pervasive Computing*, 1(1), 2002.

[105] Scalable Network Technologies, Inc. *Qualnet User's Manual Simulator, version 3.5*.

[106] S. Shakkottai, T. Rappaport, and P. Karlsson. Cross-layer design for wireless networks. *IEEE Communications Magazine*, pages 74–80, October 2003.

[107] T. J. Shepard. A channel access scheme for large dense packet radio networks. In *Proc. of ACM SIGCOMM*, pages 219–230. ACM Press, Aug 1996.

[108] M. K. Simon and M. Alouini. *Digital Communication over Fading Channels: A Unified Approach to Performance Analysis*. John Wiley & Sons, Inc., 2000.

[109] A. Stamoulis and N. Al-Dhahir. Impact of space-time block codes on 802.11 network throughput. *IEEE Trans. on Wireless Communications*, 2(5):1029–1039, September 2003.

[110] M. Stemm and R. Katz. Measuring and reducing energy consumption of network interfaces in hand-held devices. *IEICE Trans. on Communications*, 8(E80-B):1125–1131, 1997.

[111] G. L. Stuber. *Principles of Mobile Communication*. Kluwer Academic Publishers, 2000.

[112] K. Sundaresan, R. Sivakumar, M. Ingram, and T. Chang. A fair medium access control protocol for ad-hoc networks with MIMO links. In *Proc. of IEEE INFOCOM*, Hong Kong, March 2004.

[113] H. Takagi and L. Kleinrock. Optimal transmission ranges for randomly distributed packet radio terminals. *IEEE Trans. on Communications*, COM-32(3):246–257, March 1984.

[114] M. Takai, J. Martin, A. Ren, and R. Bagrodia. Directional virtual carrier sensing for directional antennas in mobile ad hoc networks. In *Proc. MobiHoc*, pages 183–193, Lausanne, Switzerland, June 2002.

[115] T. Tang, M. Park, R. Heath, and S. Nettles. A joint MIMO-OFDM transceiver and MAC design for mobile ad hoc networking. In *Proc. Int. Workshop on Wireless Ad-Hoc Networks (IWWAN)*, Oulu, Finland, May 2004.

[116] Z. Tang and J. Garcia-Luna-Aceves. A protocol for topology-dependent transmission scheduling. In *Proc. IEEE Wireless Communications and Networking Conference (WCNC)*, pages 21–24, New Orleans, USA, September 1999.

[117] V. Tarokh, N. Seshadri, and A. Calderbank. Space-time codes for high data rate wireless communications: Performance criterion and code construction. *IEEE Trans. Information Theory*, 44(2):744–765, March 1998.

[118] V. Tarokh, N. Seshadri, and A. Calderbank. Space-time block codes from orthogonal designs. *IEEE Trans. Information Theory*, 45(5):1456–1467, July 1999.

[119] E. Telatar. Capacity of multi-antenna gaussian channels. *European Trans. on Telecomm.*, 10:585–596, 1999.

[120] F. A. Tobagi. Analysis of a two-hop centralized packet radio network—part I: Slotted ALOHA. *IEEE Trans. Commun.*, COM-28(2):196–207, Feb 1980.

[121] F. A. Tobagi. Analysis of a two-hop centralized packet radio network—part II: Carrier sense multiple access. *IEEE Trans. Commun.*, COM-28(2):208–216, Feb 1980.

[122] F. A. Tobagi. Modeling and performance analysis of multihop packet radio networks. *Proc. IEEE*, 75(1):135–155, Jan 1987.

[123] F. A. Tobagi and J. M. Brazio. Throughput analysis of multihop packet radio network under various channel access schemes. In *Proc. INFOCOM'83*, San Diego, CA, Apr 1983.

[124] F. A. Tobagi and L. Kleinrock. Packet switching in radio channels: Part II - the hidden terminal problem in carrier sense multiple-access modes and the busy-tone solution. *IEEE Trans. on Communications*, COM-23(12):1417–1433, 1975.

[125] L. Tong, Q. Zhao, and G. Mergen. Multipacket reception in random access wireless networks: From signal processing to optimal medium access control. *IEEE Commun. Mag.*, 39(12):108–112, 2001.

[126] S. Toumpis and A. J. Goldsmith. Capacity regions for wireless ad hoc networks. *IEEE Trans. Wireless Communications*, 2(4):736–748, Jul 2003.

[127] D. Tse and S. Hanly. Linear multiuser receivers: Effective interference, effective bandwidth and user capacity. *IEEE Trans. Information Theory*, 45(2):641–657, Mar 1999.

[128] UN Millennium Project, New York. *Investing in Development: A Practical Plan to Achieve the Millennium Developmet Goals*, 2005.

[129] B. Vucetic and J. Yuan. *Space-Time Coding*. John Wiley & Sons Ltd., 2003.

[130] Y. Wang and J. J. Garcia-Luna-Aceves. Performance of collision avoidance protocols in single-channel ad hoc networks. In *Proc. of 10th IEEE International Conference on Network Protocols (ICNP)*, Paris, France, Nov 2002.

[131] Y. Wang and J. J. Garcia-Luna-Aceves. Directional collision avoidance in ad hoc networks. *Elsevier Performance Evaluation Journal*, 58(2-3):215–241, Nov. 2004.

[132] J. Ward and R. T. C. Jr. Improving the performance of a slotted ALOHA packet radio network with an adaptive array. *IEEE Trans. on Communications*, 40(2):292–300, February 1992.

[133] J. Ward and R. T. C. Jr. High throughput slotted ALOHA packet radio networks with adaptive arrays. *IEEE Trans. on Communications*, 41(3):460–470, March 1993.

[134] M. Weiser. The computer for the 21st century. *Scientific American*, 1991.

[135] E. Weisstein. Taylor series. From *MathWorld*—A Wolfram Web Resource. http://mathworld.wolfram.com/TaylorSeries.html.

[136] J. Winters. On the capacity of radio communication systems with diversity in a rayleigh fading environment. *IEEE Journal on Selected Areas in Communications*, SAC-5:871–878, June 1987.

[137] World Summit on the Information of Society, Geneva. *Declaration of Principles. Building the Information Society: a Global Challenge in the New Millennium*, December 2003. Document WSIS-03/GENEVA/DOC/4-E.

[138] H. Wu, Y. Peng, K. Long, S. Cheng, and J. Ma. Performance of reliable transport protocol over IEEE 802.11 wireless LAN: Analysis and enhancement. In *Proc. INFOCOM*, New York, USA, June 2002.

[139] L. Wu and P. Varshney. Performance analysis of CSMA and BTMA protocols in multihop networks (I). single channel case. *Information Sciences, Elsevier Sciences Inc.*, 120:159–177, 1999.

[140] Y. Wu, P. Chou, Q. Zhang, K. Jain, W. Zhu, and S. Kung. Network planning in wireless ad hoc networks: A cross-layer approach. *IEEE Journal on Selected Areas in Communications*, 23(1):136–150, January 2005.

[141] T. A. Wysocki and H. Zepernick. Characterization of the indoor radio propagation channel at 2.4 GHz. *Journal of Telecommunications and Information Technology*, pages 84–90, 2000.

[142] H. Yao and G. Wornell. Structured space-time block codes with optimal diversity-multiplexing tradeoff and minimum delay. In *IEEE Global Telecomm. Conf.*, pages 1941–1945, December 2003.

[143] S. Yi, Y. Pei, and S. Kalyanaraman. On the capacity improvement of ad hoc wireless networks using directional antennas. In *Proc. ACM MobiHoc*, pages 108–116, Annapolis, USA, Jun 2003.

[144] S. Yi, Y. Pei, and S. Kalyanaraman. On the capacity improvement of ad hoc wireless networks using directional antennas. In *Proc. MobiHoc*, Annapolis, USA, June 2003.

[145] T. Yum and K. Hung. Design algorithms for multihop packet radio networks with multiple directional antennas stations. *IEEE Trans. on Communications*, 40(11):1716–1724, November 1992.

[146] J. Zander. Slotted ALOHA multihop packet radio networks with directional antennas. *Electronics Letters*, 26(25):2098–2100, Dec. 1990.

[147] A. Zanella and F. Pellegrini. Mathematical analysis of IEEE 802.11 energy efficiency. In *Proc. WPMC*, Sep. 2004.

[148] L. Zheng and D. Tse. Diversity and multiplexing: A fundamental tradeoff in multiple antenna channels. *IEEE Trans. Information Theory*, 49:1073–1096, May 2003.

[149] C. Zhu and M. Corson. A five-phase reservation protocol (FPRP) for mobile ad hoc networks. In *Proc. IEEE INFOCOM*, pages 322–331, San Francisco, USA, March 1998.

[150] E. Ziouva and T. Antonakopoulos. CSMA/CA performance under high traffic conditions: throughput and delay analysis. *Computer Communications*, 25(3):313–321, 2002.

[151] M. Zorzi. Mobile radio slotted ALOHA with capture, diversity and retransmission control in the presence of shadowing. *Wireless Networks*, 4:379–388, Aug 1998.